ELECTROCODEPOSITION OF MOLYBDENUM DISULFIDE PARTICLES IN NICKEL
MATRIX

A THESIS SUBMITTED TO
THE GRADUATE SCHOOL OF NATURAL AND APPLIED SCIENCES
OF
MIDDLE EAST TECHNICAL UNIVERSITY

BY

EBRU SARALOĞLU GÜLER

IN PARTIAL FULFILLMENT OF THE REQUIREMENTS
FOR
THE DEGREE OF DOCTOR OF PHILOSOPHY
IN
METALLURGICAL AND MATERIALS ENGINEERING

JULY 2013

Approval of the thesis:

ELECTROCODEPOSITION OF MOLYBDENUM DISULFIDE PARTICLES IN NICKEL MATRIX

submitted by **EBRU SARALOĞLU GÜLER** in partial fulfillment of the requirements for the degree of **Doctor of Philosophy in Metallurgical and Materials Engineering Department, Middle East Technical University** by,

Prof. Dr. Canan Özgen
Dean, Graduate School of **Natural and Applied Sciences**   _____

Prof. Dr. C. Hakan Gür
Head of Department, **Metallurgical and Materials Engineering**   _____

Prof. Dr. İshak Karakaya
Supervisor, **Metallurgical and Materials Eng. Dept., METU**   _____

Assist Prof. Dr. Erkan Konca
Co-Supervisor, **Metallurgical and Materials Eng. Dept., Atılım U.**   _____

Examining Committee Members

Prof. Dr. Abdullah Öztürk
Metallurgical and Materials Eng. Dept., METU   _____

Prof. Dr. İshak Karakaya
Metallurgical and Materials Eng. Dept., METU   _____

Prof. Dr. Ali İhsan Arol
Mining Eng. Dept., METU   _____

Assist Prof. Dr. Yener Kuru
Metallurgical and Materials Eng. Dept., METU   _____

Assist. Prof. Dr. Metehan Erdoğan
Materials Eng. Dept., Yıldırım Beyazıt University   _____

Date:

I hereby declare that all information in this document has been obtained and presented in accordance with academic rules and ethical conduct. I also declare that, as required by these rules and conduct, I have fully cited and referenced all material and results that are not original to this work.

Name, Last name :

Signature :

ABSTRACT

ELECTROCODEPOSITION OF MOLYBDENUM DISULFIDE PARTICLES IN NICKEL MATRIX

Saraloğlu Güler, Ebru
Ph.D., Department of Metallurgical and Materials Engineering
Supervisor   : Prof. Dr. İshak Karakaya
Co-Supervisor: Assist. Prof. Dr. Erkan Konca

July 2013, 94 pages

The influence of the electroplating parameters and their interactions on hydrogen evolution reaction (HER) and the internal stress were studied during the electrodeposition of Ni and Ni-MoS$_2$ composite coatings by fractional factorial design (FFD) and analyzed by Minitab software package. The parameters and their ranges were; MoS$_2$ particle concentration (0 and 30 g/L), temperature (30 and 50 ºC), pH (2 and 4) and three surfactants, sodiumlignosulfonate (SLS), ammoniumlignosulfonate (ALS) and depramin-C (DC) (0 and 1 g/L), for voltammetric measurements of HER. The internal stress during electrodeposition was measured by deposit stress analyzer. The MoS$_2$ particle concentration (0 and 10 g/L), temperature (30 and 50ºC), pH (2 and 4), current density (1.2 and 4.8 A/dm^2) and coating thickness (25 and 50μm) were the parameters. The best combination of parameters (temperature: 50ºC, pH: 2, current density: 4.8 A/dm^2, thickness: 50 μm, in presence of MoS$_2$) for the lowest internal stress was determined. Meanwhile, the effects of mineral processing surfactants (SLS, ALS and DC) on homogeneity of MoS$_2$ particles and on internal stress were investigated. Since relatively more homogenous particle distribution was observed when SLS was added, it was used in the experiments.

The tribological behavior of Ni-MoS$_2$ composite coatings developed under above mentioned conditions were studied by using a pin–on-disc tribometer. The effects of MoS$_2$ particle concentration (5, 10 and 30 g/L), MoS$_2$ particle size (1.440 and 5.156 μm average) and the surfactant (SLS) amount (0.3 and 1 g/L) on the friction and wear behaviour were investigated. Small particle size, high MoS$_2$ and surfactant amount decreased the friction coefficient.

Keywords: Electrocodeposition, Composite Coating, Hydrogen Evolution, Internal Stress, Friction, Wear, MoS$_2$

ÖZ

NİKEL MATRİKSTE MOLİBDEN DİSÜLFÜR PARÇACIKLARININ ELEKTRO KAPLANMASI

Saraloğlu Güler, Ebru
Doktora, Metalurji ve Malzeme Mühendisliği Bölümü
Tez Yöneticisi   :Prof. Dr. İshak Karakaya
Ortak Tez Yöneticisi: Assist. Prof. Dr. Erkan Konca

Temmuz 2013, 94 sayfa

Ni ve Ni-MoS$_2$ kompozit kaplama sırasında, elektro kaplama değişkenlerinin ve bunların birbirleriyle ilişkilerinin hidrojen çıkışı reaksiyonunun zirve akım yoğunluğuna ve iç gerilim üzerindeki etkileri Minitab paket programındaki kesirli faktöriyel deney tasarımı kullanarak çalışılmıştır. Voltametrik metotla ölçülen hidrojen çıkışı reaksiyonunun zirve akım yoğunluğu için çalışılan değişkenler ve aralıkları: MoS$_2$ parçacık konsantrasyonu (0 ve 30 g/L), sıcaklık (30 ve 50 ℃), pH (2 ve 4) ve üç yüzey aktifleyici maddesi, sodyumlignosülfonat (SLS), amonyumlignosülfonat (ALS) ve depramin-C (DC) (0 and 1 g/L)'dir. Kaplama gerilim analiz cihazı ile ölçülen iç gerilim için, MoS$_2$ parçacık konsantrasyonu (0 ve 10 g/L), sıcaklık (30 ve 50℃), pH (2 ve 4), akım yoğunluğu (1.2 ve 4.8 A/dm^2) ve kaplama kalınlığı (25 ve 50μm) parametreleri kullanılmıştır. Değişkenlerin en düşük iç gerilim için en iyi kombinasyonu, sıcaklık: 50℃, pH: 2, akım yoğunluğu: 4.8 A/dm^2, kaplama kalınlığı: 50 μm, MoS$_2$ eklenmesi, olarak belirlenmiştir. Bu sırada, MoS$_2$ parçacıklarını homojen bir şekilde dağıtmak için kullanılan yüzey aktifleyici maddelerin (SLS, ALS and DC) iç gerilim üzerindeki etkileri de araştırılmıştır. Homojen parçacık dağılımı SLS eklendiğinde gözlendiği için, takip eden deneylerde bu kullanılmıştır.

Yukarıda belirtilen kombinasyonda oluşturulan Ni-MoS$_2$ kompozit kaplamaların sürtünme ve aşınma davranışları pin-on-disk tribometre ile incelenmiştir. MoS$_2$ parçacık konsantrasyonunun (5, 10 ve 30 g/L), MoS$_2$ parçacık boyutunun (ortalama 1.440 ve 5.156 μm) ve yüzey aktifleyici madde (SLS) miktarının (0.3 ve 1 g/L) etkileri araştırılmıştır. Küçük parçacık boyutu ve yüksek MoS$_2$ miktarı, sürtünme katsayısının düşmesine sebep olmuştur.

Anahtar Kelimeler: Elektro birlikte kaplama, Kompozit kaplama, Hidrojen Çıkışı, İç Gerilim, Sürtünme, Aşınma, MoS$_2$

To My Family,

ACKNOWLEDGMENTS

TABLE OF CONTENTS

x

LIST OF TABLES

LIST OF FIGURES

xiv

CHAPTER 1

INTRODUCTION

In the electrodeposition process, electric current is transported across an electrolyte and the metallic materials are usually deposited at the cathode [1]. The advantages of electrodeposition over other deposition techniques can be listed as [2, 3]:

- It is applicable in an industrial scale and it does not require high cost or post deposition treatment.
- It can be applied to complex shapes and to different substrates.
- It creates less waste which is an important problem in dipping or spraying techniques.
- The required time for electrodeposition is short due to higher deposition rate and non-porous coatings can be achieved with high purity.
- The coating thickness and the composition can easily be controlled that help to attain compositions which are impossible to obtain by other techniques.

The electroplating method can be used to produce composite plating by using dispersed fine particles in the metal plating bath so that the particles are trapped in the deposit and the process is then called electrocodeposition or composite deposition [3, 4]. The composite deposition of insoluble solid particles embedded in a metal matrix has been offered for several industrial applications such as; fuel cells, super capacitors, piezoelectric devices, biomedical implants, solar cells and in other surface modifications and protections [5].

The particles are mainly chosen from the group of metal powders, metal alloy powders and metal oxide powders of Al, Co, Cu, In, Mg, Ni, Si, Sn, V, Zn and nitrides of Al, B, Si and C (graphite or diamond) and carbides of B, Bi, Si, W and MoS_2 and organic materials such as polytetrafluoroethylene (PTFE) and polymer spheres [6]. Composite coatings based on nickel with build-in lubricant particles such as; boron nitride (BN) [7, 8], molybdenum disulphide (MoS_2) [9-13], PTFE [14-16], polyethylene [17] and graphite [18-20] were produced to have improved tribological behavior. High pressure lubricating materials; MoS_2, PTFE and graphite were added to plating baths especially to decrease the friction coefficients of coated surfaces [21]. The particles penetrate into the interface between the sliding surfaces and peel under an applied load so that these particles lead to easy sliding by covering the roughed surface [22].

A solid lubricant has to provide some important properties. For example, the friction between two sliding surfaces must be low, manageable and the lubricant must be chemically stable at operating temperature, wear resistant, non-toxic, economic and have strong adhesion to prevent catastrophic failure. Most substances are eliminated due to one or more of these restrictions leaving only the substances like graphite, MoS_2 and PTFE to find place in tribological applications [23].

MoS_2 particles that are solid lubricants can be used in cases where the temperature is high or low or under high pressure or vacuum conditions where common lubricants are inadequate for reducing surface friction [9]. It was claimed that the weight percentage of MoS_2 in the deposit increases up to a certain extent, with an increase in particle concentration in the bath [10, 13]. However, it was reported to decrease with temperature [9, 10, 12]. Besides the temperature; the current density, pH and agitation rate were also effective on the MoS_2 content in the deposit [9]. Kuo concluded that the content of MoS_2 in the deposit increases with a decrease in the current density and pH [12]. On the other hand, Ni deposits more efficiently with increase in temperature and pH [10].

Internal stress is a common problem in plated deposits if it is not controlled and it may lead to adverse effects on the properties and the performance of the coatings and may result in adhesion problems or other undesirable morphology of the deposits [24, 25]. The reasons for internal stress development in coatings can be listed as follows:

1. The differences in lattice parameters (lattice misfit) [21, 26-28] of coatings and substrates: The misfit amount depends on the substrate type and electroplating conditions [21]. The amount of lattice difference between the deposit and the substrate determines the magnitude of stress [27].
2. The differences in thermal expansion coefficients between the deposits and the substrates [26].
3. Hydrogen [21, 27, 29, 30] codeposition: Tensile stresses occur due to hydrogen dissolution and following delivery depending on current density [31] and electrolyte composition.
4. The crystalline-joining [21, 27, 29, 30] that occurs by coalescence of crystallites: Coatings grow and contact one another during three dimensional nucleation [21, 29]. This coalescence results in tensile stress since different crystallites contacted may be pulled together by a surface tension to have a decreased total free surface energy [21, 29, 30].
5. The presence of dislocations that lead to the tensile stress development [21, 27, 30].
6. The excess energy theory stems from overpotential: A metal ion has to overcome an energy barrier to be adhered to the lattice and converted from hydrated level. When the ions overcome the barrier they have higher temperature than their surroundings and cooling creates tensile stress [21, 30].
7. The bath composition [21, 27, 30, 32] and electroplating conditions [21, 26]:

Stress relievers and wetting agents that act as a stress reducer assisted to decrease internal stress [33]. Generally, increasing temperature decreased the internal stress [25, 30, 34, 35]. pH must be lower than 5 for Watts bath for tolerable stress levels [36]. In addition, increasing current density from 0.15 to 5 A/dm^2 increases internal stress [37]. The deposit stress can either be tensile (+) or compressive (-) that will try to contract or expand the deposit relative to the substrate [32, 38]. The allowable stress in electrodeposits up to 100 μm thickness was in the range of ± 30 MPa for quality electroplating [39] whereas the range was stated as 125 to 185 MPa by Di Bari [40].

Nickel is well known for its strong adhesion to substrates and MoS_2 particles embedded in nickel matrix are used due to their self-lubrication property. Therefore, in this study Ni-MoS_2 composite pair was studied. The first objective of this work was to study the effects of electroplating parameters such as; MoS_2 concentration, temperature, pH and surfactant (ammoniumlignosulfonate, sodiumlignosulfonate, depramin C) on hydrogen evolution reaction (HER) in order to determine the current density range where H_2 is not simultaneously discharged with Ni plating. This way, contribution of hydrogen to the internal stress and crystal texture could be controlled. Following this study, the effects of above electroplating parameters and coating thickness on the internal stress during Ni electroplating and Ni-MoS_2 electrocodeposition were investigated to determine the combination of parameters that produce minimum internal stress. Meanwhile from the microstructural investigation of the coatings produced by using combination of parameters that give low internal stress, the mineral processing surfactant; among ammoniumlignosulfonate, sodiumlignosulfonate and depramin C, that gives higher concentrations and homogeneous distributions of MoS_2 particles was determined. Furthermore, the effects of MoS_2 concentration, surfactant concentration and MoS_2 particle size on the friction coefficient and wear rate of electrocodeposited Ni-MoS_2 coatings were studied. During the experiments, fractional factorial design from Minitab program [41] was used to evaluate the influence of parameters and the complex variable interactions of parameters with a reasonable number of experiments.

CHAPTER 2

LITERATURE REVIEW

2.1 Electrodeposition

The schematic drawing of a typical electrolytic cell used for electrodeposition is shown in Figure 2.1. The electric current "i" is transported by ions across the electrolyte which is the surrounding and this leads to the formation of electrolysis' products at the electrodes. The positively charged cations (M^+) are attracted by the negatively charged cathode and negatively charged anions go to the positively charged anode. The products of the electrolysis are developed by neutralization of the charges on the electrodes with the help of the charges on the electrodes. The cathode is the place where reaction takes place at a potential called deposition potential. The current admitted to the cathode is directly related to the plated area so current density is defined as the current per unit area [1]. The reactions occur at the anode do not depend on the cathode reactions [1]. Various reactions can occur at the cathode in the presence of more than one ions [1]. Each electrode reaction has its own voltage to occur and the reversible electrode reaction of the deposited metal ion will be the most positive one. The most commonly used solvent which is plentiful, has low cost, dissolves many commercially used salts and ionizes the substances that dissolve in it is water. Many commercial electrolytes use water as solvent and they are called aqueous electrolytes [1]. Fused salts are nonaqueous electrolytes and generally used in electrolytic production of metals like sodium, magnesium, aluminum and in electrolytic cleaning of metals [1].
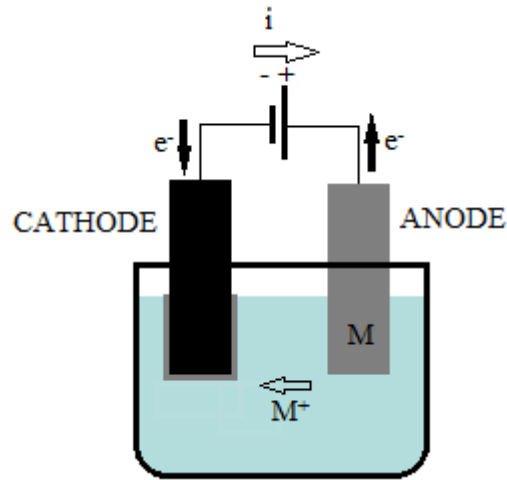
Figure 2.1 Schematic drawing of a typical electrodeposition cell

2.2 Polarization

For the operation of an electrolytic deposition process, a potential that will perform electrode reactions and carry the current across the electrolyte and the external circuit is required. The parts of the applied potential other than that required for the reaction, are resistance polarization (E_r) that includes voltage drop due to ohmic resistance in the electrolyte and voltage drop in the electrical connections and overpotentials (η) of the electrodes. In order to obtain a current flow, an external potential must be applied to an electrolytic cell if it has no net current flow [36, 40]. The applied potential during electrodeposition can be divided into several components as shown in equation 1.

$$E_{app} = E_{rxn} + \eta + E_r \tag{1}$$

Where E_{rxn} is the potential required for cell reaction to take place reversibly, η is overpotential of electrodes and E_r is potential due to resistance of the electrolyte and external connections. Therefore, application of E_{rxn} alone will not be enough for a cell to operate. The effect of overpotential of electrodes on cell potential can be seen in Figure 2.2.

The reaction rates at the anode and the cathode are equal in an unpolarized cell. The potential at the anode is increased and at the cathode is decreased by applying the polarization potential so the deposition reaction is provoked and dissolution reaction is repressed. As a result, the flow of net cathodic current and metal deposition take place [36]. The potential change in both electrodes is their polarization potential or overvoltage [36]. The sign of the overvoltage is negative for the reactions at the cathode and positive at the anode [36].
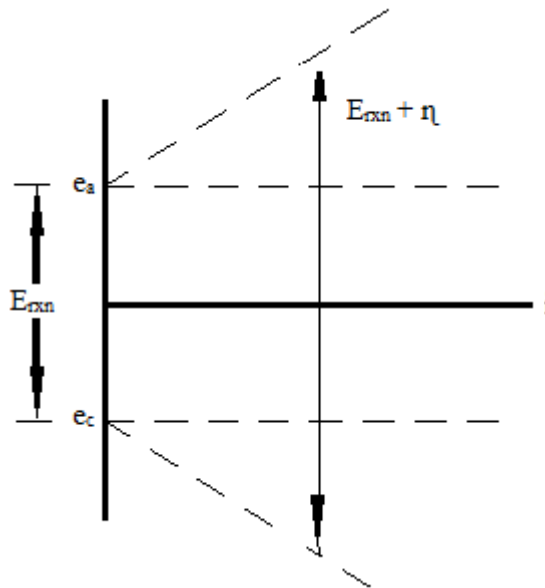
Figure 2.2 The effect of the overpotential of electrodes on cell potential

The ideal current – voltage curve that clarifies electrode reactions is shown in Figure 2.3 [1]. If the voltage is measured almost near the cathode, Figure 2.3 is obtained [1]. There is no current passing until applied potential reaches to point A, but the voltage will increase by applying a small current. Although there are ions in the solution ready to deposit, the metal deposition will not take place yet. Additional increase in the current increases the voltage up to a value where plating starts. The electrode reactions begin at this voltage which corresponds to point B in Figure 2.3. The potential difference between points A and B is the resistance polarization. Current is diffusion limited when it reaches to limiting current density (i_L) which is the maximum current density to achieve a desired electrode reaction before hydrogen or other extraneous ions are discharged simultaneously.
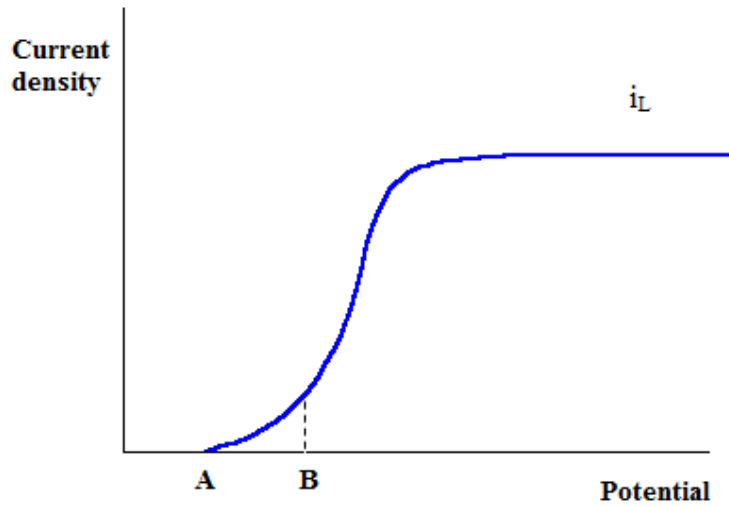
Figure 2.3 Current density versus voltage curve

2.2.1 Activation Polarization

The reactants must exceed a minimum energy barrier in order to continue the reaction in any chemical or electrochemical reaction. The closer the mean energy of reactants to activation energy the more probable that individual reactants will collect enough energy to attain activation level [36]. Activation energy is the obstacle that the reactants must overcome [36]. If the activation energy for the reaction is high then required overvoltage is high, if the energy is low necessity for overvoltage is less [42]. Activation polarization is the part of total electrode polarization that is due to activation energy. Activation polarization is a logarithmic function of the current density [36].

$$\eta(\text{act}) = \frac{R \times T}{\beta \times z \times F} \times \ln\frac{i}{io} \tag{2}$$

where
R: gas constant = 8.3143 J/(mol*K),
T: temperature (K),
β: electron transfer coefficient (0< β <1),
z: number of electrons involved,
F: Faraday constant = 96485 C/mol,
i: current density,
i_0: current exchange density,

Equation 2 can be reorganized in another form known as Tafel equation given below:

8

Tafel equation: $\eta = a + b \log i$ (3)

where b is Tafel slope and
a = [– (2.303×R×T) / ($\beta \times z \times F$)]

Tafel equation displays a linear relationship (Figure 2.4) provided that there is no concentration accumulation [42]. However deviation from the linearity is observed with additional increase in current density [42]. Insufficient amount of cations are transported through the double layer because of low diffusion rate since the production rate of cations increases at higher current densities. The ions are collected and apply repulsive force to the ions to be carried from the surface of the metal to the double layer. At this point anodic dissolution cannot be continued and current cannot be conducted by the cations regardless of the applied overvoltage. This point corresponds to limiting current density (i_L) at which current loses its dependency to the potential.
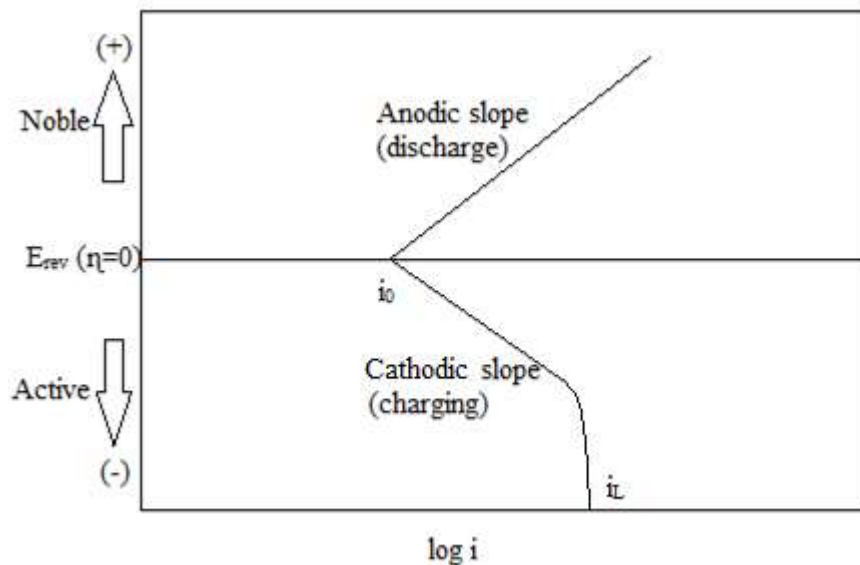
Figure 2.4 A typical Tafel plot for M $\leftrightarrow$ M^{z+} + ze$^-$

2.2.2   Concentration Polarization

The concentration of metal ions near the cathode decreases as the deposition continues because the mass transport is not enough to supply ions to be deposited The reversible potential is decreased due to this effect and the amount of decrease is given by concentration overpotential shown in equation 4.

$$\eta(conc) = \frac{R \times T}{z \times F} \times \ln \frac{Ce}{Co} \tag{4}$$

where
C_e: concentration of the ion being deposited next to the electrode surface,
C_o: concentration in the unchanged bulk of the electrolyte

Concentration polarization can be measured with the interruption of current if it is reversible electrode since the activation polarization vanishes [36]. Mass transport is more important at the cathode [42]. Agitation, temperature, velocity, concentration of ionic species and geometry are the factors that affect concentration polarization [42]. Concentration polarization is decreased by agitation and increasing temperature since diffusion layer thickness gets smaller and ionic diffusion increases [42]. Increasing velocity also decreases concentration polarization since ionic flux becomes sufficient to keep concentrations of ions in electrode/electrolyte interface and in the bulk similar [42].

2.2.3 Resistance Polarization

In addition to activation and concentration polarizations, further voltage is required to proceed electrodeposition. This part of polarization is called resistance or ohmic polarization and expressed by E_r and it is potential due to resistance of the electrolyte and external connections. If the anode cathode distance is remarkable, ohmic polarization comes into prominence [42].

2.2.4 Total Polarization

The total polarization or applied polarization is necessary to keep current at steady state through the plating bath which equals to the sum of all individual polarizations.

2.3 Nickel Electroplating

Nickel electrodeposition is one of the surface finishing processes. The applications of nickel electroplating can be divided into three main categories: decorative, functional, and electroforming [40]. Generally, nickel is electrodeposited in combination with chromium in decorative applications. A thin layer of chromium is deposited on top of a relatively thick, single layer of nickel to prevent the nickel from corruption. In most cases, decorative nickel coatings are mirror bright as deposited and do not require polishing prior to chromium plating. Multilayered nickel coatings are superior as compared to single-layer ones of equal thickness and are widely used to protect materials against corrosion [40]. Nickel coatings with improved wear and corrosion resistance can be used in automotive industry (coatings on pistons, cylinder walls, rotary engine housing liners, gear shafts, drive shafts, pump rods, hydraulic pistons) [43], cylinder rolls, mining equipment (hydraulic pistons, shafts, pump rods, and cylinders) [44] and many household applications. Moreover, the low current

density application in nickel plating was also reported to assist bonding process in electronic packaging [45].

Nickel plating process includes the dissolution of one electrode (the anode) and the deposition of metallic nickel on the other electrode (the cathode) [46]. In other words, the nickel layer is deposited on a substrate by passing current between the anode (+) and the cathode (-). The conductivity is achieved by an aqueous solution of nickel salts between the electrodes. Nickel exists as positively charged ions Ni^{2+} upon dissolution of nickel salts in water. Nickel ions react with two electrons when current flows and metallic nickel is deposited at the cathode and the reverse reaction takes place at the anode where metallic nickel dissolves to form divalent ions. The corresponding electrode reactions are shown in the schematic representation of cell in Figure 2.5. Hydrogen evolution reaction may also take place at the cathode depending on electroplating conditions.
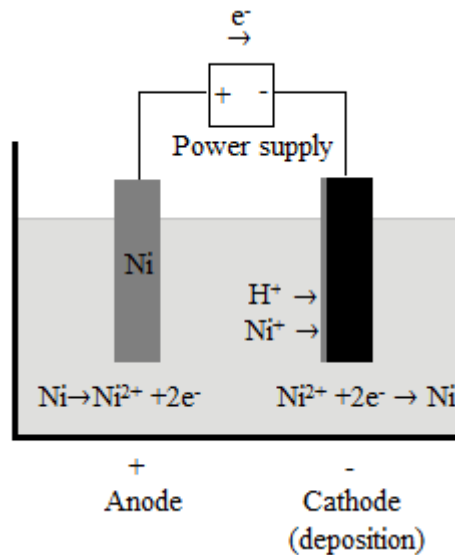
Figure 2.5 Schematic representation of nickel electroplating cell

Uniform thicknesses of nickel are desired on all surfaces to obtain foreseeable service life and to satisfy specifications that require minimum coating thicknesses at particular places on the surface. The current that reaches the surface determines the amount of metal that deposits on the surface. Embedded areas that are far from the anode on the surface gets less current and in these areas both the current density and the metal deposition rate are lower compared

to the projecting areas. So the thickness of the deposit at the areas near the anode is higher than the other parts as it can be seen in Figure 2.6.
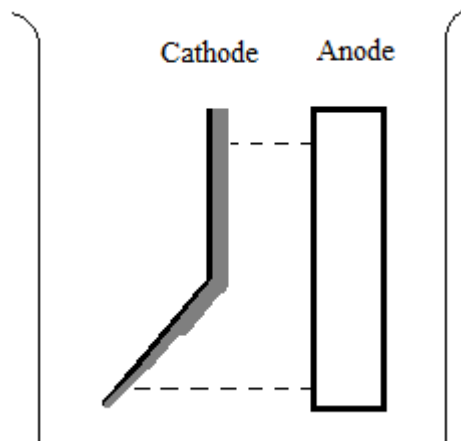
Figure 2.6 Areas far from the anode receive smaller share of the available current than areas near the anode

2.3.1 Plating baths

Nickel electroplating was first demonstrated in 1837 by Bird with the process of electrolyzing nickel chloride or sulphate solution for hours and ending up with metallic nickel on platinum electrode [21]. Afterwards, different prescriptions were patented. Nickel sulfamate plating bath was used with the concentration ranges of nickel sulfamate (329 to 493 g/L), nickel chloride (0 to 33 g/L) and boric acid (33 to 49 g/L) but it was also prepared with the concentrations of 500 g/L nickel sulfamate, 8.5 g/L nickel chloride and 26 g/L boric acid [47]. The internal stress values of electrodeposits made from sulfamate bath is low [48]. However, the widely accepted rapid plating solution is Watts bath that contains nickel sulfate, nickel chloride, boric acid and distilled water and it was formulated by O. P. Watts in 1916 [21]. Nowadays Watts bath with some adaptations are still used in most of the commercial nickel electroplating. The bath can be prepared at temperatures above room temperature and it can be used at high current densities [49]. The concentration ranges of the components are listed in Table 2.1 [21]. Each of the ingredients of the Watts bath has their own mission. Nickel sulphate is the basic source of uncomplexed nickel ions that dissolves quickly [21, 46, 49]. It has relatively low cost and it is commercially available [21]. The concentration of the nickel sulphate used in the solution is directly related to the current density [49]. The nickel activity is controlled by the concentrations of nickel salts in the

solution, their dissociation amount and the nature and amount of other ingredients in solution [21]. Burnt deposits will be obtained at low current density if available nickel ion concentration and the corresponding limiting current density are low [21]. Nickel sulphate amount in the solution is generally kept high to have sound plating [21]. Nickel chloride increases anode dissolution and the diffusion coefficient of nickel ions and increases the limiting current density [21, 46, 49]. It also leads to uniform coating thickness in the deposit [46, 49]. Boric acid helps to keep the solution pH at the desired value [21]. It improves the surface smoothness and increases the ductility of deposits [46]. Cracking is observed in the deposit as the boric acid concentration decreases whereas high boric acid concentrations do not affect the appearance of the deposit [49].

Table 2.1 Concentration ranges of Watts bath components [21]

Chemical	Concentration range (g/L)
Nickel sulphate ($NiSO_4.6H_2O$)	150 to 400
Nickel chloride ($NiCl_2.6H_2O$) or	20 to 80
Sodium chloride (NaCl)	10 to 40
Boric acid (H_3BO_3)	15 to 50

2.3.2 Additives

Wetting agents and surfactants are added to inhibit pitting by decreasing the surface tension of the solution so that air and hydrogen bubbles do not adhere to the plating substance [36, 49]. Wetting agents play an important role during brightening system since brightness cannot be achieved if the surface is not pit free. Levelers are added to obtain smoother surfaces than the substrate on which coating is applied with an increase in the coating thickness [49] and to hide surface defects [21]. The principal aim of the carriers which are the sources of sulfur codeposited with nickel is to obtain refined grains and shining deposits [49]. They have also stress reducing effects [49]. Carriers generally are added into the solution with the amounts of 1 to 25 g/L. The first class brighteners increase leveling [21, 49]. If it is used alone, complete brightening effect cannot be observed unless the specimen was previously polished [21]. The amounts are not very important, for example if the brightener is naphthalene polysulphonic acid type the 15 g/L concentration will be used or if it is one of aromatic sulphonimides especially sodium salt of saccharin, which is more commonly used then the concentrations will be in the range of 2 to 4 g/L [21]. The aim of the second class brighteners is to obtain fully bright surfaces however they cannot be added into the solution alone, they are added together with stress relievers, since they cause brittleness and internal stress in the deposits [21, 49]. Second class brighteners have more considerable effects on the physical properties of the deposits than the first class ones [21]. Therefore, concentrations of second

class brighteners are low and in the range of 0.005 to 0.2 g/L [21]. For instance, an acetylenic group is added at an amount of 0.01 g/L [21]. Synergetic effect is observed when they are used together [21].

2.3.3 Anode and Cathode Efficiencies

Cathode efficiency of nickel deposition is less than 100 % since some portion of the current is consumed to discharge hydrogen ions from water [46, 49]. This is because the standard electrode potentials, $e^0_{(Ni^{2+}/Ni)}$ = -0.25 V and $e^0_{(H^+/1/2H2)}$= 0 V, show that hydrogen discharge is preferable than nickel ion discharge if both activities are unity [21]. But the cathode efficiency of nickel deposition from Watts bath is about 95 %, that stems from the higher activity of nickel ion that changes the reversible potentials and diffusion rates of two ions into the cathode [21]. In this respect, cathode efficiency can be increased by increasing the activity of nickel ions, pH, temperature and current density [21, 50]. On the other hand, dissolution efficiency at the anode is normally 100% since the anode efficiency surpasses the cathode efficiency by a small amount and hydrogen ions are not discharged [46, 49].

The nickel amount electrodeposited at the cathode is directly related with the passage of electrical charge according to Faraday's law.

$$m = M \times \frac{I \times t}{n \times F}$$

where I is current in Amperes, t is time in seconds, M is the molar mass, n is the number of electrons take part in the reaction, F is Faraday's constant that is 96485 coulombs (amp-sec) and m is the mass of the substance liberated at an electrode in grams. The expression above gives the deposited nickel amount for a 100 % current efficiency. In order to determine the actual result the theoretical amount must be multiplied by the current efficiency [49].

2.4 Composite Electroplating

Composite coatings with metal base have been produced by several methods, like hot isostatic pressing, a combination of physical and chemical vapor deposition and electrocodeposition [51]. Since electrocodeposition is carried out at a normal pressure and ambient temperature, it is accepted as one of the most advantageous techniques to produce composite coatings [51]. Moreover, electrodeposition has the advantages of low cost, homogeneous particle distribution and high deposition rate [51].

Although electrodeposited nickel satisfies most of the requirements like high tensile strength, good toughness and corrosion resistance, engineering applications sometimes require additional properties [21, 51]. So attempts were made to improve the properties of nickel coatings by introducing a second phase by dispersing soft and/or hard reinforcements to improve wear resistance and/or anti-friction behavior [21, 43, 51]. These deposits were then

called composite coatings composed of an electrodeposited metal matrix and non-metallic particles [52]. The method underlies the composite deposition to apply coating process using conventional plating baths including solid particles that stay in suspension by stirring [21]. Agitation prevented particle agglomeration and led to homogeneous distribution of fine dispersoids [53]. In addition, high stirring rate assisted ion transportation during electrodeposition procedure [35]. Generally mechanical stirring was applied but other methods were air agitation and prolonged circulation with pumps [21]. For most applications that required smooth composite coatings; particles with 1-12 μm size were used commonly [21]. The general composition range for the embedded particles were 2-200 g/L in plating baths was restricted if the particle amounts were below an optimum value due to the low particle supplement [3]. On the other hand, very high particle amounts led to tensile stress in the deposits [21] and settling were observed [3].

In one of the applications, composite coatings are produced to obtain better lubricity in the form of metal, ceramic and polymer-matrix composites [54]. Solid lubricants were categorized in two groups that are soft and hard coatings [54]. The wear resistance was higher in hard coatings compared to soft ones so especially wear and lifetime were important for soft coatings [54]. Hard coatings contain oxides, nitrides, carbides, borides and diamond or low hydrogenated diamond-like carbon based compositions whereas soft coatings contain soft metals, polymers, halides, sulfates of alkaline earth metals, high hydrogenated diamond-like carbon based compositions, well known lamellar solids like transition metal dichalcogenides and graphite [54].

2.4.1   MoS$_2$-Nickel Composite Electroplating

The modern self-lubricating coatings were introduced to satisfy the increasing demand for decreased friction in severe applications [54].The metal dichalcogenides MX$_2$ (where M is molybdenum or tungsten and X is sulphur or selenium) especially MoS$_2$ particles that are very interesting due to enhanced frictional properties. It is used in applications involving ultra-high vacuum, automotive or space systems including satellites and launch vehicles where liquid lubricants fail [9, 55, 56]. Low friction is required especially in vacuum mechanics to decrease the power consumption and heat generation [57]. The main aim of the application of these coatings is improved dry-running due to reduction in friction [52].

The lubricating property of MoS$_2$ can be regarded due to its lamellar structure and inert basal planes existing in the individual crystallites that helps easy shearing [58]. Their crystal structures have multiple slip planes and do not work-harden significantly during sliding [54]. Dislocations and point defects produced during shear deformation are rapidly nullified by the frictional heat generated during sliding. However, MoS$_2$ containing films are soft that lead to low wear resistance [58].

There are several electrocodeposition studies including MoS_2-nickel composite pair. The best plating parameters were determined as 50g/L MoS_2 concentration in the electrolyte, 4 A/dm^2 current density, pH=4 and 45ºC plating temperature to have maximum MoS_2 content in the deposit [9]. On the other hand, Kuo stated that optimized parameters were 30g/L MoS_2, 4 A/dm^2 current density, pH=3 and 50ºC [12]. It was also stated that the amount of surfactant was critical since it restricted the transfer of electrons during electrochemical processes that led to decrease MoS_2 content of the deposit even though surfactants were beneficial to disperse MoS_2 particles in the solution [12]. The optimum surfactant amount was determined as 20 mg/g MoS_2 [12]. According to Chang and his coworkers, the temperature that exerted an adverse effect and the particle concentration in the bath which exhibited positive effect on MoS_2 content in the deposit were the main parameters. This conclusion was arrived from the results of tests done by using statistical experimental design [10]. Moreover, increasing MoS_2 concentration in the bath decreased the friction coefficient of the coating whereas increased the wear volume [13].

2.4.2   General Mechanisms

General codeposition process mechanisms based on particle transportation due to electrophoresis, mechanical entrapment, adsorption and convective-diffusion have been studied [59]. The commonly accepted model involves combination of three steps in the movement of solid particles from solution to the cathode surface, as stated by Kurozaki [60, 61]. The dispersed particles are carried to the Helmholtz's double layer by mechanical stirring in the first step. They are charged due to the high potential gradient and carried to the cathode by electrophoresis in the second step. In the third step, Coulombic forces present between particles and adsorbed anions led to adsorbtion and incorporation of particles at the cathode surface where adsorped ions are reduced. On the other hand, Martin and William claimed that electrophoresis is irrelevant but the process is completely mechanical entrapment [3]. The expansion of the three-step mechanism to five steps [62] is shown in Figure 2.7. The figure includes; double layer formation of adsorbed species around each particle transportation of particles to hydrodynamic layer limit by stirring, diffusion of only positively charged particles to the cathode due to the electric field affect, reduction of free or adsorbed electro active species at the cathode and incorporation of the particle in the deposit due to the reduction of adsorbed ion species on the particles.

16
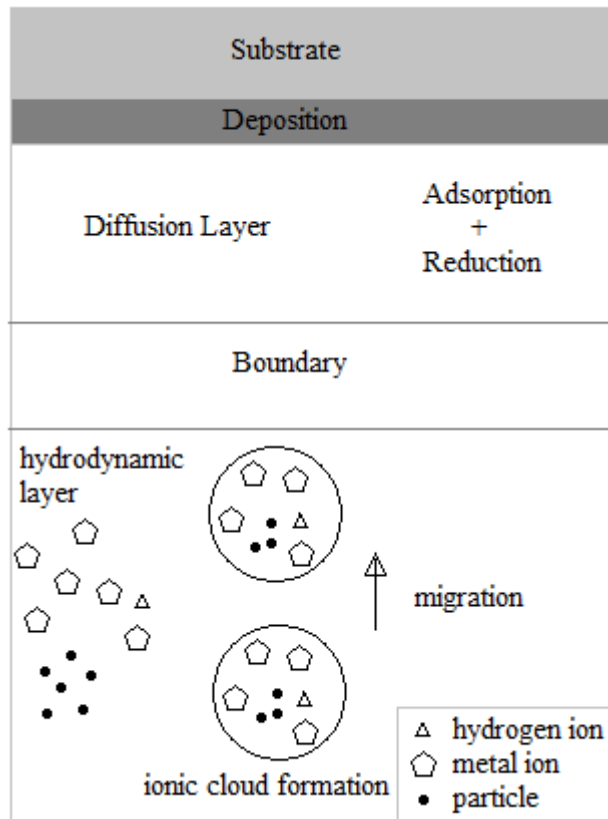
Figure 2.7 The steps of dispersed particles in composite coating by electroplating

A two-step mechanism suggested by Guglielmi covers only the part of the process involving the integration of particles to the coating [59]. The first one was the bonding of adsorbed particles by loose Van der Waals forces [60, 63] and the second step was electrochemical in nature and exhibited strong particle adsorption by Coulomb forces on to the substrate [60, 63]. This model included the effects of particle concentration and current density on encapsulation rate of particles in the deposit whereas hydrodynamic effects and particle characteristics were not considered [59]. Studies were conducted to include a corrective factor to overcome these omissions [15] but the function was only valid for a limited range of experimental parameters [59]. A more extensive mechanism included particle transportation by agitation and encapsulation of particles in the metal matrix as a result of reduction of ions shown in Figure 2.8 [64, 65]. Particle concentration, agitation and growth mechanism were the most significant parts of the mechanism [64]. Nickel was coated both on the substrate and on the incorporated particle during MoS_2-Ni electrocodeposition [13]. Nickel coating around the particle became larger, and dendritic growth was observed due to the preferred deposition at the sharp edges of MoS_2 since those parts possess lower resistance

[13]. Because conducting particles like MoS_2 are attracted by the cathode that they act as a depositing site later which resulted in cluster formation and increased roughness seen in (Figure 2.9) [66]. On the other hand, when the added particles were non-conductive, smoother deposits with low porosity were observed because deposition did not occur selectively on the conductive parts [9, 66].
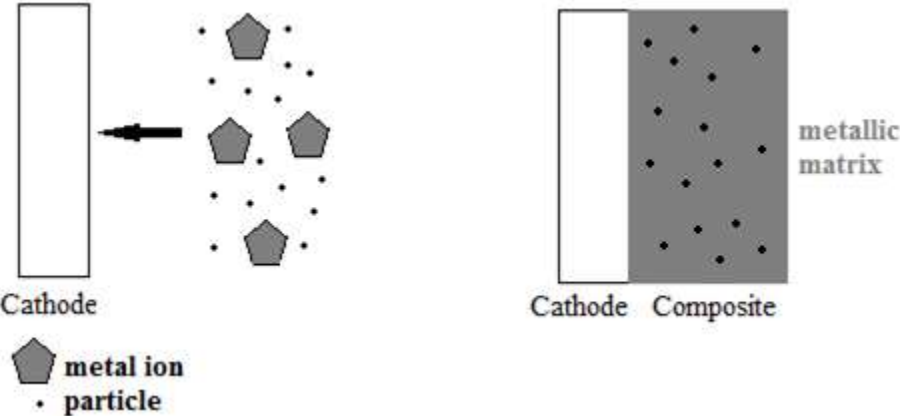
Figure 2.8 Encapsulation of particles in metal matrix
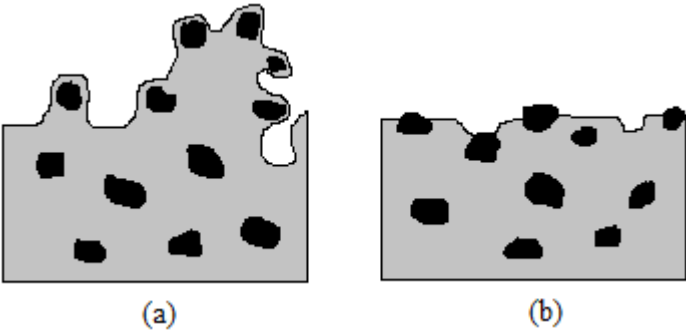
Figure 2.9 Schematic view of composite coating containing a) conducting particles and b) nonconducting particles

2.4.3   Zeta Potential

The zeta potential that is a quantitative measure for the particle surface charge indicates the degree of repulsion between similarly charged particles and stability of the colloidal system [53]. Higher zeta potential decreases agglomeration of particles in the electrolyte. The

18

particles with near to zero zeta potentials form aggregates and lead to low suspension stability [34, 67]. It was claimed that positively charged particles codeposit more easily since the particles are electrostatically attracted to cathode [53, 64, 68]. However, according to the study of Shawki and Abdel Hamid, negatively charged particles were covered by positive ions and they all together move to the cathode [13, 69].

When the pH of the plating bath was 2, the highest zeta potential value was reached and this resulted in a huge repulsive force between particles and consequently particle agglomeration in the plating bath was the lowest [70]. In addition, it was found that cationic surfactant addition to the bath changed the zeta potential from negative to positive values and affected particle distribution [71].

2.5 Hydrogen Evolution

Hydrogen evolution is the secondary electrode reaction that takes place at the cathode during electrodeposition from aqueous solutions. It can be disregarded in many cases, but it could become very important especially when hydrogen evolution affects the structure and morphology of the deposits. Hydrogen is absorbed in the substrate metal as H atoms, not H_2 molecules, but may come together to form molecule bubbles in voids or vacancies resulting in hydrogen embrittlement during hydrogen co-deposition [72]. Hydrogen bubbles that are adsorbed and stuck to the surface lead to the growth of pores during deposition before they are released whereas hydrogen bubble evolution can help important bubble raft at the free surface of the solution by providing a stirring effect [72]. The overall rection for hydrogen deposition at the cathode in acidic solutions is:

$$2H^+ + 2e^- \rightarrow H_2$$
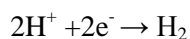
The steps can be listed as [73]:
a) transportation of hydrogen ions to the cathodic double layer,
b) hydrogen ion discharge at the metal by accepting an electron in other words, transition from solvation bond (solv) to adsorption bond (ad): $H^+_{solv} + e^- \rightarrow H_{ad}$,
c) molecular hydrogen formation (H_2) on the metal surface by holding the adsorption bond. The reaction can be carried out in two ways, Tafel reaction: $H_{ad} + H_{ad} \rightarrow H_{2,ad}$ and Heyrovsky reaction: $H^+_{solv} + H_{ad} + e^- \rightarrow H_{2,ad}$,
d) desorption of $H_{2,ad}$ (adsorbed hydrogen) from the metal surface and its travel into the solution,
e) gaseous hydrogen removal by diffusion.

Normally gaseous hydrogen overwhelms. The hydrogen ion transportation to the double layer given in a) is not so important for cathodic hydrogen deposition since hydrogen ions are ready for use in aqueous solutions. Hydrogen discharge is controlled by the activation polarization (reactions b and c) and Tafel and Heyrovsky reactions to form adsorbed molecular hydrogen because the concentration polarization can be ignored [73]. Since the

desorption process and the removal as gas or dissolved hydrogen steps (d and e) carried out very quickly, they do not control the deposition process. The slower reaction between b and c will be the hydrogen deposition controlling step depending on the deposition conditions like the nature of cathode material surface and electrolyte composition [73]. The variation of hydrogen overvoltage (η) with current density is given by Tafel equation.

Preferred crystal orientation in electrodeposits was observed due to the inhibition of the growth of certain crystal directions and allowing others to grow according to recent studies [74]. Various textures can be developed by controlling the plating parameters like current density, pH, additive type and their concentrations and metal ion concentration [74]. Mainly, pH and current density were emphasized to promote one mode of growth and lead to deposit [75, 76]. The relationship between texture and current density together with the pH of Watts' electrolyte was in general agreement [77], but there are some differences in the values of the current densities. At low current densities, the (110) texture was favored due to the inhibition of growth which was attributed to hydrogen adsorption, because the metallic surface was mostly H_{ads} that inhibits the deposition. On the other hand, (100) texture was observed at the high current densities because of uninhibited growth (free growth mode) of nickel [76-80]. In accord with above observations, dominated orientation was stated as (110) at 0.15 A/dm^2 and (100) at 0.5 A/dm^2 [37]. Similar to above results, Fritz et. al. claimed that increasing mean current density changes texture from (110) to (100) due to HER [78]. (111) is the strongest peak in the standard pattern of randomly oriented polycrystalline Ni when preferential orientation decreased in the coating [81]. The stronger Ni (111) peaks were dominant in the orientation of Ni-PTFE composite films [82]. In Ni-Al$_2$O$_3$ composite coatings, increasing randomness was attributed to alumina particles that impede grain growth of primary columnar grains which are oriented in fastest growing [100] direction and yield nucleation sites for the growth of new randomly oriented grains [81].

2.6 Electroplating Parameters
2.6.1   Current Density
The deposition of incorporated particles is directly related to the metal deposition rate and the flux of particles to the cathode that directly depends on the applied electric field profile [65]. The growth rate of metallic deposition is governed by the current density [65]. Therefore, particle concentration in the deposit increases with the increase in the current density [65, 83]. It was claimed that the concentration of titania particles during Ni-titania electrocodeposition increased by rising the current density [21]. Nickel ions were assumed to be adsorbed by titania particles and the particles were incorporated by discharging of adsorbed nickel ions Since transportation of nickel ions dissolved from the anode is slow and inssufficient to be adsorbed on particles, lower concentrations of Al$_2$O$_3$ particles were observed in the deposit at lower current densities [60].

Contrary to above observations, the effect on the increase of metal deposition rate can overwhelm the increasing effect of current density on particle incorporation and could lead to decrease in particle concentration of the deposit at very high current densities [65]. For instance, in Al_2O_3-Ni system, the Al_2O_3 content of the deposit increased sharply up to the current density of 1.5 A/dm^2 and then decreased dramatically upon further increase current density. This can be explained by rapid deposition of the metal and less incorporation of particles in the coating due to domination of metal deposition over codeposition process [84]. In addition, according to the study of Saha and Khan, at high current densities nickel ions dissolved from the anode transported faster than the Al_2O_3 particles carried by the mechanical agitation and led to low concentration of incorporated Al_2O_3 particles in the deposit during electrodeposition of Al_2O_3-Ni [60].

Therefore, there is an optimum current density that allows the maximum concentration of the co-deposited particles in the composite coatings [60]. Another study reveals that current density is independent of $BaCr_2O_4$ particle content in nickel matrix [85].

2.6.2   pH

The effect of pH on particle incorporation is dependent on the nature of the particles. The amount of embedded particles in the deposit was not affected too much by pH when it was greater than 2, whereas the incorporated particle concentrations decreased explicitly for Al_2O_3–Ni system when pH was dropped below 2 [3]. The particle content in SiC-Ni deposit increased with raising pH up to 5 [83]. In MoS_2-Ni deposit, optimum pH was determined as 3 [12] and 4 [9] for the maximum MoS_2 content in the deposit.

2.6.3   Temperature

The increase in temperature increases nickel deposition rate [35], but increases energy consumption to operate at higher temperatures and supply heat for bath evaporation. Therefore, an optimum plating temperature is used to satisfy energy consumption and the coating quality.

No effect of temperature on particle incorporation was observed in $BaCr_2O_4$-Ni [85] and Al_2O_3-Ni systems [3]. On the other hand, deposited amount of WC increased with raising temperature up to 50ºC and after that it decreased in WC-Ni composite coatings [50]. In addition, WC was uniformly distributed in the deposit when the temperature was 50ºC. Optimum temperature was determined as 50 ºC for MoS_2-Ni composite coating [12]. Therefore, 50 ºC is the best temperature for particle concentration and their distribution in composite coatings [50].

2.6.4   Particle Concentration in Composite Coating

Energies that exist between the particles determine whether the particles will separate or agglomerate when two particles approach one another in an electrolyte solution. Usually,

larger attraction energy results in agglomeration of particles. The agglomeration tendency of nanoparticles was higher than micron and submicron size particles due to their high activity [86]. The number of effective particles decrease due to agglomeration and larger agglomerated particles cause roughness in deposits and particle flake off from the matrix because of weak bonding [86].

Incorporated particles in the deposit increase with an increase in the amount of particles added to the plating solution up to a limited value [3, 84, 87]. On the other hand, the increase in the particle concentration in the electrolyte increased agglomeration and made it difficult to maintain the suspension of uniformly mixed particles in the bath in SiC embedded in Ni-Co [88] and in bronze-PTFE composite coatings after 50g/L PTFE concentration in the bath [16]. In addition, the effect of current density decreased when the particle concentration was increased [21].

Particle agglomeration was inhibited by surfactant addition [88] and stirring [53] and formed uniform particle distribution in coatings. Furthermore, since surfactant addition decreased the particle agglomeration, the amount of effective particles increased significantly and led to higher amounts of SiC in the SiC-nickel deposit [86].

2.6.5 Surfactant

Surfactant addition to plating solution in codeposition affects the amount of particles and their dispersion in the deposit [89]. Especially, hydrophobic particles (fluorographite, MoS_2) need surfactants in order to be dispersed in the aqueous electrolytic solution [18]. Suitable surfactant addition improved the suspension stability by diminishing the surface tension [88]. In addition, surfactants like sodium lauryl sulphate enhanced the electrostatic adsorption of suspended particles on cathode surface by increasing their positive charges [88]. Similarly, azobenzene (AZTAB) promoted particle deposition into the nickel matrix by their more positive reduction potential than that of nickel [90]. The advantage of the surfactant cetyl trimethyl ammonium bromide (CTAB) was to increase the volume percentage of SiC in the deposit besides homogeneous and non-agglomerated distribution of particles in SiC-nickel composite coatings [51, 91]. It was also claimed that addition of cationic surfactant, CTAB increased the amount of carbon nanotubes and $BaCr_2O_4$ particles [85] in nickel matrix whereas anionic surfactant, sodium dodecyl sulphate (SDS) led to a slight decrease. However the detrimental effects of CTAB on mechanical property and corrosion resistance of the depsoit were also mentioned [92]. Moreover, according to Shrestha and coworkers cationic surfactants increased the particle incorporation in the coating [8, 93, 94], but anionic surfactant SDS did not effect the codepositon of particles [94].

The surface charge of the particles determined the particle percentage in the deposit because if the particle had negative surface charge, cationic surfactants would be easily adsorbed on the particle [8]. Therefore, a net positive charge was formed by the adsorption of cationic

surfactants that inhibited the formation of particle clusters and led to more stable particle suspension in the bath [8, 53, 93]. Moreover, this positive charge improved the tendency of particles to move towards cathode and increased the amount of particles in the deposit [8, 93]. For instance, addition of cationic surfactant Benzyl Ammonium Salts (BAS), increased the amount of MoS_2 codeposition [9]. In addition, BAS adsorbed on MoS_2 particles decreased the conductivity of the particles and resulted in homogeneous deposition of nickel and MoS_2 particles [9, 66]. Furthermore, the strongest adhesion between the deposit and the substrate was achieved by the addition of cationic surfactant BAS compared to anionic, nonanionic and amphoteric surfactants [9].

On the contrary, it was stated that anionic surfactant in the electrolyte helps the particles to gain a negative charge and make them able to move towards the positively charged anode surface as a result of electrophoresis [95]. In addition, it was stated that anionic surfactants sodium dodecyl-glycol were necessary to inhibit agglomeration in SiC-nickel composite coating [96]. Furthermore, anionic surfactants dodecyl sodium sulfate and saccharine were used to disperse Si_3N_4 particles in nickel matrix [97]. However, it was claimed that non-ionic surfactants provoked solid particle incorporation in the study of Popov et. al. [64]. On the other hand, anionic SDS or cationic CTAHS (cetyltrimethylammonium hidrogensulfate-$C_{19}H_{43}NO_4S$) surfactants were added to determine the charge effect and it was concluded that the presence of surfactant was more important than its charge since both SDS and CTAHS showed a decrease in the amount of incorporated particle concentrations in NiP-SiC composite coatings [89]. In addition, it was claimed that there was no relation between the amount of particle incorporation and surfactant charge since just the wetting of the particles increased as a result of adsorbed surfactants [68].

Surfactants may even lead to flotation of smaller particles and let just the larger ones to suspend [89]. The use of surfactants was more advantageous for the particles which are hydrophobic like MoS_2 [8, 9]. Adding surfactant regardless of its charge, can alter the hydrophobic behavior of the particles [89]. Surfactants were adsorbed on the hydrophobic parts of the particles and the particles shifted to hydrophilic owing to surfactant cover [89]. In addition, it was stated that hydrophilic particles must rotate to stay away from the water molecules that adsorb on the surface in order to be incorporated in the deposit whereas hydrophobic particles do not encounter this problem [89].

The disadvantage of the surfactants may occur if there are unadsorbed free surfactants, because they could lead to stress development and brittleness in the deposit [53]. Since the amount of incorporated surfactant is generally very small, their undesirable effects may be ignored [53]. However, increasing surfactant (CTAB) amount caused an increase in the internal stress due to the high possibilty of embedded CTAB in the nickel matrix [98].

2.7 Internal Stress

Internal stresses can either be tensile or compressive and they affect the deposition coherency that can lead to blistering, cracking or distortion [99, 100]. The adhesion is decreased and even peeling of the deposit is observed due to the stress [100]. The liberation of the stored elastic strain energy may led to detachment of the deposit and the substrate [100]. When the average atomic distance in the lattice is larger than the equilibrium value, it causes a tensile stress by trying to attract atoms closer [99]. The compressive stress is developed when atoms are closer to each other than the average equilibrium distance [99].

2.7.1   Suggested Theories for Internal Stress

One of the theories of the internal stress in coatings was *lattice misfit* that takes place when a metal was electrodeposited on a different substrate [21]. Its highest value was attained at the initial stage of the deposition [28]. The misfit amount was based on the substrate type, surface characteristics and electroplating conditions [21]. Moreover, the quantity of the stress was directly related to the amount of difference between the lattice parameters of the coating and the substrate since the mismatch determines the associated strain energy [27]. If the lattice parameter of the deposit is smaller than that of the substrate, as in the case of nickel deposition on copper, the stress was tensile that stems from the nickel atoms that were taken apart to arrange themselves in order to adapt the copper substrate structure [28].

Another reason for the stress is the difference in the *thermal expansion coefficients* of the deposit and the substrate [26, 101]. Thermal stresses are inevitable when the processing temperatures are very high and can become significantly large since coating and substrate generally have different thermal expansion coefficients [102].

One of the theories considers *codeposited hydrogen* as responsible for internal stress development during electroplating [21, 27, 30, 31]. According to the theory, hydrogen codeposition on the metal causes lattice expansion [21] that leads to tensile stress [31]. However, Lin et. al. claimed that the codeposition of hydrogen may lead to both tensile and compressive stresses [29]. The tensile and compressive stresses were considered to be formed when hydrogen departure or hydrogen diffusion takes place respectively [30].

In *crystalline joining theory,* stress is considered to be caused by coalescence of crystallites that grow and contact each other during three dimensional nucleation [21, 29]. Consequently, the coalescence lead to tensile stress since crystallites will be pulled together by surface tension to decrease total free surface energy [21, 29, 30]. The pulling force affects the size and the shape of the grains and preferred orientations [29]. Larger column grains lead to increase the internal stress due to the higher boundary mismatch however less unfilled gaps associated with larger grains would decrease the internal stress [29]. Foreign substances decreases tensile stress by hindering crystallite coalescence or by settling to the gaps

between crystallites [21]. However, this theory does not explain the development of compressive stresses [30].

The *dislocation theory* assumes that vacancy formation or dislocations in the deposit was the cause of internal stress [21, 30]. The resultant surface tension took place at the top of the substrate within 0.2 nm depth of deposit [21]. The tensile stress decreased as the deposit thickness increased, due the low dislocation density [21, 27]. However in the case of rapid deposition, some tension would remain until the equilibrium was reached [21]. In addition, compressive stresses can be developed when proper amount of stress reducers added create edge dislocations of the opposite sign [21]. Furthermore, effect of organic additives on the internal stress during electrodeposition was claimed to be related to absorption of the additive on the deposits, and explained by the dislocation-sorption theory of internal stresses [103].

According to the *excess energy theory* the reason for the internal stress was the overpotential [30]. A metal ion in solution must overcome an energy barrier to be converted to a metal durably adhered to the lattice [30]. When the metal ions jump the barrier, they have excess energy and have a higher temperature than their surroundings [21, 30]. The contraction that takes place upon cooling results in tensile stress [21, 30]. This theory could not clarify the reasons for compressive stress [30].

2.7.2 Factors Effecting Internal Stress

The *electroplating parameters* affect the internal stress in coatings [26]. The most important electroplating parameters that affect the stress [38] were listed as; current density, additive and impurity concentration, temperature of the bath and agitation rate. In most cases, raising the *temperature* decreased the internal stress [25, 30, 34, 35] but its effect was also claimed to be insignificant [40] or inconsistent depending on current density [36]. Generally, tensile stress was directly related to the *current density* [36]. Increase in current density from 0.5 to 1.5 A/dm^2 increased stress but further increase in current density led to a decrease in the internal stress in Al_2O_3-Cu(Sn) composite coatings [84]. A complex reaction was observed in talc–Cu(Sn) and CaF_2–Cu(Sn) coatings; the internal stress decreased initially; it then increased between 2.0 and 2.5 A/dm^2 current density and then decreased again upon increasing the current density [84]. The effect of *pH* on the internal stress changed with the bath contents and it was recommended that pH must be lower than 5 for Watts bath [36]. Similarly, the minimum value of stress was observed at pH=4 and the stress increased below 4 in sulfamate bath [33].

Internal stresses can be controlled by adjusting the *bath composition* [21, 26, 27, 32, 34]. For instance, high amount of nickel chloride in the Watts bath led to an increase in the internal stress [36, 49]. Stress relievers and wetting agents that act as a stress reducer assisted to decrease internal stress [33]. Carriers also reduce internal stress especially when they include

amido or imido nitrogen as in the case of saccharin [49]. Furthermore, stress was decreased with addition of compounds that contain sulfur even at small quantities (0.01 - 0.1 g/L) [30]. The contaminants that somehow entered to the solution accidentally or due to the uncontrolled plating conditions can also affect stress [30]. When these contaminants were involved in the deposit, they led to some changes that generates volume change [30]. On the other hand, the most important advantage of the nickel sulfamate [Ni(NH$_2$SO$_3$)$_2$] solution is the low stressed deposits [21, 30]. The low tensile stress in the sulfamate bath can even be changed into compressive stress by adding stress reducers.

2.7.3   Measurement Techniques

The first stress measurement that included metal electrodeposition on a thermometer bulb by silvering was done by Mills in 1877 [21]. Many measurement techniques used nowadays depend on flexible strip basis which was first employed by Stoney in 1909 [21]. Richardson and Stein stated that the widely used ones are spiral contractometer and bent strip methods that can be seen in Figure 2.10 and Figure 2.11[104]. The comparison of these two methods are listed in Table 2.2 [104].

In spiral contractometer, helix that is formed by winding of a flat strip is used to measure the stress with one end fixed and the external side of the helix is allowed to be plated. The stress in the deposit causes the helix to wind more tightly or to unwind, depending on the stress type whether it is compressive or tensile [105]. Tightening of the helix is observed due to compressive stress during plating and unwinding is seen if the stress is tensile [21, 104]. The change in the radius of curvature measured by angular displacement of the free end of the helix is then used to calculate the internal stress [21]. However it was restricted with high stress value range having upper stress limit of 140 MPa and it is not applicable in the low stress value range [32]. The spiral contractometer is slow and expensive compared to the bent strip method [32, 104].

The faster and sufficiently precise measurements can be done by the bent strip method. Two legged copper or steel strips of 0.0508 mm thickness are used directly in the plating tank. In this method, one side of the legs of the strips were previously insulated to allow plating only on the other side [38, 73]. The leg bending either toward (compressive) or away (tensile) from the plated surface was observed [21, 38, 104]. Stress calculation [32] is given as:

$$t = \frac{\Delta m}{D \times A \times 2.54} \qquad S = \frac{U \times K}{3 \times t} \qquad (5)$$

Where; t: thickness of deposit (inch), Δm: weight gain (gram), D: density of nickel (g/cm^3), A: area (cm^2), S: stress (psi), U: number of increments, K: strip constant (psi x inch)
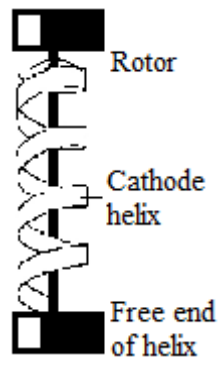
Figure 2.10 Spiral Contractometer

Figure 2.11 Photographs of Bent Strip and Deposit Stress Analyzer

Table 2.2 Summary of the most important characteristics of the three stress measurement techniques

	Bent Strip	*Spiral Contractometer*
Resolution (4 μm/.00015 in deposit)	~10.3 MPa	~55.2 MPa
Resolution (8 μm deposit)	~2.1 MPa	~13.8 MPa
Resolution (16 μm deposit)	- - -	~4.1 MPa
Typical Setup Time	5 min	25 min
Typical Test Duration	~20 min	~60 min
Maximum Test Frequency	2 per hour	1 per day per available helix
Substrate cost	$3.00 ea.	$75.00 ea. (reusable)
Ability to Use Different Substrates	No	Yes, with purchase of add-l helix
Cost of Measuring System	<$250	$1000 ($2000 w/ ext. Anode)

2.7.4   Particle Incorporation

Addition of particles may lead to further increase or decrease in stress due to mismatch of lattice parameters. Adding MoO_2 (4.2 g/L) and TiO_2 (1 g/L) particles decreased the average internal stress of nickel deposit from 47.69 MPa to 27.98 and 35.17 MPa, respectively [106]. The introduction of higher concentrations of particles in nickel matrix such as; 40 g/L B_4C and 150 g/L SiC could even change the stress behavior from tensile, 118 MPa, to compressive, 39 MPa and 42 MPa, respectively [107]. Compressive stresses were yielded by increasing particle content (TiC) of the matrix [26]. On the other hand, in the study of Wang, the stress increased by incorporation of dispersed Al_2O_3 particles higher than 6 % (by volume) in Cu(Sn) alloy matrix [84]. It was also claimed that the phosphorous content in Ni-P composite coatings up to 2wt % increases tensile stress and further phosphorus addition (up to 6wt %) decreased tensile stress since phosphorus incorporation led to refined grain structure and caused randomly oriented fibrous grains [29]. The high mismatch between random fibrous grains and empty gaps accompanied with the finer grains led the internal stress to increase and the coalescence of the grains could end up with lattice distortions caused by a larger pulling force [29]. However increase in phosphorus content prevented the formation of long fibrous grains and equiaxed grains led to a decrease in the tensile stress, because smaller crystallites, combine together and induce smaller pulling force [29].

2.8 Friction and Wear

Friction is the force acting against the relative motion of surfaces sliding against each other. It occurs at the interface between the contacting surfaces and influences all mechanical

systems [108]. Friction mainly depends on interfacial environment such as lubricants, dry films or foreign matters between the surfaces [108].

Wear can be defined as the damage on the solid surface which is in relative motion with a substance that includes growing material loss [109]. Wear resistance was mainly related to mechanical properties of the materials but friction was more complex than wear and related to materials properties and system parameters [110]. Friction was affected by physical, mechanical and chemical properties of the surfaces in sliding contact [110]. Despite the previous judgments, no relation was stated between friction coefficient and wear resistance [111].

The friction and wear was decreased in tools and molds with the help of electrolytic metal depositions. For instance, chromium plating was used to protect against wear and led to a significant increase in the service life of machines [73]. Electroplated nickel coatings have high friction coefficients reported as 0.9 [112], 1.1 [51] and 1.2 [113] when measured against sliding stainless steel. Therefore, composite coatings attracted attention. Progress in composite coatings resulted in production of new generations of adaptative, self-lubricating coatings [54].

Composite electroplating is an effective way to obtain improved tribological properties. Addition of WC [114], WS_2 [22], diamond [34, 115], polyethylene [17], MoS_2 [13, 22], MoS_2-Al_2O_3 [13], MoS_2-W [11], Al_2O_3 [116], SiC [117] and CeO_2 [118] particles to the matrix displayed low frictional properties. The friction coefficient decreased with an increase in particle concentration [34]. On the other hand, incorporation of BN particles in nickel matrix had no significant effect on the friction coefficient [7]. The particles penetrate into the contact face between the surfaces and peel under an applied load so the particles led to easy sliding by coating the roughed surface [22]. Moreover, part of the load can be carried especially by the soft particles with low shear strength that stuck in the interface so the direct contact of substrate and counterface was impeded that led to decrease in friction [113]. On the other hand particles such as Al_2O_3 [69, 81, 116, 119], SiC [69, 91, 93, 120-124], diamond [34, 115, 116, 125, 126], diamond-Cr [127], B_4C [90], WC [114], TiO_2 [116, 128], Si_3N_4 [116], CeO_2 [118], BN [7] were added to improve wear resistance. The wear volume decreased with an increase in particle concentration [34, 81].

Pin-on-disk tribometer is the most widely used equipment to determine the friction coefficient of materials. Furthermore, the wear rate of the materials can be calculated by using the track obtained by the tribometer. The tester consists of a stationary pin under an applied load (P) in contact with a rotating disk seen in Figure 2.12 [129]. Either the pin or the disk can be tested. A load cell attached to the pin-on-disk tester is used to measure the evolution of the friction coefficient with sliding distance [129].
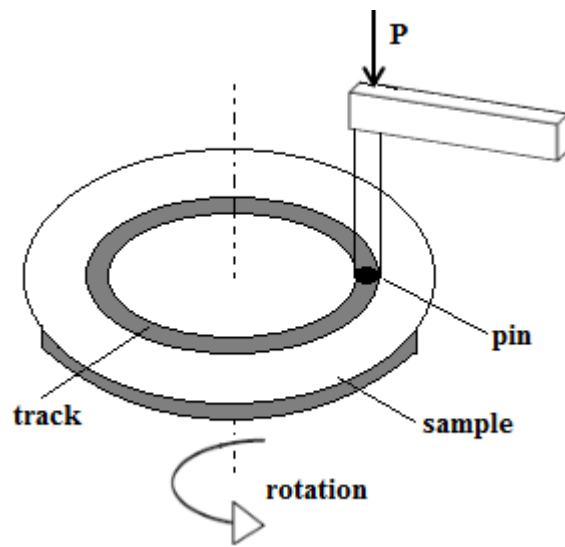
Figure 2.12 Schematic view of pin on disk tribometer

CHAPTER 3

EXPERIMENTAL PROCEDURE

3.1 Preparation of Watts Solution

The Watts bath containing 300 g/L $NiSO_4.6H_2O$ (63035981; Umicore, Belgium), 50 g/L $NiCl_2.6H_2O$ (7791-20-0; Selnic, France), and 40 g/L boric acid (minimum % 99.9 H_3BO_3, Etibank, Turkey) was prepared for the study. Above components were dissolved in deionized water at 60°C according to the procedure given in Surtec 855 [130]. The following additives; 4 mL/L carrier (SurTec 850), 10 mL/L leveler (SurTec 855), 1 mL/L brightener (SurTec 855), and 1 mL/L wetting agent (SurTec 850) were added to the Watts bath. The proper amounts of two different size MoS_2 particles, 1.440 μm (Merck-product no: 1122570250) and 5.156 μm (Sigma Aldrich-product no: 69860) average diameter, were agitated for 5 hours within 50 ml Watts solution to make a slurry that was then completed up to the desired volume and agitated for 1 hour [10].

3.2 Cleaning cathode surface:

The surfaces of the AISI 304 stainless steel specimens containing (by weight): 71.56 % Fe, 18.21 % Cr, 8.18 % Ni, 1.58 % Mn, 0.396 % Si, 0.05 % C, 0.031 % P and 0.002 % S were subjected to an alkaline soak cleaning first to remove oil, grease and solid particles for voltammetric studies, microstructural analysis and friction measurements. Alkaline solution containing 51 g/L NaOH and 49 g/L Na_2CO_3 was at 80°C [131]. Following the alkaline immersion treatment for 2 minutes, stainless steel samples were water rinsed and then subjected to electrolytic acid treatment to remove oxide film and activate the surface for reception. 18 g/L sulfuric acid solution at room temperature was used as electrolyte for this purpose. Anodic acid treatment was applied to each AISI 304 stainless steel specimen at a current density of 0.048 A/cm^2 for 60 seconds [132]. Since the surface areas of the parts immersed in the bath were 10 cm^2, applied current was 0.48 A. Following the electrolytic acid treatment, the parts were water rinsed again to prepare them for coating. The copper strips having weight percent chemical composition of Cu (97.5), Fe (2.35), P (0.03) and Zn (0.12) that used to measure internal stress of deposits were only acid treated in 150 mL/L HCl solution [133]. Following the electrolytic and acid treatments, the parts were water rinsed again.

3.3 Voltammetric Response of Hydrogen Evolution Reaction (HER)

In order to determine the current density for nickel electroplating and at the same time avoid hydrogen evolution, the voltammetric response experiments were conducted. As indicated before (110) texture was favored in nickel deposition in the presence of hydrogen evolution. The growth of FCC nickel of above texture could be strained since it is not the lowest energy plane. Furthermore, hydrogen diffusion and departure during coating cause stresses. Therefore, it was possible to discard one of the possible causes of internal stress, by applying

31

coatings under conditions that do not permit HER. To identify the effects of 5 electrodeposition variables on hydrogen evolution profile with the reasonable number of experiments, 2^{5-1} fractional factorial design, regression analysis and mixture design were used. The variables were determined as; A: MoS_2 concentration (1.44 µm, Merck-product no: 1122570250), B: Temperature, C: pH and D: Surfactant. The low (-1) and high (1) levels of above variables are given in Table 3.1 which were determined after a comprehensive literature survey. The experimental route obtained by 2^{5-1} fractional factorial design using the statistical analysis software Minitab is given in Table 3.2. The peak current density (i_p) and the peak voltage (V_p) values in the process were chosen as the response values in the design.

Table 3.1 Factors and Levels for Fractional Factorial Design (FFD)

	LEVEL	
Factor	**-1**	**1**
A MoS_2 concentration (g/L)	0	30
B Temperature(°C)	30	50
C pH	2	4
D Surfactant (g/L)	0	1

The AISI 304 stainless steel substrates of 40x40x0.5 mm were placed in the electrodeposition cell schematically shown in Figure 3.1. They were placed into the electrolyte to have only 10 cm^2 of exposed area since 2.5 cm of the specimen were merged into the solution. In addition, one of the sides was covered with electroplating tape to not to allow deposition. The stainless steel cathode (working electrode) was connected to W pole, while nickel anode (counter electrode and acting as reference electrode at the same time) was connected to both C and R poles of a GAMRY Reference 3000 Potentiostat.

The voltammetric responses between the working electrode (cathode) and the nickel anode were recorded during electrodeposition of nickel and Ni-MoS_2 composite coatings from Watts' bath according to the conditions given in Table 3.2. The potentials were swept linearly from 0 to 2.5 V at two different scan rates of 20 mV/s and 100 mV/s. "Echem Analyst" program was used to determine the i_p and V_p values associated with HER. The use of two electrode voltammetric measurements of the potentiostat, enabled the direct determination of conditions for HER in cells used in electrodeposition. Therefore, the results could be directly taken into account in the subsequent coating experiments.

32

Table 3.2 Experimental conditions for 2^{5-1} Fractional Factorial Design: -1 = low values 1 = high values for the variables

Experiment #	A (MoS$_2$)	B (Temp.)	C (pH)	D (Surfactant)	E (Thickness)
1	-1	-1	-1	-1	1
2	-1	1	1	-1	1
3	1	-1	-1	1	1
4	1	1	-1	-1	1
5	1	1	1	1	1
6	-1	-1	1	1	1
7	1	-1	1	-1	1
8	-1	1	-1	1	1
9	1	1	-1	1	-1
10	1	-1	-1	-1	-1
11	-1	1	-1	-1	-1
12	-1	1	1	1	-1
13	-1	-1	-1	1	-1
14	1	1	1	-1	-1
15	-1	-1	1	-1	-1
16	1	-1	1	1	-1

Figure 3.1 Schematic view of the voltammetry set-up. W, C and R are poles for working, counter and reference electrodes respectively

3.4 Measurements of Particle Size and Zeta Potentials:

The magnitude of the zeta potential of the particles is a measure of particle interaction. The zeta potential is a quantitative measure for the particle surface charge that gives information about the degree of repulsion between similarly charged particles. The particle size and zeta potentials of the MoS_2 particles in pure water and Watts solution were determined by a Zetasizer Nano ZS (Malvern Instruments). Dynamic light scattering was used to measure particle size by measuring the diffusion of particles that move under Brownian motion, and this was converted to size and a size distribution using the Stokes-Einstein relationship [134]. Laser Doppler micro-electrophoresis was used to measure zeta potential by applying electric field to the solution of dispersed particles that then move with a velocity related to their zeta potential. This velocity is measured using a patented laser interferometric technique called phase analysis light scattering [134]. The velocity of a particle in an electric field is commonly referred to as its electrophoretic mobility and it is converted to zeta potential by using theoretical equations.

3.5 Internal Stress Measurements:

Deposit stress analyzer, model 683, and copper alloy-194 bent strips received from Specialty Testing & Development Co. with a constant, K, of 0.3449 (psi x inch) were used directly in the electroplating cell to measure internal stress developed during plating. Schematic drawing of the cell and locations of coatings during tensile and compressive stress developments are shown in Figure 3.2. The cell was composed of a 5x5 cm nickel anode (Falconbridge, 99.98 % Ni) and a copper strip cathode placed inside a rectangular Pyrex container holding the Watt's solution. The electrodes were connected to an Instek PPS-3635 single output programmable D.C. power supply. The anode to cathode distance was 4 cm.
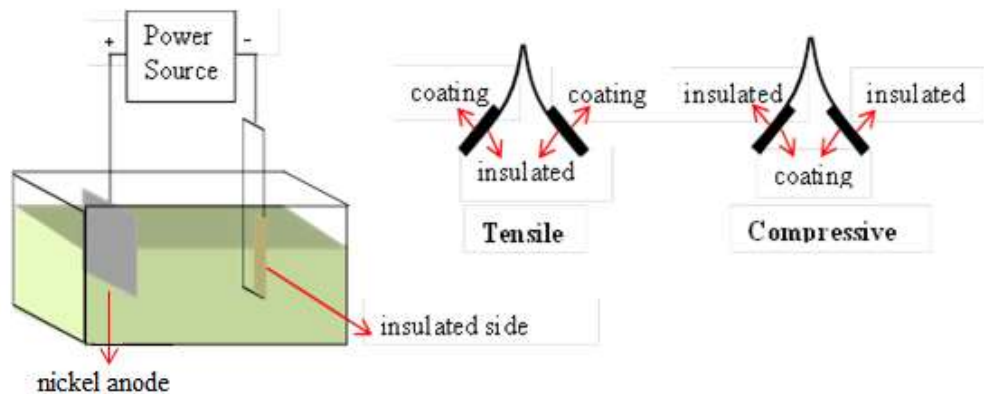
Figure 3.2 Schematic drawing of the cell showing nickel anode and one side insulated copper strip cathode in Watts bath (left). Locations of coatings on strips during tensile and compressive stress developments are shown on right

The experimental route for internal stress measurements obtained by 2^{5-1} fractional factorial design (FFD) that gives reasonable number of experiments are listed in Table 3.3. The variables were determined as *A: MoS₂ concentration, B: Temperature, C: pH, D: Surfactant* and *E: Coating thickness* and their low (-1) and high (1) fixed limit values for levels of FFD are listed in Table 3.4.

Table 3.3 Experimental routes for 2^{5-1} FFD: -1 = low values 1 = high values for the variables

Run	MoS₂ concentration	Temp	pH	Current density	Coating thickness
1	1	-1	-1	1	1
2	1	1	-1	1	-1
3	1	-1	1	-1	1
4	-1	-1	-1	1	-1
5	-1	-1	1	1	1
6	1	1	1	1	1
7	-1	-1	1	-1	-1
8	-1	1	1	-1	1
9	-1	1	-1	1	1
10	1	-1	1	1	-1
11	-1	1	-1	-1	-1
12	1	1	1	-1	-1
13	-1	-1	-1	-1	1
14	-1	1	1	1	-1
15	1	1	-1	-1	1
16	1	-1	-1	-1	-1

Table 3.4 Factors and their low (-1) and high (1) fixed limit values for Levels of FFD

		LEVEL	
Factor		**-1**	**1**
A MoS₂ concentration (g/L)		0	10
B Temp (ºC)		30	50
C pH		2	4
D Current density (A/dm²)		1.2	4.8
E Coating thickness (μm)		25	50

3.6 X-ray Diffraction Measurements

X-ray diffraction patterns of the samples were taken by FT (counts) scanning via Rigaku D/Max 2200/PC model X-Ray Diffractometer. Cu K_α radiation at a wavelength of 0.154183 nm was used. The generator settings were 40 kV and 40 mA. The diffraction data were collected over 2θ range of 10° to 90° with increments of 0.02°.

3.7 Deposition of Coatings for Friction and Wear Measurements and Microstructural Analysis

The pre-polished and cleaned 4x4 cm AISI 304 stainless steel specimens (cathodes) were immersed, to depth of 2.5 cm, into a rectangular Pyrex container holding the Watts bath and coated with nickel or Ni-MoS$_2$ composite. A 5x5 cm nickel (Falconbridge, 99.98 % Ni) anode and the cathode, separated from each other by 4 cm were connected to an Instek PPS-3635 single output programmable D.C. power supply during coating. Previously optimized combination of the parameters [135] was used to produce samples that had coatings with low internal stress (thickness: 50 μm, pH: 2, temperature: 50ºC and current density: 4.8 A/dm^2). Sodiumlignosulfonate that provided homogenous distribution of particles was added in amounts of 0.3 and 1 g/L. Composite coatings were deposited from the electrolytes by using three different MoS$_2$ concentrations (5, 10 and 30 g/L) and two different sizes (1.440 and 5.156 μm average diameter). The microstructures of the specimens were examined by an Olympus PME 3 optical microscope and a FEI Nova NanoSEM 430 scanning electron microscope equipped with energy dispersive x-ray spectroscopy (EDX) unit.

3.8 Coefficient of Friction and Wear Rate Measurements

Uncoated, pure Ni coated and Ni-MoS$_2$ coated 4x4 cm AISI 304 stainless steel specimens were tested under dry sliding conditions using a pin-on-disk tribometer (CSM Instruments) and a photograph of the test machine is seen in Figure 3.3. 6 mm diameter 100Cr6 steel balls (ISO 683-17:1999) were used as the counterface material. Tests were performed in ambient air with 45-60 % relative humidity. A constant load of 1N was applied in all tests. The linear sliding speed was 5cm/s and the wear track radius was 2 mm. The tests were run for 4000 laps corresponding to a total sliding distance of 51.07 m.

The worn volumes of the specimens subjected to the pin-on-disk tests were calculated by measuring the wear track width under the optical microscope according to ASTM standard G99 with the assumption of no significant pin wear [129]. The volume lost was then divided by the total sliding distance to obtain the wear rate.

$$\text{Disk volume loss, mm}^3 = \frac{\pi \times R \times (d^3)}{6 \times r} \tag{6}$$

Where **R:** wear track radius (2mm), **d:** wear track width, **r:** pin end radius (3mm)
In addition, surface profiler (Taylor Hobson, Surtonic 3+) was used to obtain a 2D-profile of the wear track perpendicular to the sliding direction as a representative cross-section. The

loss of material was also found by using profiles over the wear track. For three different experiments, the average cross-sectional areas were calculated from 3 measurements at different locations to get a representative value and the software readily provided the area covered by the profile. The wear volumes were calculated by multiplying the average cross-sectional area of the wear track with the circumferential contact length.

Figure 3.3 A photograph of the pin-on-disk tribometer

CHAPTER 4

RESULTS AND DISCUSSION

4.1 Characterization of MoS$_2$ Particles

MoS$_2$ particles of two different batches were used in this study. The distributions of MoS$_2$ particle size are given in Figure 4.1 and Figure 4.2. It was found that 50 % of the volume was below 1.440 μm and 5.156 μm respectively for the two batches.

The zeta potentials of MoS$_2$ particles of d(0.5) = 1.440 μm and d(0.5) = 5.156 μm in nickel plating solution including anionic surfactant sodiumlignosulfonate (SLS) were measured as -15.1 mV and -15.4 mV respectively. Previously, the zeta potential of MoS$_2$ particles of d(0.5) = 1.440 μm was measured -34.5 mV in water. Therefore, positively charged Ni ions in solution were adsorbed on negatively charged MoS$_2$ particles and the particles with adsorbed ions could move to cathode where Ni^{2+} ions were reduced to Ni atoms to form the deposit with captured particles. This result can be considered as a sign for collection of MoS$_2$ particles in Ni during electroplating, because the zeta potential values more negative than 35 mV can lead to decrease in particle concentration in the deposit. Because increase in zeta potential will increase the number of Ni ions surrounding particles and end up with heavy weight couples with low mobility [69].

The SEM images and EDX analysis spectrums of two different MoS$_2$ particles are given in Figure 4.3 and Figure 4.4 for d(0.5) = 1.440 μm and Figure 4.5 and Figure 4.6 for d(0.5) = 5.156 μm respectively. The particles exist in the form of aggregate with loose and fluffy surfaces (Figure 4.3 and Figure 4.5). Both microstructures have web-like morphology.
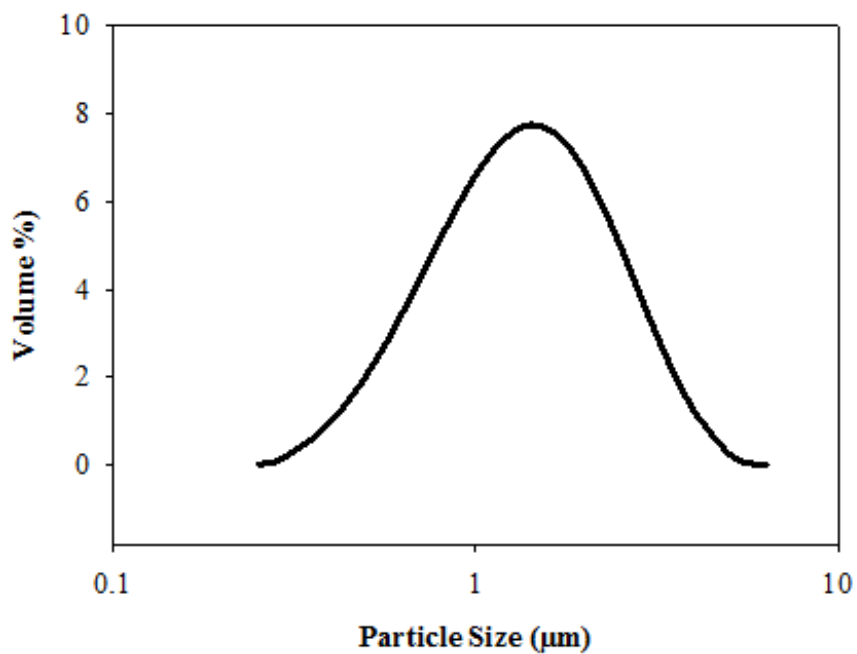
Figure 4.1 The distribution of MoS$_2$ particle size (d(0.5) = 1.440 μm)
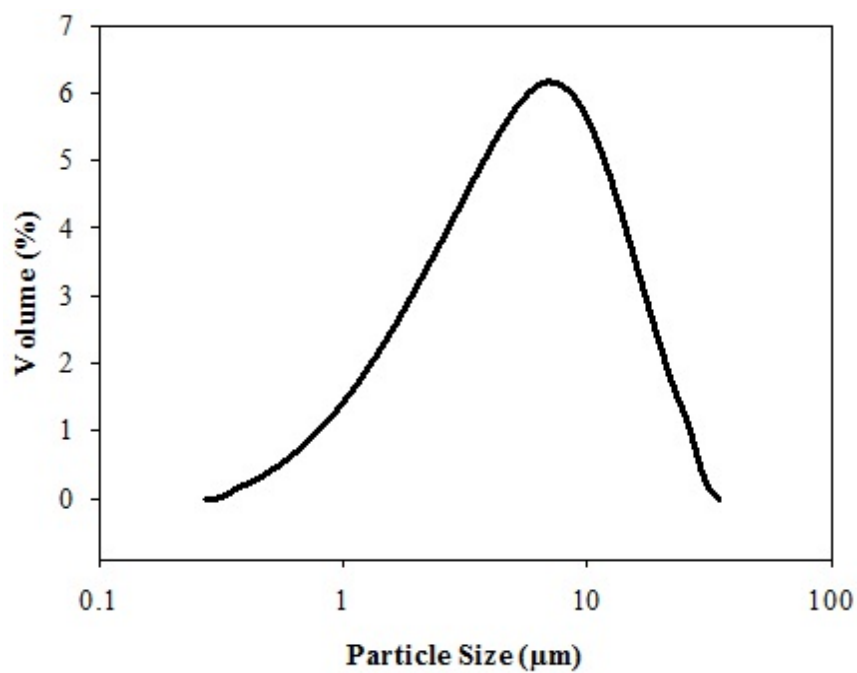
Figure 4.2 The distribution of MoS$_2$ particle size (d(0.5) = 5.156 μm)
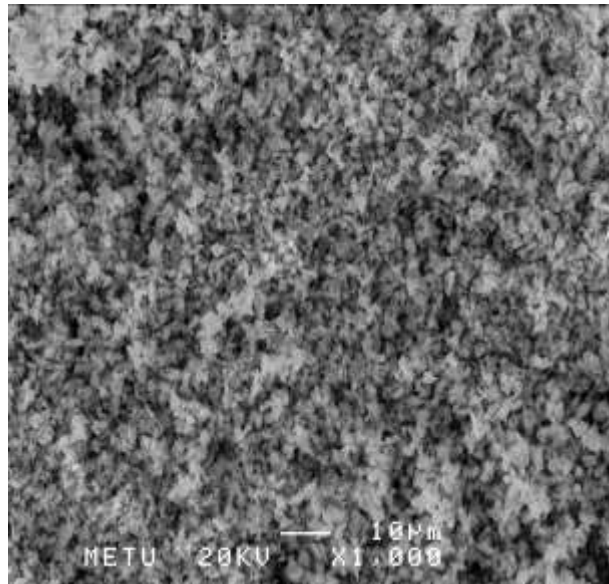
Figure 4.3 SEM image of MoS$_2$ particles (d (0.5) = 1.440 μm)
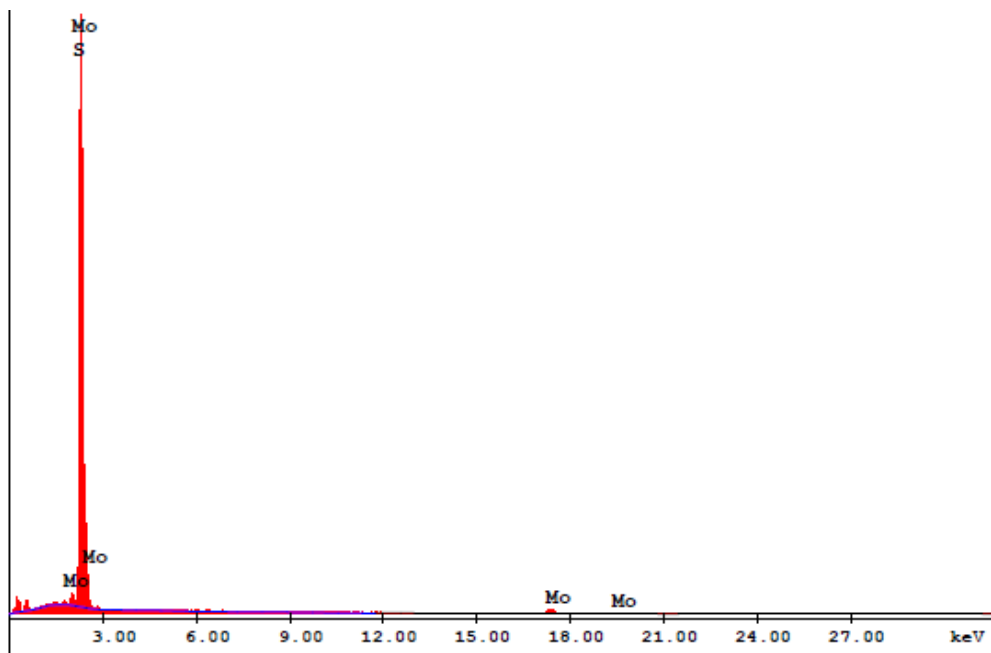
Figure 4.4 The EDX analysis of the MoS$_2$ particles (d(0.5) = 1.440 μm)
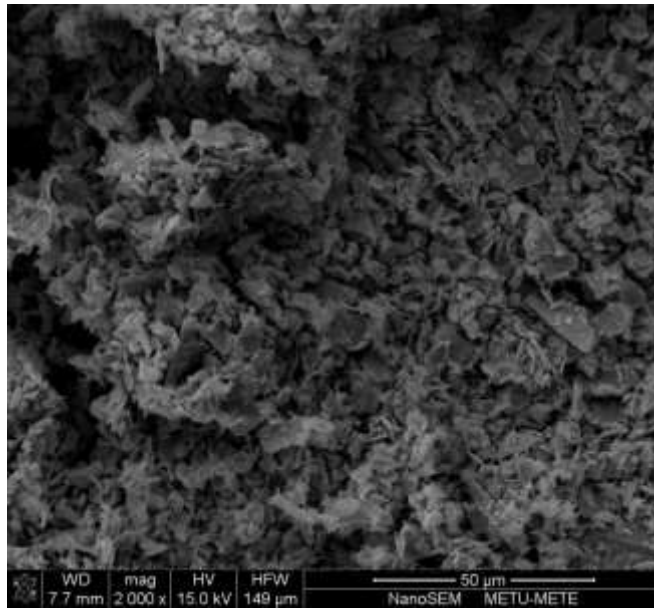
Figure 4.5 SEM image of MoS₂ particles (d (0.5) = 5.156 μm)
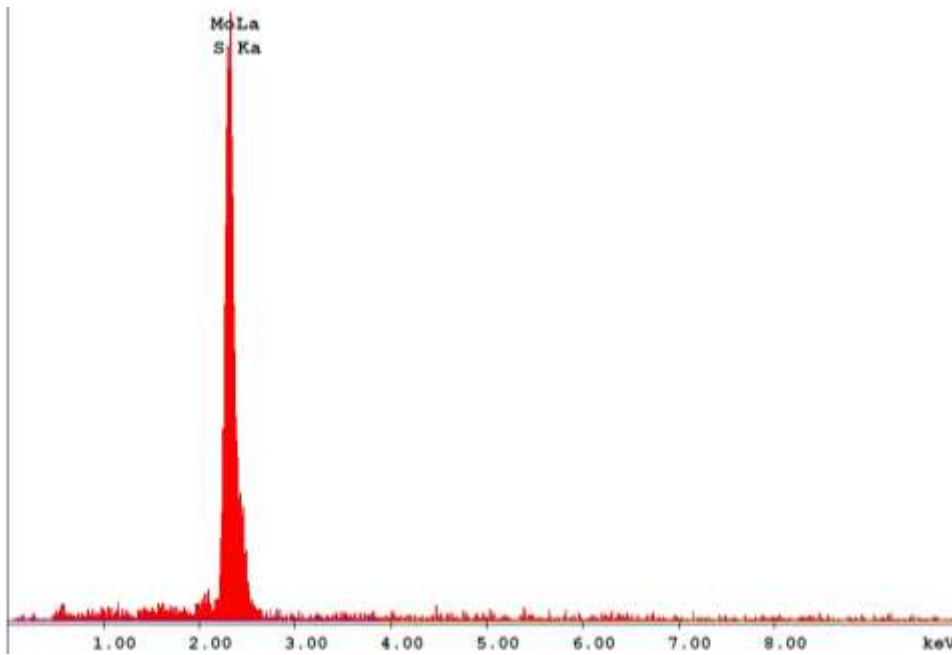
Figure 4.6 The EDX analysis of the MoS₂ particles (d(0.5) = 5.156 μm)

4.2 Voltammetric Response of HER

The effect of scan rate on the voltammogram is illustrated in Figure 4.7 for experiment 2 under conditions given in Table 3.2. It is apparent that total current density at extremum increases with increasing scan rate as expected [136, 137]. Therefore, 100 mV/s was chosen as the scan rate in the successive experiments since i_p's were well determined and predominant when potential scan rate increased. From Figure 4.7, it can be seen that the current density is almost zero until the onset of reduction of nickel and/or hydrogen ions at the cathode. Then, it continuously increases and reaches to a maximum. The irregularity of the voltammogram after the maximum indicates the decay of one of the primary electrode reactions.
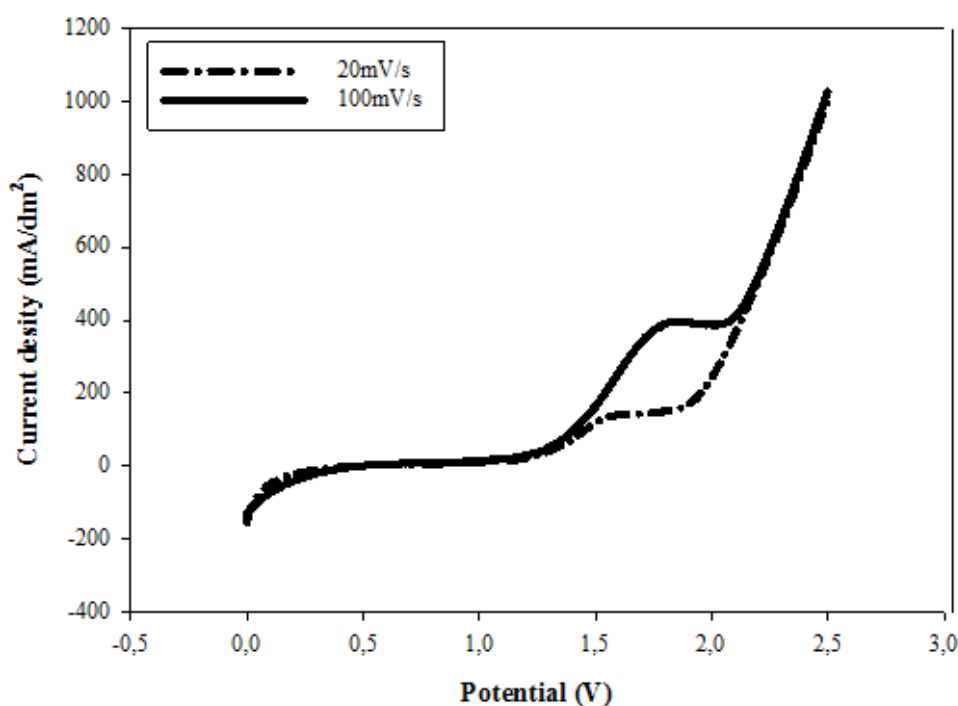
Figure 4.7 The effect of scan rate on the voltammogram for experiment 2 under conditions given in Table 3.3

To test the decay of HER, current efficiencies of nickel plating were determined at 3 different current densities selected from the voltammogram. One of the selected current density values was the peak value. The other two were the values before and after the peak value. Under the conditions of experiment 15, for 2 and 8 hours of depositions, the average current efficiency for nickel were determined as 90 %, nearly 100 % and 68 % for the current densities before, after and at the peak value, respectively. The decrease in the current efficiency at the peak position can be attributed to the HER [29] since cathodic current

efficiency of nickel deposition in Watts bath decreases due to the hydrogen evolution at a current density of about 0.65 A/dm^2. The typical volammograms and the positions of i_p values for the first four experiments are shown in Figure 4.8. All of the voltammograms for sixteen experiments (Table 3.2) are shown in Appendix A and the values of the peak current, I_p, the peak current density, i_p, and the peak voltage, V_p, determined from these figures are given in Table 4.1 for all experiments together with surfactant designations. Sodiumlignosulfoneate (SLS), ammoniumlignosulfonate (ALS) and depramin C (DC) were the three surfactants used in this study. The peak current densities obtained are comparable with the study of Ibrahim [138].
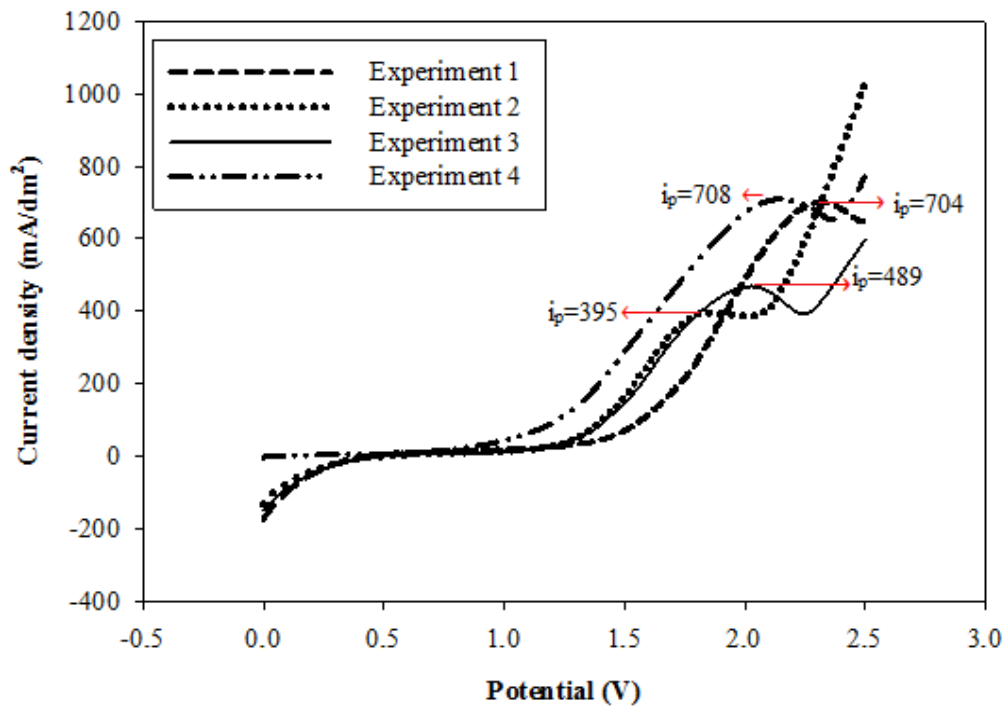
Figure 4.8 The typical voltammograms at 100 mV/s scan rate and the positions of ip values, in mA/dm^2, for the first four experiments

44

Table 4.1 I_p (cathode 10 cm^2), V_p and i_p values for experiments from 1 to 16

Experiment #	Surfactant	I_p (A)	V_p (V)	i_p (A/dm^2)
1	-	0.07040	2.323	0.704
2	-	0.03950	1.861	0.395
3	SLS	0.04686	2.027	
	DC	0.05772	1.926	0.577
	ALS	0.06210	2.059	0.621
4		0.07079	2.160	0.708
5	SLS	no peak	no peak	no peak
	DC	0.03944	1.879	0.394
	ALS	0.05628	1.728	0.563
6	SLS	0.02887	2.027	0.289
	DC	0.02672	1.865	0.267
	ALS	no peak	no peak	no peak
7	-	no peak	no peak	no peak
8	SLS	0.03541	2.027	0.354
	DC	0.01056	1.915	0.106
	ALS	0.01412	2.142	0.141
9	SLS	0.0196	1.572	0.196
	DC	0.05273	1.686	0.527
	ALS	0.04745	1.716	0.474
10	-	0.03090	1.609	0.309
11	-	0.07180	2.023	0.718
12	SLS	0.04009	1.866	0.401
	DC	0.02182	1.498	0.218
	ALS	0.02053	1.535	0.205
13	SLS	0.0334	1.629	0.334
	DC	0.04153	1.676	0.415
	ALS	0.04187	1.719	0.419
14	-	0.03243	1.649	0.324
15	-	0.01989	1.595	0.199
16	SLS	0.02032	1.860	0.203
	DC	0.02084	1.592	0.208
	ALS	0.03631	1.706	0.363

The parameters that have decreasing effect on the peak current density yielded negative coefficients in the regression analysis given in Equations 7, 9 and 11 and on the peak voltage given in Equations 8, 10 and 12 when DC, ALS and SLS were used as surfactant, respectively. The magnitudes of the coefficients indicate the weights of their effects. In addition, the results were subjected to factorial design analysis to obtain the interaction effects of surfactants on i_p and on V_p, illustrated in Figure 4.9 and Figure 4.10 respectively where i_p and V_p variations are indicated by the vertical axes as shown at right. The scale of the vertical axes is not given since it is different for three surfactants. The effects of parameters shown on horizontal axis on i_p and V_p values are for low (-1) and high (1) limits of the parameters shown on left according to codes given in the box at lower left.

$$i_p \ (mA/dm^2) = 557 - 48.6 \ A + 81.4 \ B - 204 \ C + 16.7 \ D \qquad \text{(DC)} \quad (7)$$
$$V_p \ (V) = 1.99 + 0.0035 \ A - 0.0407 \ B - 0.0865 \ C - 0.0983 \ D \qquad \text{(DC)} \quad (8)$$

$$i_p \ (mA/dm^2) = 675 - 113 \ A + 95 \ B - 186 \ C + 135 \ D \qquad \text{(ALS)} \quad (9)$$
$$V_p \ (V) = 2.02 - 0.0298 \ A - 0.0506 \ B - 0.148 \ C - 0.0694 \ D \qquad \text{(ALS)} \ (10)$$

$$i_p \ (mA/dm^2) = 465 - 25.9A + 11.2 \ B - 149 \ C - 75.2 \ D \qquad \text{(SLS)} \ (11)$$
$$V_p \ (V) = 2.02 - 0.0366 \ A - 0.0822 \ B - 0.111 \ C - 0.0740 \ D \qquad \text{(SLS)} \ (12)$$

where A: MoS_2 concentration, B: temperature, C: pH, D: surfactant changing between -1 and 1 corresponding to limit values given in Table 3.1.

It can be concluded that parameters A (MoS_2) and C (pH) have decreasing while the parameter B (temperature) has increasing effect on the peak current density regardless of the surfactant type used [139]. Among surfactants, decreasing effect on the peak current density was observed only in the case of SLS addition to the bath. The decrease in i_p with MoS_2 particles (A) that is also observed in Figure 4.9a at low temperature, may be explained by the adsorption of positively charged hydrogen ions in solution on negatively charged MoS_2 particles [9, 140]. Particles with adsorbed ions move to cathode where H^+ ions are reduced to hydrogen gas. This adsorption will end up with heavy weight couples which lead to decrease in mobility and thus increase in polarization. On the other hand, the adverse effect of MoS_2 was seen in Figure 4.9a at low temperature. The increase in pH, in other words; the decrease in the concentration of hydrogen ions will decrease the rate of the hydrogen gas evolution reaction that will lead to diminishing effect on i_p. The same result was seen in Figure 4.9b for both high and low levels of temperature and MoS_2 content. Since the temperature improves ion diffusion rate, i_p was increased due to retardation in polarization. Using ALS and DC increased the peak current density. However, the weight of surfactant effect in ALS is more significant compared to DC. Voltammetric response was apparently improved with decreasing the overpotential in the presence of anionic surfactants [141, 142] and the peak current density values for H^+ reduction were increased. This is in accord with the expectations that anionic surfactants can promote both oxidation and reduction processes [143]. On the other hand, SLS decreased the peak current density. This result supported by

46

Popov et. al. who claimed that saccharin which is an anionic surfactant was effective in suppressing the hydrogen evolution reaction [144]. In addition, the hydrogen evolution peak decreased with increasing the saccharin concentration [144]. According to Equations 8, 10 and 12, adding MoS_2 (parameter A) decreased peak voltage. Moreover, increasing temperature (parameter B) decreased peak voltage (V_p) since hydrogen overvoltage decreased with increasing temperature [73] but this result was observed when there was no MoS_2 in the solution (Figure 4.10a). The parameters C (pH) and D (all surfactants) had decreasing effects on the peak voltage (V_p) independent of the surfactant type, as can be seen in Figure 4.10b, Figure 4.10c, Figure 4.10d and Figure 4.10e with slight deviations. The addition of MoS_2 increased V_p when DC is added to the solution whereas decreased V_p in case of SLS and ALS addition.
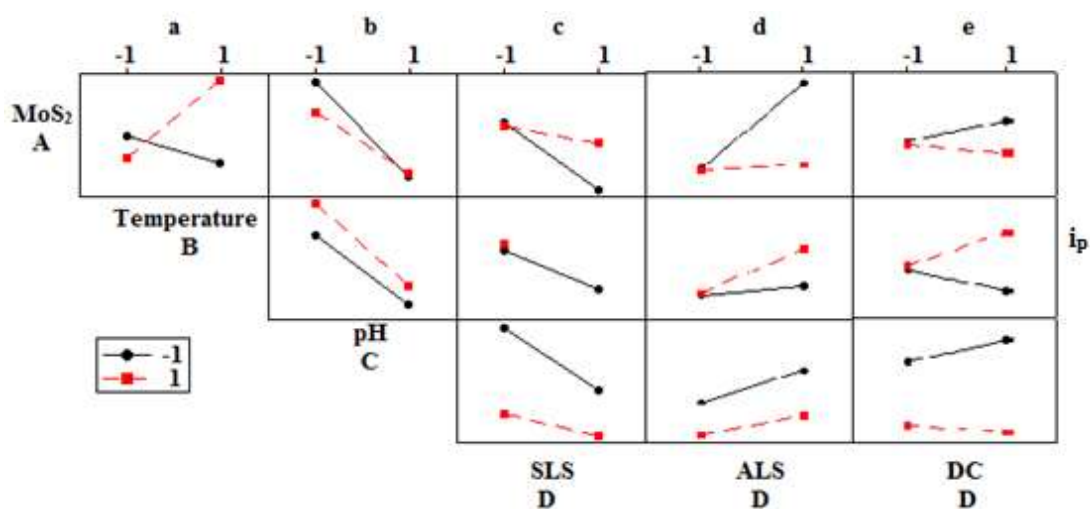
Figure 4.9 Interaction plot for peak current densities; the columns are showing; (a) A-B (b) A-C and B-C (c) A-D, B-D and C-D interactions for Surfactant SLS, (d) for Surfactant ALS, (d) for Surfactant DC
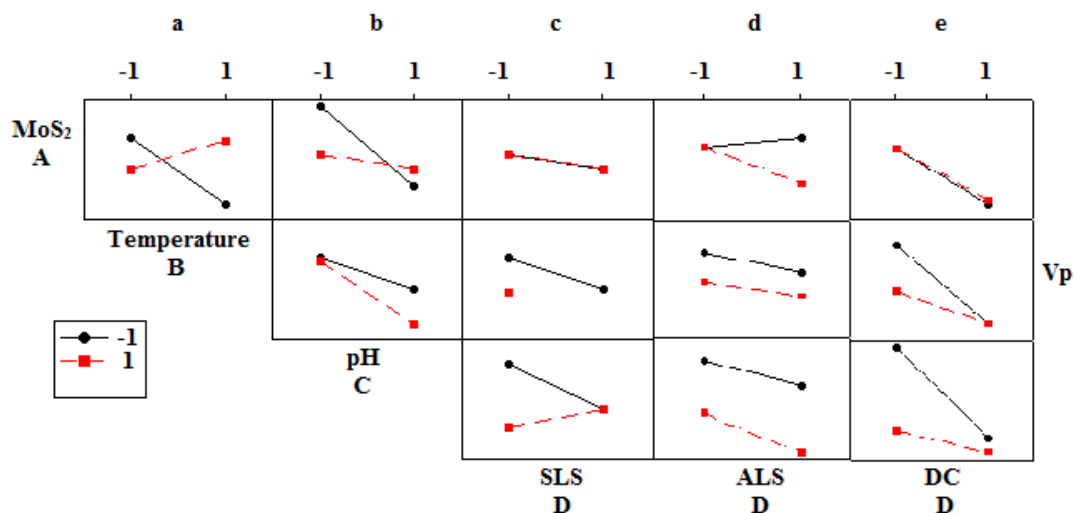
Figure 4.10 Interaction plot for peak voltages; the columns are showing; (a) A-B (b) A-C and B-C (c) A-D, B-D and C-D interactions for Surfactant SLS, (d) for Surfactant ALS, (d) for Surfactant DC

The contour plots in mixture design analysis given in Figure 4.11, Figure 4.12 and Figure 4.13 show the bands of current densities for the surfactants DC, ALS and SLS respectively. The hold value, taken as 0.5, means that the middle value of the fourth parameter was used in each plot. For instance; in ABC plot; surfactant (parameter D) was taken as 0.5 g/L which is the mean value of low, 0 and high, 1 g/L levels and for ABD plot, pH (parameter C) taken as 3 was the average of low, 2 and high, 4 values of pH. The peak current densities were higher than 650, 700 and 650 mA/dm^2 when there was no MoS$_2$, at pH 2 and temperature 50°C with surfactant 0.5 g/L, as seen in Figure 4.11, Figure 4.12 and Figure 4.13 respectively (corner B of ABC plots). Whereas according to ACD plot of Figure 4.11; when pH was 2, the peak current density was higher than 650 mA/dm^2 independent of MoS$_2$ and surfactant concentration. On the other hand, peak current densities were lower than 400 mA/dm^2, when pH was 3 at 30°C in the presence of MoS$_2$ without surfactant (see corner A of ABD plots of Figure 4.11 and Figure 4.12).
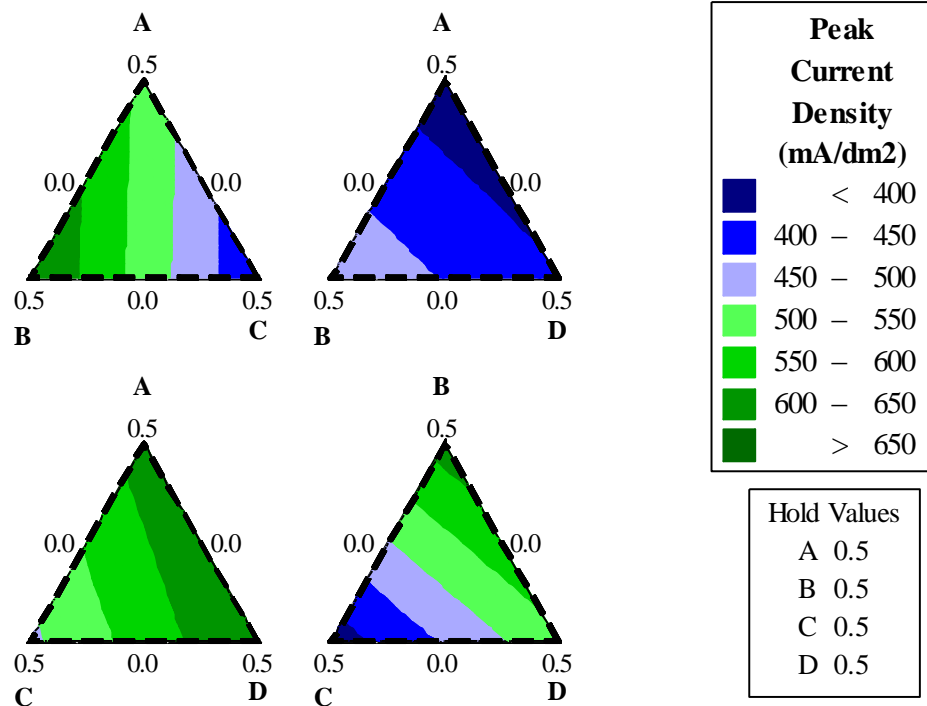
Figure 4.11 Matrix of mixture contour plots for the peak current densities (mA/dm^2) A: MoS$_2$, B: Temperature, C: pH, D:Surfactant-DC
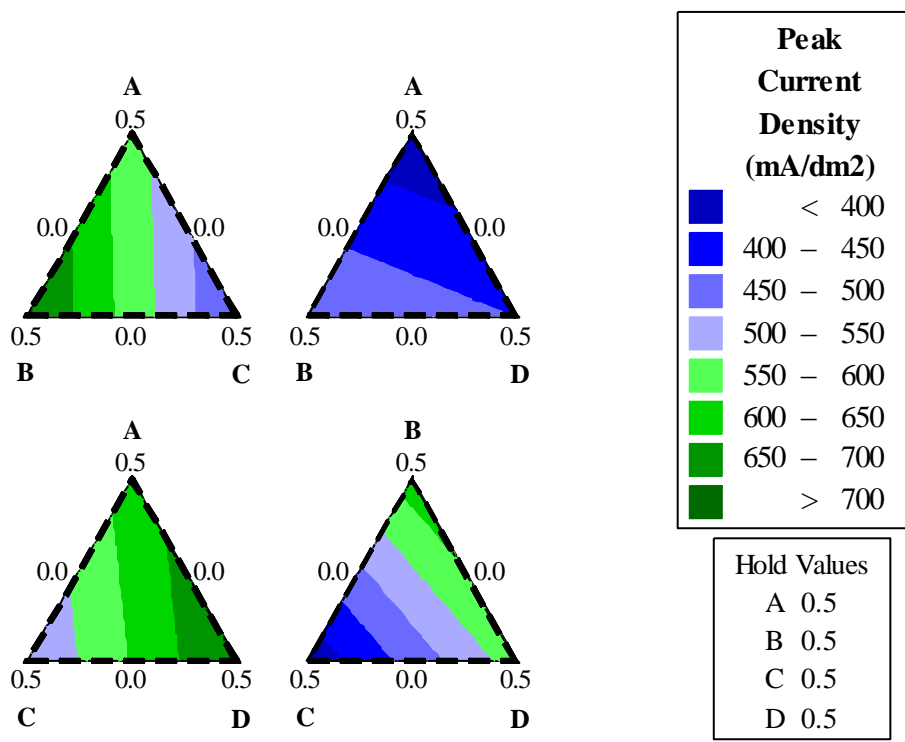
Figure 4.12 Matrix of mixture contour plots for the peak current densities (mA/dm^2) A: MoS$_2$, B: Temperature, C: pH, D:Surfactant-ALS
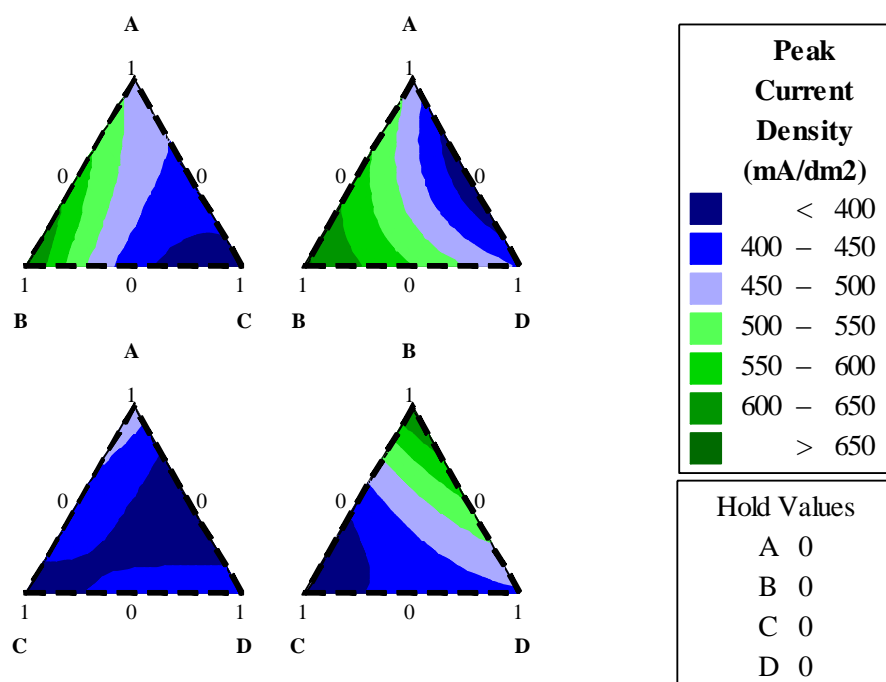
Figure 4.13 Matrix of mixture contour plots for the peak current densities (mA/dm^2) A: MoS$_2$, B: Temperature, C: pH, D:Surfactant-SLS

4.3 Internal Stress

The internal stresses developed during nickel or Ni-MoS$_2$ composite coatings were determined for 16 experimental routes given in Table 1. The current density (CD) and temperature (T) together with observed weight gain during deposition (Δm), calculated thickness of the deposit (t), number of increments (U) and calculated internal stress (S) for each run are given in Table 4.2. The stress values were calculated from equation 5 by using the mass of the deposit (Δm) determined by weighing the substrates prior to and following deposition and the number of increments observed in the analyzer. For instance, the number of increments (U) in run 11 was 7.5 as it can be read from Figure 4.14. The stress values were small in accordance with expectations, because the bath additions recommended by the supplier of plating chemicals were followed to produce deposits with low stress [46]. Thus small effects of plating parameters on internal stress in coatings could be determined with high precision. The reproducibility of stress values tested for some of the runs yielded consistent directions and ±1.2 MPa deviations at most.

Figure 4.14 Deposit stress analyzer showing number of increments, U, in run 11.

Table 4.2 The current density (CD), temperature (T), weight of deposit (Δm), calculated thickness (t), number of increments (U) and internal stress (S) for each run

Run	CD (A/dm^2)	T (ºC)	Δm (g)	t (μm)	U: number of increments	S:stress (psi)	S:stress (MPa)
1	4.8	30	0.835	37	6	-479.1	-3.3
2	4.8	50	0.8498	23	7	-896.0	-6.2
3	1.2	30	0.8468	41	3.5	-246.5	-1.7
4	4.8	30	0.1556	23	17	-2156,3	-14.9
5	4.8	30	0.1492	22	35	4630.0	31.9
6	4.8	50	0.8621	46	7	-442.3	-3.0
7	1.2	30	0.1515	22	39	5080.8	35.0
8	1.2	50	0.2772	41	32	2278.4	15.7
9	4.8	50	0.2942	44	16.5	-1106.9	-7.6
10	4.8	30	0.846	33	2	178.0	1.2
11	1.2	50	0.1467	22	7.5	1009.0	7.0
12	1.2	50	0.8472	21	7	-957.5	-6.6
13	1.2	30	0.2802	45	2	-129.8	-0.9
14	4.8	50	0.0833	12	30	7108.1	49.0
15	1.2	50	0.8479	32	9	-812.2	-5.6
16	1.2	30	0.8419	23	1.5	-189.6	-1.3

The application of regression analysis to above stress data yielded;

$$S \ (MPa) = 5.54 - 8.86 \ A - 0.21 \ B + 9.64 \ C + 0.34 \ D - 2.36 \ E \qquad (13)$$

where A: MoS_2 concentration, B: temperature, C: pH, D: current density and E: coating thickness changing between -1 and 1 corresponding to limit values given in Table 4.2. According to the equation 13 and Figure 4.15, addition of MoS_2 particles decreased internal stress with a factor of -8.86 [135]. This result supports the observations of Garcia et. al. [145], Chou et. al. [146] and Wielage et. al. [120] who reported decreasing effects of different particles on internal stress of composite nickel coatings. The incorporation of SiC particles (Ø 0.3-5 μm) also decreased the internal stress of the deposit in the Ni [145] and Ni-P alloy matrix [146]. TiO_2 (Ø 5-10 μm) [120] and TiC particle (Ø 50-200 nm) additions [26] in the amounts of 20 g/L and 6g/L, respectively in Ni matrix [120] also decreased internal stresses. The dispersed particles generally have a reasonably homogeneous stress field and certainly average out if they do not have a preferred orientation [145]. In this study, it was concluded that the compressive stress effect overwhelms due to the addition of MoS_2 particles. The lattice parameters of Ni, Cu and MoS_2 are 3.517, 3.608 and 3.148 A° respectively [21, 147]. Since the lattice parameter of Ni is smaller than that of Cu, Ni deposit will normally exert a compressive stress on the Cu lattice and it will be under tension if there were not any other internal stress [21, 28]. In accord with the expectations due to Watts solution additives, small stresses were measured for all cases of coatings in this study. The addition of MoS_2 therefore caused compression of the nickel coatings and decreased stress levels. In addition, the codeposition of particles may reduce stress levels by interrupting the nickel grain growth [145] which causes tensile stress.

The second output of the equation was the decrease in internal stress with increase in temperature; which agrees with Dini [25, 30]. Moreover, small decrease in internal stress in the presence of MoS_2 (see Figure 4.15a), complements the observations of Wang [9] who showed slight increase in MoS_2 content of the deposit with increasing temperature. However; in one of the studies [40], it was claimed that temperature of the Watts bath did not have a significant effect on the internal stress. Accordingly, very small temperature dependency of internal stress can be seen in Figure 4.15e and Figure 4.15h upon changing the current density and the coating thickness. Figure 4.15h shows that increase in temperature has a small increasing effect on stress when the coating thickness is low (25 μm) and decreasing effect when the thickness is high (50 μm).

The third output of the equation was; increasing pH has an ascending effect on the stress with a factor of 9.64 (see Figure 4.15f and Figure 4.15i). It is asserted that increasing pH has slight effect on internal stress below pH 5 but increases significantly above 5 [36, 40, 73]. Effect of pH seems to be insignificant within the range studied here when MoS_2 was present in the deposit but increasing pH increases the internal stress of the nickel coating (see Figure 4.15b). It was also stated that MoS_2 content of the deposit is constant between the pH values of 2 and 4 [10] that is compatible with this result because it is known that there is a relation

between MoS_2 content of the deposit and internal stress. Hydrogen permeation in nickel was related to electroplating parameters [139]. Especially, pH determined the adsorption of hydrogen [148] so increase in internal stress at high pH may be attributed to the change in growth direction of nickel cathode from (100) to (211) [149] with decrease in hydrogen discharge [78].

It can also be deduced from the equation that, internal stress was almost constant with an increase in current density (Figure 4.15d). It was also stated that the current density has no effect on the MoS_2 content of the deposit [10] that is compatible with this result due to the information of the relationship between MoS_2 content of the deposit and internal stress. On the other hand, slight decrease in the internal stress was observed upon increasing the current density at low temperature (Figure 4.15e) and low pH (Figure 4.15f). Nickel growth is inhibited by adsorbed hydrogen at low current densities and low pH, while the (100) texture at high current densities is the result of uninhibited growth [77]. The observations showed that (100) textured Ni deposits exhibit the lowest internal stress that may be explained by the less adsorption of hydrogen [150]. Internal stress increased with current density at high pH (Figure 4.15f), because growth direction different from (100) takes place [149].

Finally the inverse relationship between internal stress and coating thickness can be seen in above regression equation. This result agrees with the argument that stress decreases with increasing coating thickness [30, 73, 151, 152] and Figure 4.15g, Figure 4.15h, Figure 4.15i and Figure 4.15j illustrates above mentioned behavior. Because, stress induced by larger Cu lattice in nickel coating is distributed to a larger cross-sectional area with increasing thickness. In addition; the factor, -2.36 given in the regression equation, indicating the mild effect of plating thickness is in accord with Czerwinski's observations [153] that the decrease in the stress was drastic up to 20 μm but smaller up to 50 μm thickness.

The combinations of parameters that give low internal stress (temperature: 50ºC, pH: 2, current density: 4.8 A/dm^2, thickness: 50 μm) were used to produce samples for microstructural examination and tribological investigation. When the regression equation was considered; the most effective parameters were the presence of MoS_2, pH and coating thickness with factors -8.86, +9.64 and -2.63 respectively. Therefore, 10 g/L MoS_2, pH = 2 and 50 μm thickness were chosen. Furthermore, with reference to the interaction plots, high temperature and high current density were selected. The reason for selecting high temperature can be seen in Figure 4.15c and Figure 4.15h, because internal stress was not influenced by temperature at low pH and it decreases with increasing temperature when plating thickness was high. Finally, current density was selected as 4.8 A/dm^2, because internal stress decreased with increasing current density when pH was low (Figure 4.15f). The samples for micrographic examinations were prepared by using above plating parameters. Three surfactants; sodiumlignosulfonate, ammoniumlignosulfonate and Depramin C were added to Watts bath to examine their effects on the internal stress and distribution of MoS_2 particles. No significant effects of surfactants on internal stress were

observed and measured stresses of Ni-MoS$_2$ composite coatings were compressive and they were around 3 MPa.
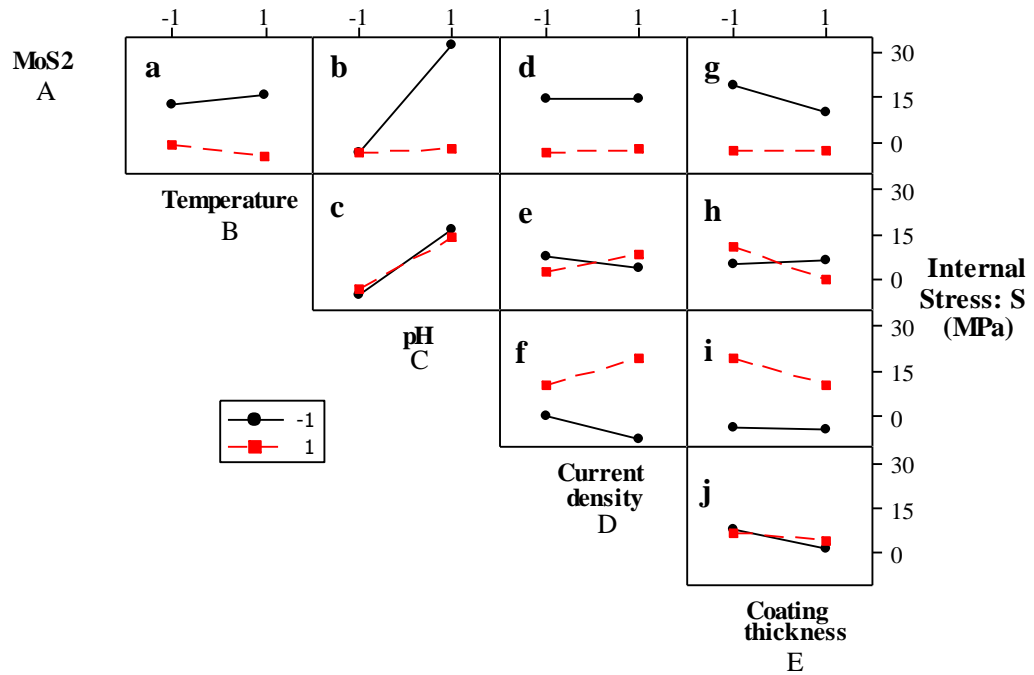
Figure 4.15 Plot of the interaction effects of the electroplating parameters. The measured internal stress values (MPa) are shown on vertical axes at right. The effects of parameters shown on horizontal axis on internal stress are for low (-1) and high (1) limits of the parameters shown on left according to codes given in the box at lower left

4.3.1 Guglielmi Model of Codeposition

Guglielmi found a relationship for the ratio of volume percentages of particles in the deposit (α) and in the bath (C) as given in equation 14.

$$\frac{C}{\alpha} = \frac{M \times i_0}{n \times F \times d \times V_0} \exp((A-B)\eta)\left(\frac{1}{k} + C\right) \tag{14}$$

where

α: volume % of particles in the deposit

η: overpotential of the electrode reaction (V)

A: constant in Tafel equation for metal deposition (V^{-1})

B: constant in Tafel equation for particle deposition (V^{-1})

C: volume % of particles in suspension in the bath

d: density of the electrodeposited metal (g/dm^3)

F: Faraday's constant = 96485 C/mol
i_0: exchange current density (A/dm^2)
k: coefficient of adsorption (vol.%$^{-1}$)
M: molecular weight of the electrodeposited metal (g/mol)
z: valence of the electrodeposited metal
V_0: constant for particle deposition (dm/s)

According to this codeposition model, C/α versus C graphs can be plotted at different current densities. The relationship of C/α (y) and C (x) can be fitted as a straight line (y = a x + b) based on equation 14, the point where C/α (y) is zero represents the value of -1/k (-b/a) that makes it possible to obtain the adsorption coefficient value (k) [15, 83]. The amount of interaction between particles and cathode mainly determines the adsorption coefficient [83]. The ratio C/α according to the MoS$_2$ concentration in the bath is given in Figure 4.16 for 4.8 A/dm^2. The linear equation is y = 1.1073x + 0.7847. Figure 4.17 shows C/α versus volume percent of particles in suspension in the bath for 1.2 A/dm^2 current density. The linear equation is y=1.1342x+0.5703. The average k value obtained from these figures is 1.7. 'k' values higher than 1 indicates that the adsorption rate of particles is faster than desorption rate [83].

The slope (tan φ) of the line is given by:

$$\tan\varphi = \frac{M \times i_0}{n \times F \times d \times V_0} \exp(A-B)\eta \tag{15}$$

An approximation of the current density i = i_0 exp(Aη) can be made since the assumption of the particles is incorporated at the cathode by electrochemical discharge of the adsorbed cations is agreed. The ratio B/A can be calculated using the following substitution [15].

$$i_0 \times \exp\big((A-B)\eta\big) = i_0 \times \exp\big((1-\frac{B}{A}) \times A \times \eta\big) = i_0^{(\frac{B}{A})} \times i^{(1-\frac{B}{A})} \tag{16}$$

Substituting equation 16 into 15 and taking the logarithm gives the relationship between slope tan φ and the current density i as:

$$\log\tan\varphi = \log\frac{M \times i_0^{(\frac{B}{A})}}{n \times F \times d \times V_0} + (1-\frac{B}{A})\log i \tag{17}$$
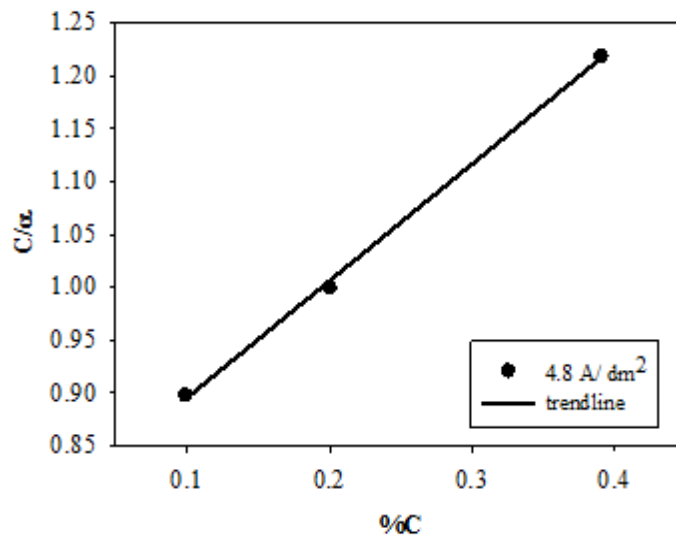
Figure 4.16 The C/α ratio according to the MoS$_2$ concentration in the bath at 4.8 A/dm^2 current density
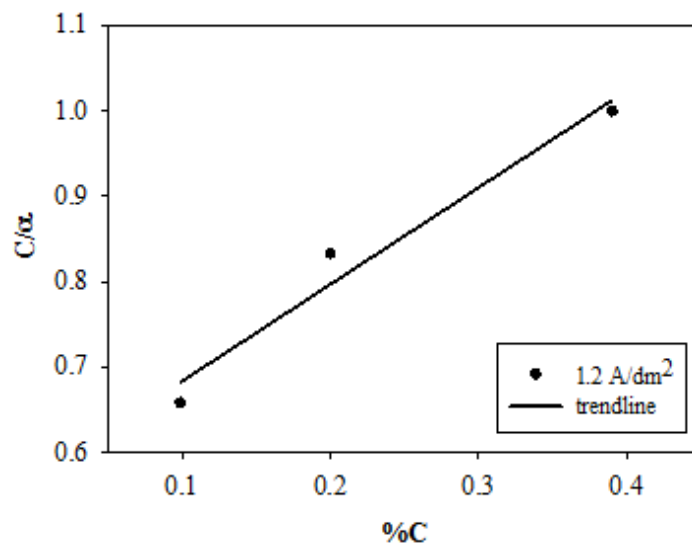

Figure 4.17 The C/α ratio according to the MoS$_2$ concentration in the bath at 1.2 A/dm^2 current density

The slope of the y = -0.0075x + 1.1432 linear equation drawn in Figure 4.18 is -0.0075. This yields B/A value as 1.0075.
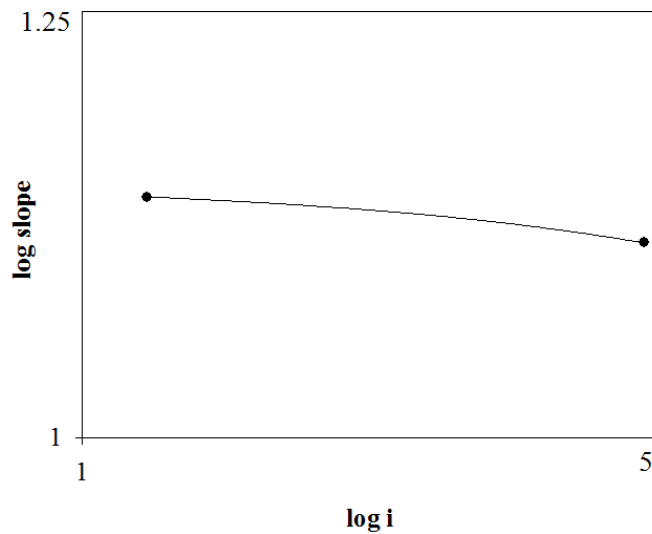
Figure 4.18 Logarithmic graph of the slope (tan φ) versus current density

The parameters A and B are related to metal deposition and particle deposition respectively. B being higher than A represents that the increase in current density increases the particle content in the deposit [63, 83]. B being lower than A indicates that Ni cations adsorbed on the particles are reduced more slowly than the solvated Ni cations that resulted in decrease in volume percent of particles in the deposit when the current density increases [15, 63]. In the present system, B/A is 1.0075 that is B is slightly higher than A meaning that as the current density increases there will be a slight increase in the MoS_2 content of the deposit which is compatible with the regression analysis given in equation 13 where current density has an effecting factor of 0.34 on the internal stress. This is because, the internal stress decreased by an increase in the MoS_2 content of the deposit. It was also stated that the Guglielmi model is valid for the codeposition of MoS_2 and nickel from Watts bath at current densities of 1 to 6 A/dm^2 [10].

4.4 X-ray Diffraction Measurements

X-ray diffraction patterns of nickel and nickel-MoS_2 composite coating on AISI 304 stainless steel substrates are given in Figure 4.19 and Figure 4.20. The coatings were obtained by using Watts solution containing 1g/L SLS and 10g/L MoS_2. It can be seen from these figures that both nickel and MoS_2-nickel coatings have Fe peak together with Ni and MoS_2 peaks. It was believed that Fe diffractions were probably coming from the substrate. According to the quantitative analysis performed by Rigaku software by excluding Fe, there were ~100 % nickel in nickel deposit and 92.9 % nickel and 7.1 % MoS_2 in MoS_2-nickel composite coating.
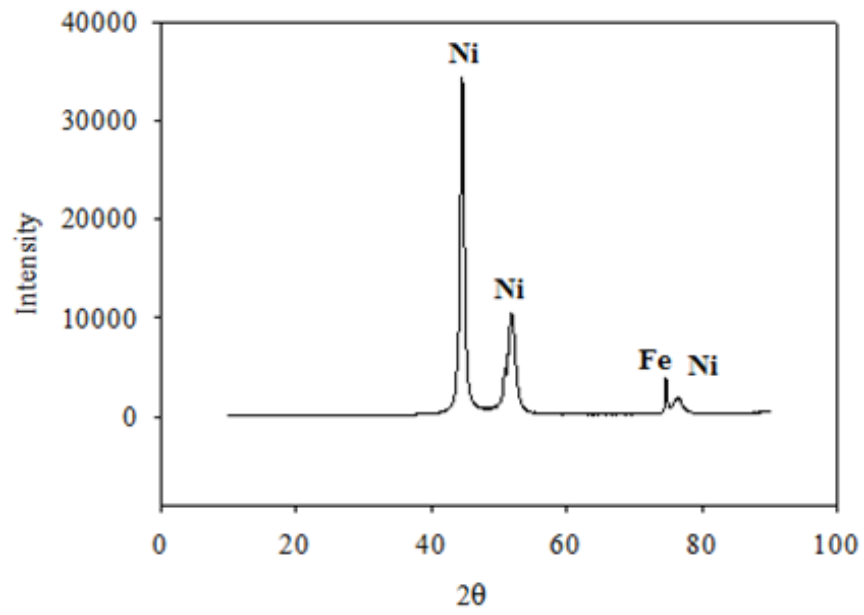
Figure 4.19 X-ray diffraction pattern of the Ni coating on AISI 304 stainless steel substrate
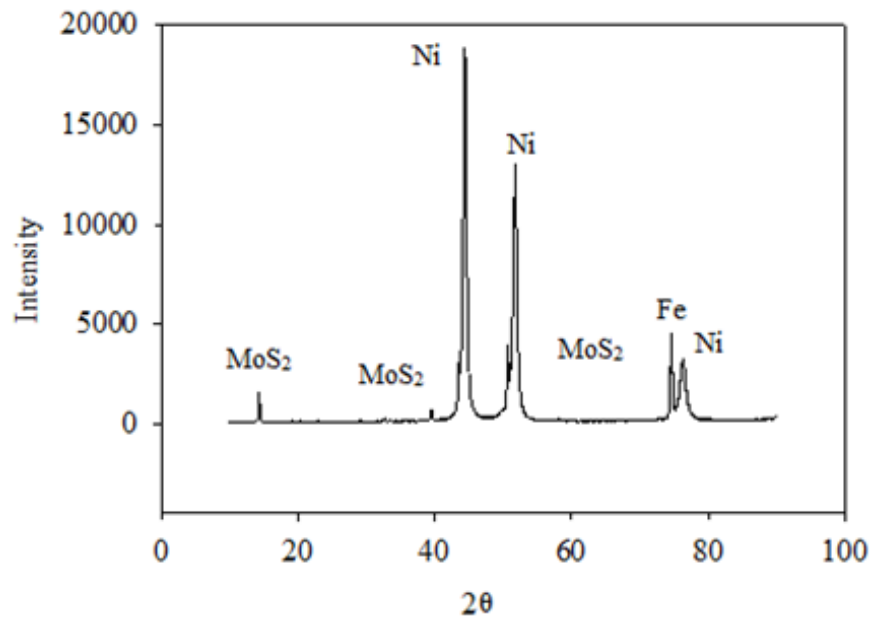

Figure 4.20 X-ray diffraction pattern of the Ni-MoS$_2$ composite coating on AISI 304 stainless steel substrate

4.5 Microstructural Examination

Among the three surfactants; sodiumlignosulfonate, ammoniumlignosulfonate and Depramin C used to prepare samples for micrographic examinations, it was observed that homogenous particle distribution and high particle concentrations were observed when SLS was added to Watts bath. A typical top view of the Ni-MoS$_2$ composite coating on AISI 304 stainless steel substrate is shown in Figure 4.21. It was produced from a Watts solution containing 1 g/L SLS and 10 g/L MoS$_2$. The cross-sectional optical microscope and SEM images of the Ni-MoS$_2$ deposit are given in Figure 4.22 and Figure 4.23. EDX analysis spectrum of the coating is shown in Figure 4.24 and percentages are given in Table 4.3. From the table it can be seen that summation of Mo and S concentrations yields 7.18 % MoS$_2$ by weight in the coating. This result is similar to approximately 9 % by volume MoS$_2$ particles determined from selected area of Figure 4.23. In addition the weight percent of MoS$_2$ was 6.3 according to XRD result that corresponds to 10 % by volume. The MoS$_2$ content in the deposit increased when 30 g/L MoS$_2$ was added to the bath (see Figure 4.25 as compared to the composite coating formed by using 10 g/L MoS$_2$ in the bath. EDX analysis of the Ni-MoS$_2$ composite deposited from 30 g/L MoS$_2$ in the bath is shown in Figure 4.26 and the percentages are given in Table 4.4. The summation of Mo and S concentrations yields 14.3 % MoS$_2$ by weight in the coating.
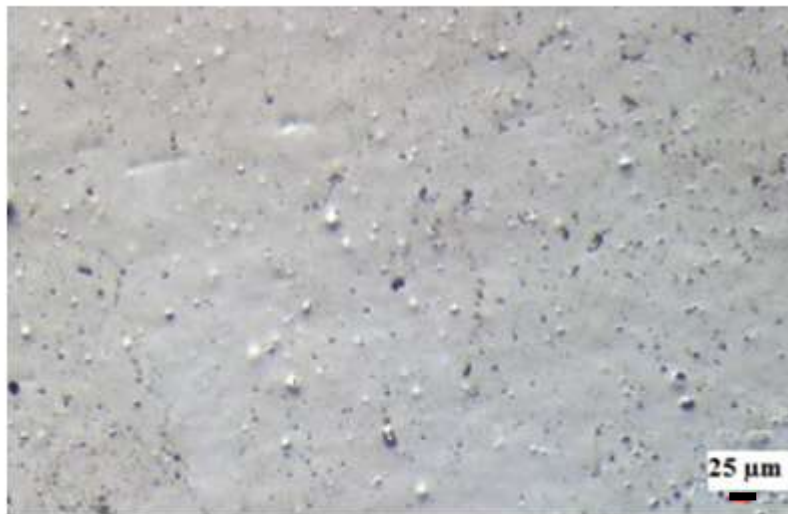
Figure 4.21 Top view of the Ni-MoS$_2$ composite coating on AISI 304 stainless steel substrate
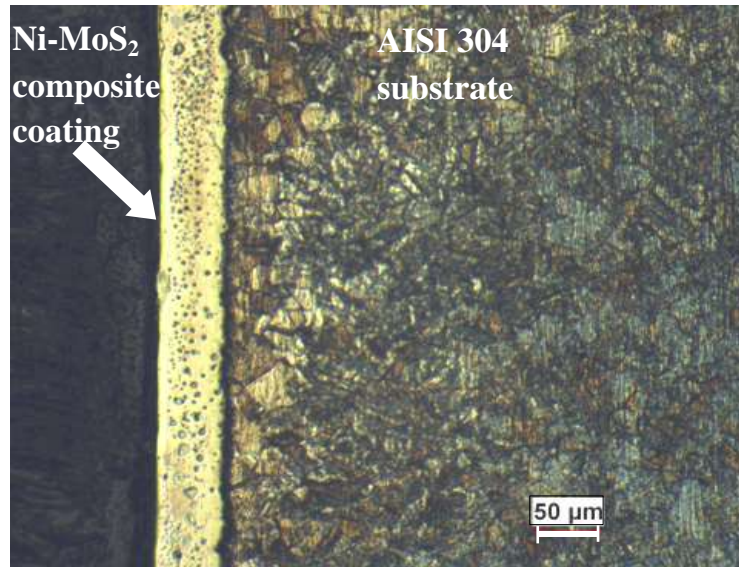
Figure 4.22 Cross-sectional optical microscope image of the Ni-MoS₂ composite coating on AISI 304 stainless steel substrate

Figure 4.23 Cross-sectional SEM image of the Ni-MoS₂ composite coating on AISI 304 stainless steel substrate

Figure 4.24 The EDX analysis of the Ni-MoS$_2$ composite coating formed by using 10g/MoS$_2$ and 1g/L SLS

Table 4.3 Weight and atomic percentages of elements in the Ni-MoS$_2$ deposit based on the EDX analysis given in Figure 4.24

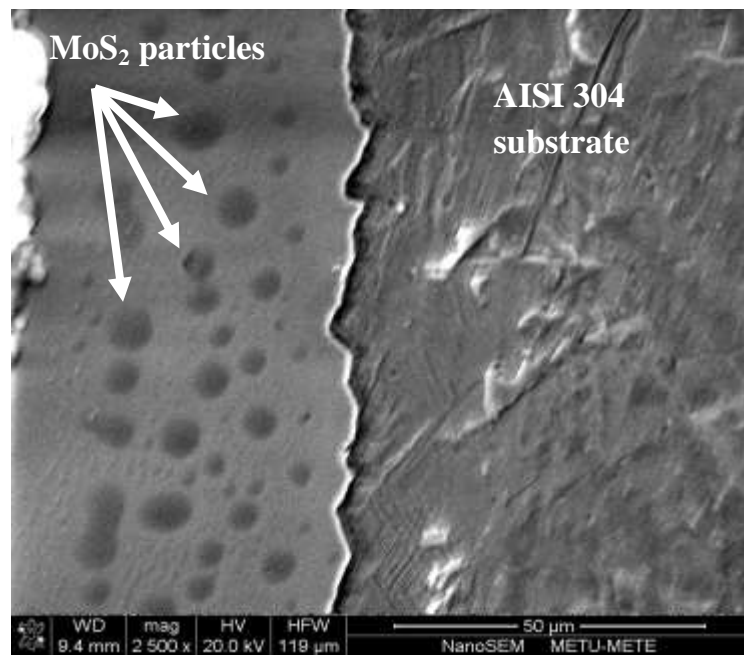| Element	wt.%	at.%
Mo	5.66	3.50
S	1.52	2.80
Ni	92.82	93.70
Total	100.00	100.00

Figure 4.25 Cross-sectional SEM image of the Ni-MoS₂ composite coating on AISI 304 stainless steel substrate from 1g/L SLS and 30g/L MoS₂ containing electrolyte
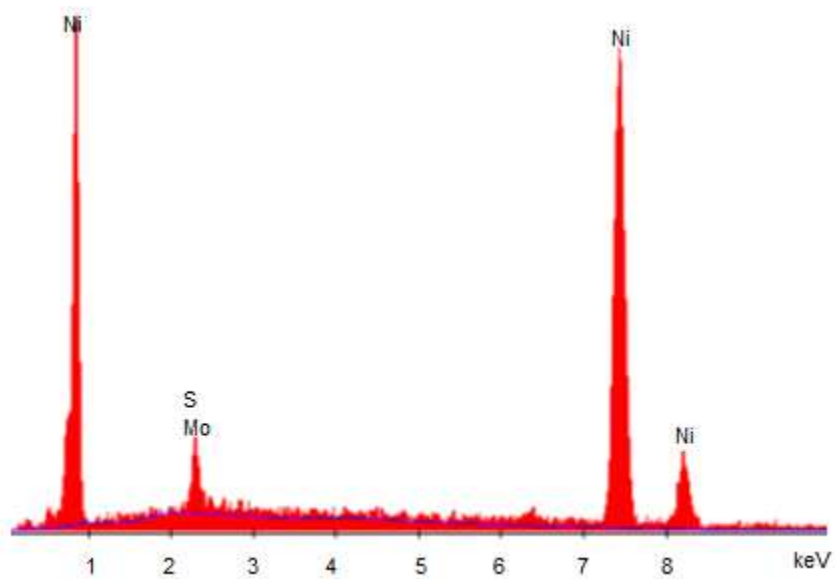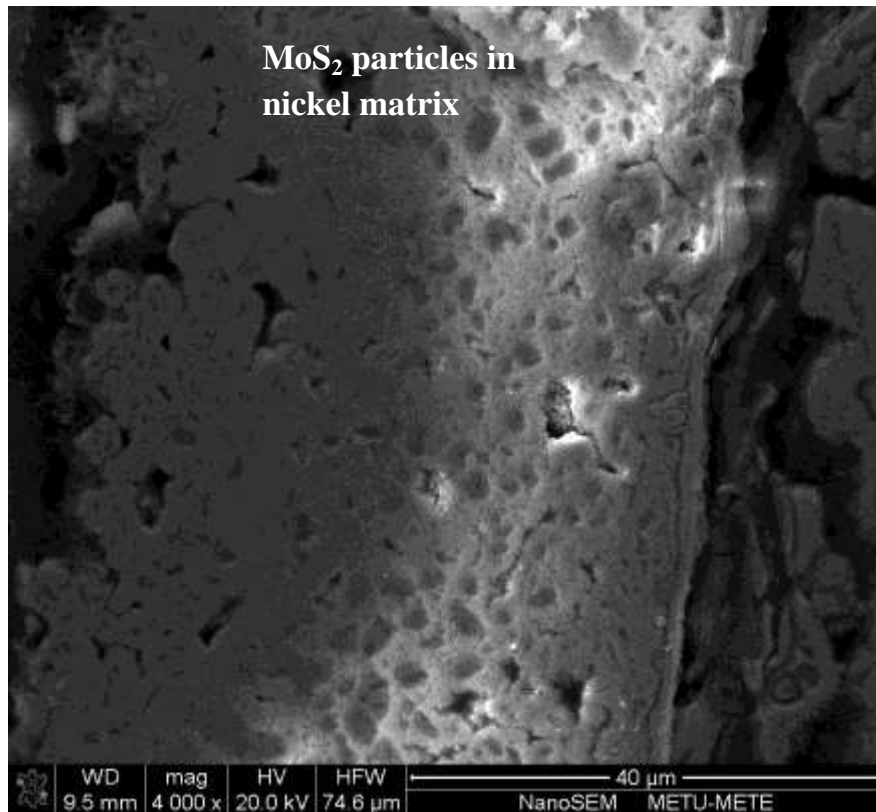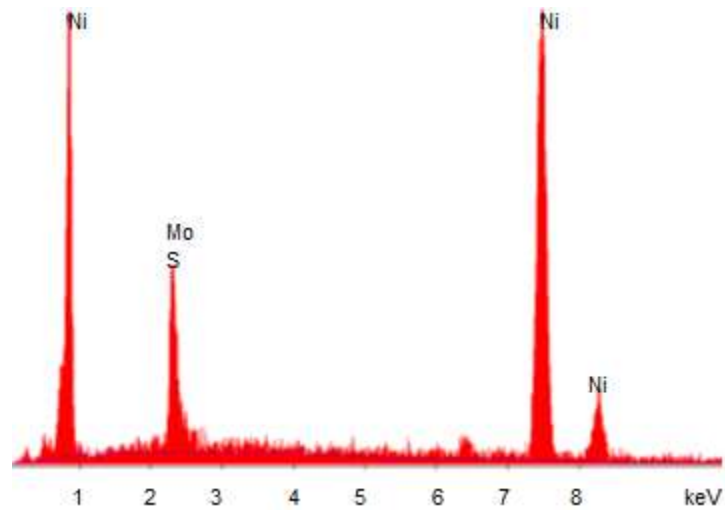

Figure 4.26 The EDX analysis of the Ni-MoS₂ composite coating formed by using 30g/MoS₂ and 1g/L SLS

Table 4.4 Weight and atomic percentages of elements in the Ni-MoS2 deposit based on the EDX analysis in Figure 4.26

Element	wt.%	at.%
Mo	10.59	6.51
S	3.69	7.40
Ni	85.72	86.09
Total	100.00	100.00

4.6 Tribological Investigations

Table 4.5 summarizes the composite plating conditions and the measured average friction coefficients of the samples used in this study within 1.6 % deviation. The average friction coefficients, μ, for the uncoated and pure nickel coated AISI 304 stainless steel were 1.03 and 1.12, respectively as shown in Figure 4.27. Figure 4.28 shows the variation of the dry sliding friction coefficients as a function of number of revolutions for the first six composite coating specimens of Table 4.5. Figure 4.29 shows the friction coefficient values of experiments 6, 7, 8 and 9. The friction coefficients of the composite coatings significantly decreased from 1.12 to as low as 0.40 when the μ for pure Ni and Ni-MoS$_2$ coated specimens are compared. This corresponds to more than 60 percent decrease in friction coefficient. Although, friction and wear properties are system properties and direct comparison among data obtained by different researchers can not be made, similar percentage decreases were also obtained when 0.5 g/L MoS$_2$ of 3 μm average particle size codeposited with Ni-W was tested against steel ball as the static partner [11]. In the study of Huang and Xiong, the friction coefficient of Ni-plated steel specimen was 0.45 and then decreased to 0.2 upon addition of 30 g/L MoS$_2$ to Watts bath [13]. This difference may stem from the differences in test conditions: ceramic ball (Al$_2$O$_3$) was used as the counterface material, the sliding velocity was 35.5cm/s and the relative humidity was 65–85 % [13] which were both higher than the values used in this study. In addition, increase in sliding velocity and humidity led to decrease in friction coefficient [154]. The interaction effects of surfactant and MoS$_2$ concentration on the average friction coefficient are seen in Figure 4.30. Increasing the concentration of MoS$_2$ in the bath led to a decrease in the friction coefficient. This is mainly due to increase in MoS$_2$ in the coating and this result matched up with the study of Huang and Xiong [13]. Notable lubrication was obtained as a result of the layered structure of MoS$_2$ [11, 58]. The layered structure can be seen in Figure 4.27 [155]. Molybdenum atoms are placed between the two layers of sulfur atoms (S-Mo-S) and this structure is strongly bonded with covalent bonding whereas these layers are weakly connected to each other with Van der Waals bonding that led to easy shearing between basal planes [11, 58]. Such anisotropy of mechanical properties provides the combination of low coefficient of friction and high carrying load capacity to MoS$_2$. As it can be seen in the Figure 4.27, the distance between C and B or B and C is shorter than the distance between A and B; an easy shearing may occur transversely between A and B due to the weak bonding between them [156]. Friction forces

64

led the MoS_2 particles to orient in the sliding movement direction where hexagonal layers are parallel to this direction. The sulfur layers of molybdenum disulfide have an affinity for very strong adherence to the metal substrate atoms therefore a strong lubrication film is formed on the substrate surface that decreased the friction coefficient. Figure 4.30 also shows the interaction effects of surfactant and MoS_2 amounts according to results of the first 6 experiments given in Table 4.5. Increasing the amount of surfactant in the bath decreased the coefficient of friction for all MoS_2 concentrations. The effect of surfactant was more pronounced at lower MoS_2 concentrations. The increase in surfactant concentration of the electrolyte, reduced particle agglomeration and led to more homogeneous distribution of particles that increased the effect of MoS_2 [9, 90, 91].
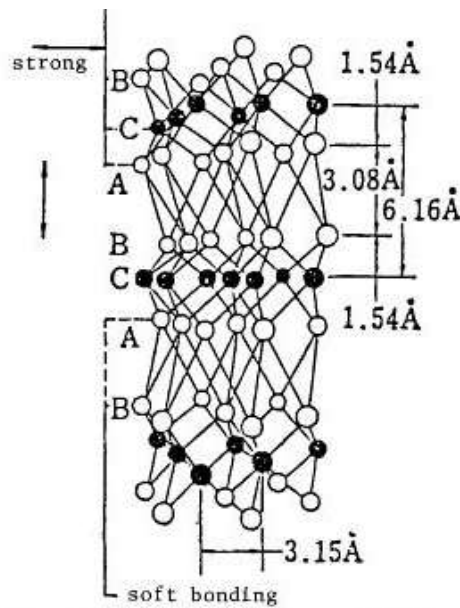
Figure 4.27 The crystal lattice showing the layered structure of the MoS_2 crystal [158]

Figure 4.30 also shows the interaction effects of surfactant and MoS_2 amounts according to results of the first 6 experiments given in Table 4.5. Increasing the amount of surfactant in the bath decreased the coefficient of friction for all MoS_2 concentrations. The effect of surfactant was more pronounced at lower MoS_2 concentrations. The increase in surfactant concentration of the electrolyte, reduced particle agglomeration and led to more homogeneous distribution of particles that increased the effect of MoS_2 [9, 90, 91].

Table 4.5 The plating conditions and the average friction coefficients of the Ni-MoS$_2$ electrocodeposited AISI 304 stainless steel specimens

Experiment No	MoS$_2$ amount (g/L)	MoS$_2$ size (µm)	SLS amount (g/L)	µ
1	5	1.440	1	0.51
2	5	1.440	0.3	0.66
3	10	1.440	1	0.46
4	10	1.440	0.3	0.49
5	30	1.440	1	0.41
6	30	1.440	0.3	0.40
7	5	1.440	0.05	0.45
8	30	5.156	0.3	0.42
9	5	5.156	0.05	0.60

Figure 4.28 Variation of the friction coefficients of uncoated and Ni-plated stainless steel as a function of number of laps
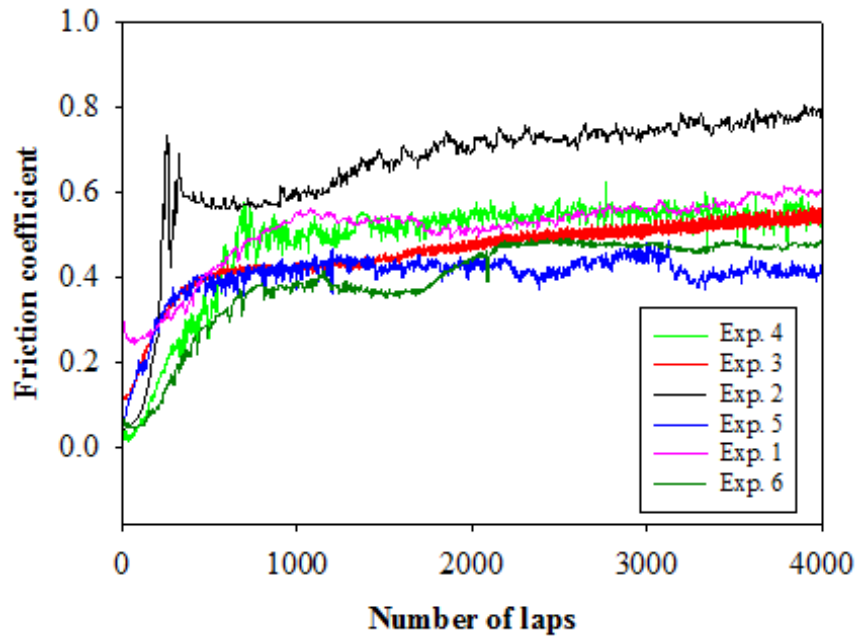
Figure 4.29 Variation of the friction coefficients of composite coatings that have experiment numbers from 1 to 6 as a function of number of laps coating specimens
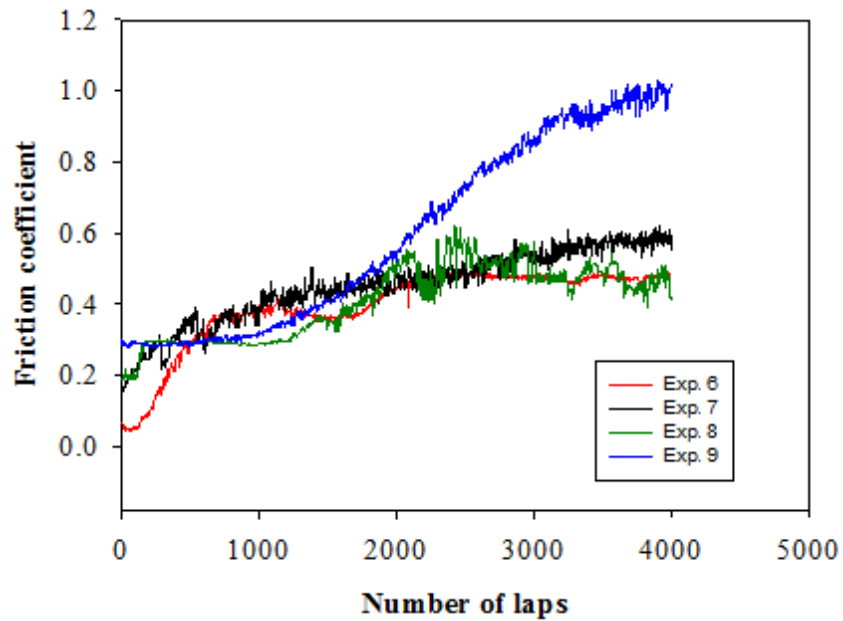
Figure 4.30 Variation of the friction coefficients of composite coatings that have experiment numbers

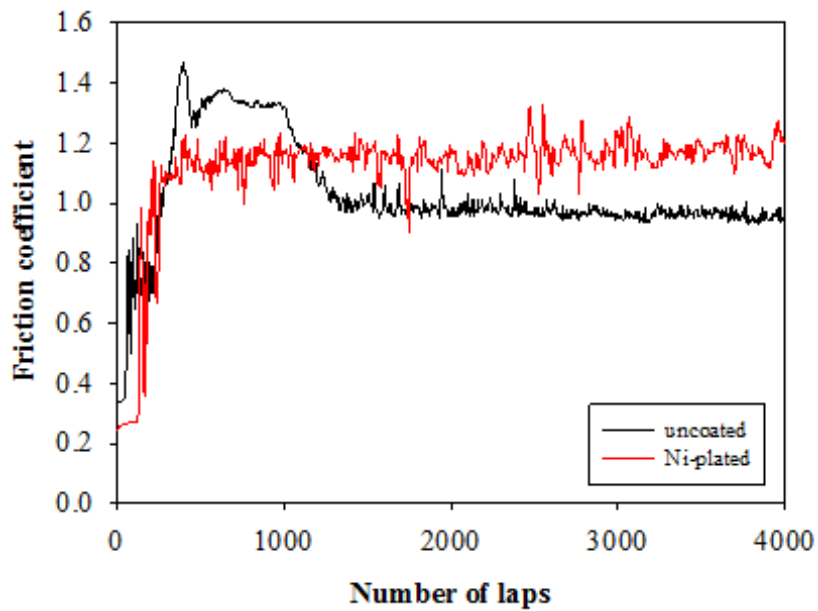The interaction plot of MoS$_2$ particle size and concentration are exhibited in Figure 4.31 according to experiments 6, 7, 8 and 9 where surfactant amount was 0.01 g/g MoS$_2$. From the figure it can be seen that increasing MoS$_2$ content and decreasing MoS$_2$ size decreased the friction coefficient and the effect of MoS$_2$ amount is overwhelming. This result is supported by the regression equation:

$$\mu = 0.522 + 0.0770 \, A - 0.114 \, B \qquad (18)$$

where A and B are the size and the concentration of MoS$_2$ particles, both varying between 0 and 1 where 0 corresponds to 1.44 μm for size and 10 g/L for concentration and 1 corresponds to 5.156 μm for size and 30 g/L for concentration. It should be noted that, above equation is obtained for parameters within the limits covered in this study, because incorporated particles in the deposits increase with increase in MoS$_2$ concentration of the electrolyte up to a limit, beyond which particle settling is observed [3, 13, 87].
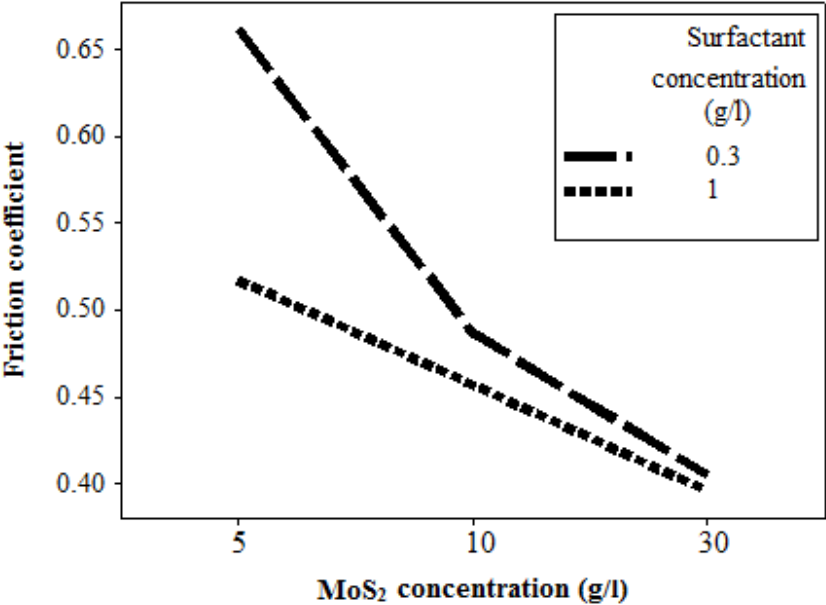
Figure 4.31 Effect of surfactant and MoS$_2$ concentration of the electrolyte on the average coefficient of friction of Ni-MoS$_2$ composite coatings
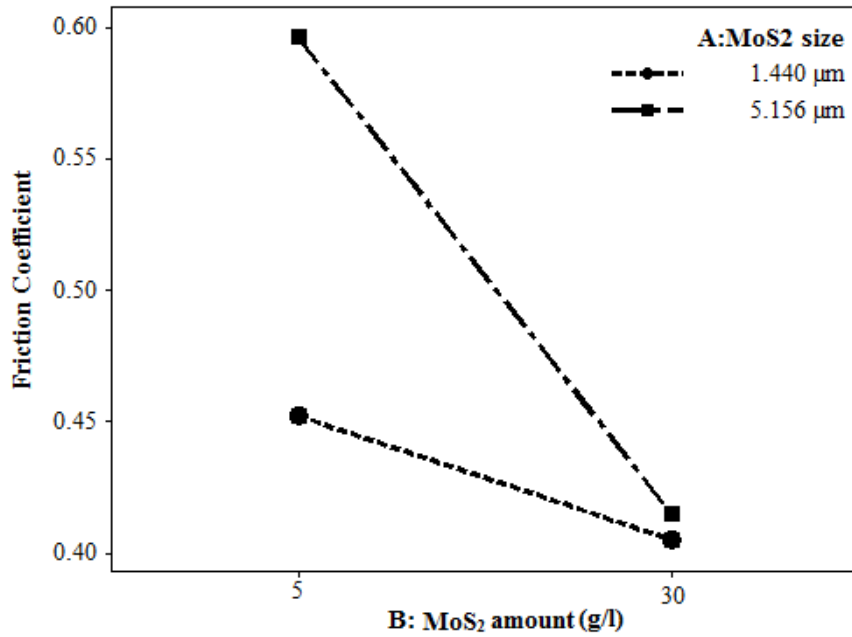
Figure 4.32 Interaction plot of MoS$_2$ size and amount

Volume loss is the scientific way of measuring wear [157]. The wear volumes of the specimens that were subjected to the pin-on-disk tests were calculated by measuring the widths of the wear tracks under the optical microscope according to ASTM standard G99 [129]. There was no noticeable wear on the contact surfaces of the 100Cr6 balls used for the wear testing of the coatings produced. As an example, an optical image showing a part of the wear track of the experiment 3 specimen is given in Figure 4.33. Continuous and wide grooves parallel to sliding direction seen in Figure 4.33 can be attributed to plastic deformation under loading that is indicative of poor wear resistance [81]. Table 4.6 gives the calculated worn volumes, wear rates and the corresponding MoS$_2$ contents of the plating solutions. The results show that wear rate is proportional with MoS$_2$ (known as soft lubricating material [158]) concentration in the bath. As the amount of MoS$_2$ in the coating increases it becomes easier to wear it out because of the soft nature of MoS$_2$. The same trend was observed by Huang and Xiong [13]. It is known that the hard coatings that increase wear resistance lead to high friction coefficients. Moreover, improperly matched particle sizes may also result in decrease in the wear resistance.

Another way of determining the volume loss is to measure the wear track profile area. As an example, the average cross-sectional areas were calculated from 3 measurements for three experiments within 20 % deviation (no:1, 3 and 4) and the volume losses given in Table 4.7 were calculated by multiplying the average cross-sectional area of each wear track with the circumferential contact length (12.57 mm). It was observed that the worn volumes found by two different methods were following the same trend and may be considered consistent to

each other when small wear volumes are compared. The cross-sectional wear track profiles for the experiments 1, 3 and 4 are given in Appendix B.
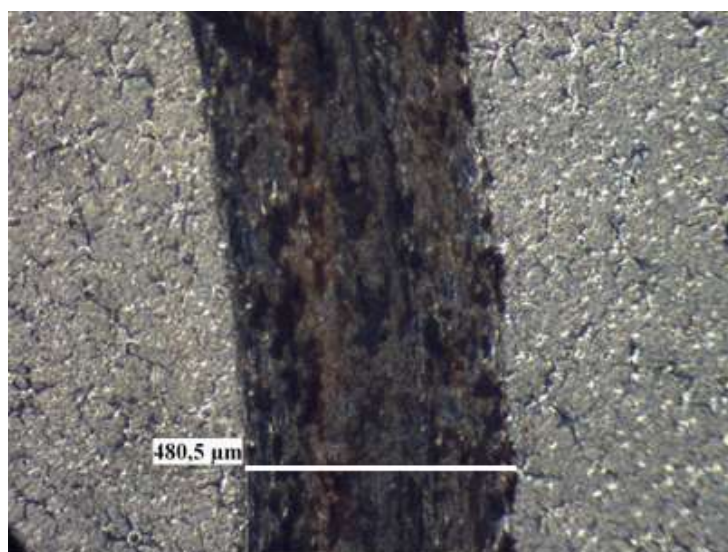
Figure 4.33 An optical image of a part of the wear track of the Ni-MoS$_2$ composite coating electrodeposited from the electrolyte containing 10g/L MoS$_2$ and 1g/L SLS

Table 4.6 Calculated volume losses and wear rates

Experiment No	Wear Volume (mm^3)	Wear Rate (mm^3/N.m)
1	0.0048	0.000094
2	0.0086	0.000168
3	0.0387	0.000759
4	0.0575	0.001126
5	0.0679	0.001329
6	0.0686	0.001342

Table 4.7 Volume losses calculated using wear track profiles

Experiment No	Volume Loss (mm^3)
1	0.0072
3	0.0241
4	0.0700

CHAPTER 5

CONCLUSION

The effects of deposition parameters on the peak current density (i_p) for the hydrogen evolution reaction during the electrodeposition of Ni and Ni-MoS$_2$ composits were studied by fractional factorial design. Interaction effects for the parameters were evaluated including the effects of three commonly used mineral processing surfactants sodiumlignosulfonate (SLS), ammoniumlignosulfonate (ALS) and Depramin C (DC). It was found that adding MoS$_2$, decreasing acidity and decreasing temperature lead to a decrease in i_p for all of the surfactants. Moreover, addition of the anionic surfactants ALS, DC increased and SLS decreased i_p. Moreover, temperature, pH and all surfactants decreased the peak voltage (V_p). However, MoS$_2$ addition increased V_p when DC was added and decreased V_p when SLS or ALS was added to the solution.

The effects of basic electroplating parameters and particle addition on the internal stress of Ni and Ni-MoS$_2$ composite coatings were determined by following the routes of a statistical experimental design. The incorporation of MoS$_2$ particles decreased the internal stress. Presence of these particles even changed the nature of the stress from tensile to compressive. Both temperature and current density did not have an important effect on the internal stress. Whereas low pH and high coating thickness led to a decrease in the value of internal stress.

The effects of surfactants (SLS, ALS and DC) on the internal stress were insignificant. More homogeneous distribution of MoS$_2$ particles was obtained in the deposited layer when SLS was added to Watts bath.

According to XRD results, the weight percent of MoS$_2$ was 6.3 that corresponds to 10 volume percent in the deposit when 10 g/L MoS$_2$ was added to the Watts bath. The microstructural analysis and EDX results confirm the findings from XRD.

Tribological behavior of Ni-MoS$_2$ composite coatings electrodeposited from electrolytes by using three different concentrations of MoS$_2$ and two different surfactant (SLS) amounts was investigated under dry sliding conditions. The wear resistances were inversely proportional to MoS$_2$ amount in the solution. Increase in the MoS$_2$ content and surfactant amount significantly decreased the friction coefficients of the deposits. In addition, increasing MoS$_2$ content decreased the effect of surfactant.

Original Contributions

In this thesis, the influence of the electroplating parameters and their interactions on hydrogen evolution reaction (HER) and the internal stress were studied during the electrodeposition of Ni and Ni-MoS$_2$ composite coatings by fractional factorial design (FFD). In the previous studies the interaction effects of parameters were not considered and only the effect of parameters on MoS$_2$ content in the deposit was investigated.

Present research adds results to previous and ongoing work on the decreasing effect of MoS$_2$ in composite coatings on friction coefficient. Present study supplies results of investigations on the effects of the surfactant and its amounts on the friction coefficient.

In this study, homogeneous distribution of MoS$_2$ particles was observed with addition of surfactant sodiumlignosulfonate which was not examined in the previous studies.

Suggestions for Futurework

As was discussed in the thesis, MoS$_2$ particles have an important effect on decreasing the friction coefficient but wear properties are not pleasant. To improve wear porperties together with frictional properties other particles like W, SiC or other hard particles can be added to the Watts bath.

Effects of electroplating parameters and MoS$_2$ and /or other particle addition on texture formation and effect of texture on tribological properties can be studied.

REFERENCES

1. J. B. Mohler and H. J. Sedusky, *Nickel Plating*, in *Electroplating* Chemical Publishing Co.: New York, 1951.
2. I. Gurrappa and L. Binder, *Electrodeposition of Nanostructured Coatings and Their Characterization - A Review.* Science and Technology of Advanced Materials, 2008, 9(4): p. 043001.
3. J. L. Stojak, J. Fransaer and J. B. Talbot, *Review of Electrocodeposition*, in *Advances in Electrochemical Science and Engineering* Wiley-VCH Verlag GmbH, p. 193, 2001.
4. T. Saji and N. K. Shrestha, *Composite Plating Method*, US 6635166 B2, Japan: Japan Science and Technolgy Coorperation, 2003.
5. I. Zhitomirsky, *Electrodeposition of Ceramic Materials and Composites.* Surface Engineering, 2011, 27(6): p. 403.
6. I. Brooks, U. Erb, F. Gonzalez, D. Glenn Hibbard, J. Mccrea, G. Palumbo and K. Tomantschger, *Process for Electroplating Metallic and Metall Matrix Composite Foils, Coatings and Microcomponents*, EP 1516076 A1, 2005.
7. E. Pompei, L. Magagnin, N. Lecis and P. L. Cavallotti, *Electrodeposition of Nickel-BN Composite Coatings.* Electrochim. Acta, 2009, 54: p. 2571.
8. N. K. Shrestha, K. Sakurada, M. Masuko and T. Saji, *Composite Coatings of Nickel and Ceramic Particles Prepared in Two Steps.* Surf. Coat. Tech., 2001, 140(2): p. 175.
9. L. M. Wang, *Effect of Surfactant BAS on MoS_2 Codeposition Behaviour.* J. Appl. Electrochem., 2008, 38(2): p. 245.
10. Y. C. Chang, Y. Y. Chang and C. I. Lin, *Process Aspects of the Electrolytic Codeposition of Molybdenum Disulfide with Nickel.* Electrochim. Acta, 1998, 43(3-4): p. 315.
11. M. F. Cardinal, P. A. Castro, J. Baxi, H. Liang and F. J. Williams, *Characterization and Frictional Behavior of Nanostructured $Ni-W-MoS_2$ Composite Coatings.* Surf. Coat. Tech., 2009, 204(1-2): p. 85.
12. S. L. Kuo, *The Influence of Process Parameters on the MoS_2 Content of $Ni-MoS_2$ Composite Coating by the Robust Design Method.* JCIE, 2004, 27(2): p. 243.
13. Z.-J. Huang and D.-S. Xiong, *MoS_2 Coated with Al_2O_3 for $Ni-MoS_2/Al_2O_3$ Composite Coatings by Pulse Electrodeposition.* Surf. Coat. Tech., 2008, 202(14): p. 3208.
14. Y. Kunugi, R. Kumada, T. Nonaka, Y.-B. Chong and N. Watanabe, *Electrolysis Using Composite Plated Electrodes: Part III. Electroorganic Reactions on a Hydrophobic Ni/PTFE Composite Plated Nickel Electrode.* Journal of Electroanalytical Chemistry and Interfacial Electrochemistry, 1991, 313(1-2): p. 215.
15. P. Berçot, E. Pena-Munoz and J. Pagetti, *Electrolytic Composite Ni-PTFE Coatings: An Adaptation of Guglielmi's Model for the Phenomena of Incorporation.* Surf. Coat. Tech., 2002, 157(2-3): p. 282.
16. R. Balaji, M. Pushpavanam, K. Y. Kumar and K. Subramanian, *Electrodeposition of Bronze-PTFE Composite Coatings and Study on Their Tribological Characteristics.* Surf. Coat. Tech., 2006, 201(6): p. 3205.

17. Z. Abdel Hamid and I. M. Ghayad, *Characteristics of Electrodeposition of Ni-Polyethylene Composite Coatings.* Mater. Lett., 2002, 53: p. 238.

18. F. Plumier, E. Chassaing, G. Terwagne, J. Delhalle and Z. Mekhalif, *Electrolytic Co-deposition of a Nickel / Fluorographite Composite Layer on Polycrystalline Copper.* Applied Surface Science, 2003, 212-213: p. 271.

19. P. Dabo, H. Menard and L. Brossard, *Electrochemical Characterization of Graphite Composite Coated Electrodes for Hydrogen Evolution Reaction.* International Journal of Hydrogen Energy, 1997, 22(8): p. 763.

20. M. Ghorbani, M. Mazaheri, K. Khangholi and Y. Kharazi, *Electrodeposition of Graphite - Brass Composite Coatings and Characterization of the Tribological Properties.* Surf. Coat. Tech., 2001, 148(1): p. 71.

21. J. K. Dennis and T. E. Such, *Nickel and Chromium Plating*, 1993, Woodhead Publishing Limited: England.

22. M. Redlich, A. Gorodnev, Y. Feldman, I. Kaplan-Ashiri, R. Tenne, N. Fleischer, M. Genut and N. Feuerstein, *Friction Reduction and Wear Resistance of Electro-co-deposited Inorganic Fullerene-like WS$_2$ Coating for Improved Stainless Steel Orthodontic Wires.* J. Mater. Res., 2008, 23(11): p. 2909.

23. A. Shankara, P. L. Menezes, K. R. Y. Simha and S. V. Kailas, *Study of Solid Lubrication with MoS$_2$ Coating in the Presence of Additives using Reciprocating Ball-on-Flat Scratch Tester.* Sadhana, 2008, 33(3): p. 207.

24. A. Bund and D. Thiemig, *Influence of bath composition and pH on the electrocodeposition of alumina nanoparticles and nickel.* 2007, 201: p. 7092.

25. W. Blum and G. B. Hogaboom, *Principles of Electroplating and Electroforming* Toronto: McGraw-Hill Book Company, 1949.

26. M. Karbasi, N. Yazdian and A. Vahidian, *Development of Electrocodeposited Ni–TiC Nano-particle Reinforced Nanocomposite Coatings.* Surf. Coat. Tech., 2012, 207(0): p. 587.

27. S. E. Hadian and D. R. Gabe, *Residual Stresses in Electrodeposits of Nickel and Nickel - Iron Alloys.* Surf. Coat. Tech., 1999, 122(2-3): p. 118.

28. W. Reil, *Material Science of Electrodeposits* Plating & Surface Finishing, 1982, 69(12): p. 46.

29. C. S. Lin, C. Y. Lee, F. J. Chen and W. C. Li, *Structural Evolution and Internal Stress of Nickel-Phosphorus Electrodeposits.* Journal of The Electrochemical Society, 2005, 152(6): p. C370.

30. J. W. Dini, *Stress*, in *Electrodeposition The Materials Science of Coatings and Substrates* Noyes Publications: California, 1993.

31. I. Mizushima, P. T. Tang, H. N. Hansen and M. a. J. Somers, *Residual stress in Ni–W electrodeposits.* Electrochim. Acta, 2006, 51(27): p. 6128.

32. F. H. Leaman, *A New Frontier for Deposit Stress Measurements.* Specialty Testing and Development Company, Inc., 2007.

33. R. C. Barrett, *Nickel Plating From the Sulfamate Bath.* Forty-First Annual Convention of the American Electroplaters' Society, 1954.

34. I. Timoshkov, V. Kurmashev and V. Timoshkov, *Electroplated Nanocomposites of High Wear Resistance for Advanced Systems Application*, in *Advances in Nanocomposite Technology*, A. Hashim, Editor, 2011.

35. P. Wang, Y.-L. Cheng and Z. Zhang, *A Study on the Electrocodeposition Processes and Properties of Ni–SiC Nanocomposite Coatings.* Journal of Coatings Technology and Research, 2011, 8(3): p. 409.

36. F. A. Lowenheim, *Modern Electroplating*, in *Nickel*, H. Brown and B.B. Knapf, Editors., John Wiley and Sons: Toronto, p. 287, 1974.

37. S. Pathak, M. Guinard, M. G. C. Vernooij, B. Cousin, Z. Wang, J. Michler and L. Philippe, *Influence of lower current densities on the residual stress and structure of thick nickel electrodeposits.* Surf. Coat. Tech., 2011, 205(12): p. 3651.

38. B. Stein, *A Practical Guide to Understanding, Measuring and Controlling Stress in Electroformed Metals.* AESF Electroforming Symposium, 1996.

39. B. Stein, *Fast and Accurate Internal Stress Determination.* Proceedings of the AESF Sur/Fin, 2000.

40. M. Schlesinger and M. Paunovic, *Electrodeposition of Nickel* in *Modern Electroplating*, G.A. Di Bari, Editor John Wiley & Sons, p. 79 2010.

41. Minitab, *Statistical Software.* 2007.

42. Z. Ahmad, *Coatings*, in *Principles of Corrosion Engineering and Corrosion Control* Elsevier Ltd.: Oxford, UK, 2006.

43. C. S. Ramesh and S. K. Seshadri, *Tribological Characteristics of Nickel based Composite Coatings.* Wear, 2003, 255(7–12): p. 893.

44. Astm-B-689-97, *Standard Specification for Electroplated Engineering Nickel Coatings*, 2003, ASTM International.

45. L. W. Pan, L. Lin and J. Ni, *A flip-chip LIGA assembly technique via electroplating.* Microsystem Technologies, 2001, 7(1): p. 40.

46. G. A. Di Bari, *Nickel Plating* in *Electroplating Engineering Handbook*, L.J. Durney, Editor Van Nostrand Reinhold Company: New York, 1984.

47. G. Vidrich, J.-F. Castagnet and H. Ferkelz, *Dispersion Behavior of Al_2O_3 and SiO_2 Nanoparticles in Nickel Sulfamate Plating Baths of Different Compositions.* Journal of The Electrochemical Society, 2005, 152(5): p. C294.

48. D. Baudrand, *Nickel Sulfamate Plating, Its Mystique and Practicality.* Metal Finishing, 1996, 94(7): p. 15.

49. J. R. Davis, *Nickel Coatings.* ASM Specialty Handbbok: Nickel, Cobalt and Their Alloys, 2000.

50. M. Surender, R. Balasubramaniam and B. Basu, *Electrochemical Behavior of Electrodeposited Ni-WC Composite Coatings.* Surf. Coat. Tech., 2004, 187(1): p. 93.

51. F. Kılıç, H. Gül, S. Aslan, A. Alp and H. Akbulut, *Effect of CTAB Concentration in the Electrolyte on the Tribological Properties of Nanoparticle SiC Reinforced Ni Metal Matrix Composite (MMC) Coatings Produced by Electrodeposition.* Colloids and Surfaces A: Physicochemical and Engineering Aspects, 2013, 419(0): p. 53.

52. N. Kanani, *Electroplating: Basic Principles, Processes and Practice*. Metal Finishing - A Key Technology Berlin: Elsevier Ltd., 2004.

53. A. Hovestad and J. J. Janssen, *Electrochemical Codeposition of Inert Particles in a Metallic Matrix.* J. Appl. Electrochem., 1995, 25(6): p. 519.

54. C. Donnet and A. Erdemir, *Historical Developments and New Trends in Tribological and Solid Lubricant Coatings.* Surf. Coat. Tech., 2004, 180–181(0): p. 76.

55. M. Chhowalla and G. a. J. Amaratunga, *Thin Films of Fullerene-like MoS_2 Nanoparticles with Ultra-low Friction and Wear.* Nature, 2000, 407: p. 164.

56. M. R. Hilton and P. D. Fleischaure, *Applications of Solid Lubricant Films in Spacecraft*, 1994.

57.	M. R. Hilton and P. D. Fleischauer, *Lubricants for High Vacuum Applications* in *ASM Handbook - Friction, Lubricaiton and Wear Technology*, P.J. Blau, Editor, p. 150, 1992.

58.	L. Shi, C. Sun and W. Liu, *Electrodeposited Nickel - Cobalt Composite Coating Containing MoS₂.* Applied Surface Science, 2008, 254(21): p. 6880.

59.	C. T. J. Low, R. G. A. Wills and F. C. Walsh, *Electrodeposition of Composite Coatings Containing Nanoparticles in a Metal Deposit.* Surf. Coat. Tech., 2006, 201(1-2): p. 371.

60.	R. K. Saha and T. I. Khan, *Effect of Applied Current on the Electrodeposited Ni - Al₂O₃ Composite Coatings.* Surf. Coat. Tech., 2010, 205(3): p. 890.

61.	S. K. Kim and H. J. Yoo, *Formation of Bilayer Ni - SiC Composite Coatings by Electrodeposition.* Surf. Coat. Tech., 1998, 108-109(1-3): p. 564.

62.	L. Benea, *Electrodeposition of Zirconia Particles in a Copper Matrix.* Materials and Manufacturing Processes, 1999, 14(2): p. 231.

63.	N. Guglielmi, *Kinetics of the Deposition of Inert Particles from Electrolytic Baths.* Journal of The Electrochemical Society, 1972, 119(8): p. 1009.

64.	K. I. Popov, S. S. Djokic and B. N. Grgur, *Fundamental Aspects of Electrometallurgy* New York: Kluwer Academic Publisher, 2002.

65.	B. Reddy, *Advances in Nanocomposites - Synthesis, Characterization and Industrial Applications*, in *Electrodeposition of Metal Matrix Nanocomposites: Improvement of the Chemical Characterization Techniques*, A. Gomes, et al., Editors., InTech, 2011.

66.	H. Abi-Akar and C. Riley, *Electrocodeposition of Nickel-Diamond and Cobalt-Chromium Carbide in Low Gravity.* Chem. Mater., 1996, 8: p. 2601.

67.	H.-K. Lee, H.-Y. Lee and J.-M. Jeon, *Codeposition of micro- and nano-sized SiC particles in the nickel matrix composite coatings obtained by electroplating.* Surf. Coat. Tech., 2007, 201(8): p. 4711.

68.	A. Hovestad and L. J. J. Janssen, *Electroplating of Metal Matrix Composites by Codeposition of Suspended Particles*, in *Modern Aspects of Electrochemistry*, B. Conway, et al., Editors., Springer US, p. 475, 2005.

69.	S. Shawki and Z. Abdel Hamid, *Deposition of High Wear Resistance of Ni-Composite Coatings.* Aircr. Eng. Aerosp. Tech., 1997, 69(5): p. 432.

70.	H. Simunkova, P. Pessenda-Garcia, J. Wosik, P. Angerer, H. Kronberger and G. E. Nauer, *The fundamentals of nano- and submicro-scaled ceramic particles incorporation into electrodeposited nickel layers: Zeta potential measurements.* Surf. Coat. Tech., 2009, 203(13): p. 1806.

71.	E. Zuurdeeg, *Process for electro-codepositing inorganic particles and a metal on a surface*, 1980.

72.	N. D. Nikolic and K. I. Popov, *Hydrogen Co-deposition Effects on the Structure of Electrodeposited Copper Electrodeposition*, in *Modern Aspects of Electrochemistry*, S.S. Djokic, Editor Springer New York, p. 1, 2010.

73.	E. Raub and K. Müller, *Fundamentals of Metal Deposition* London: Elsevier Publishing Company, 1967.

74.	C. B. Nielsen, A. Horsewell and M. J. L. Østergård, *On Texture Formation of Nickel Electrodeposits.* J. Appl. Electrochem., 1997, 27(7): p. 839.

75.	T. Lampke, B. Wielage, D. Dietrich and A. Leopold, *Details of Crystalline Growth in Co-deposited Electroplated Nickel Films with Hard (Nano)particles.* Applied Surface Science, 2006, 253(5): p. 2399.

76.   J. Amblard, I. Epelboin, M. Froment and G. Maurin, *Inhibition and Nickel Electrocrystallization.* J. Appl. Electrochem., 1979, 9(2): p. 233.

77.   T. Fritz, H. S. Cho, K. J. Hemker, W. Mokwa and U. Schnakenberg, *Characterization of Electroplated Nickel.* Microsystem Technologies, 2002, 9(1-2): p. 87.

78.   T. Fritz, W. Mokwa and U. Schnakenberg, *Material Characterisation of Electroplated Nickel Structures for Microsystem Technology.* Electrochim. Acta, 2001, 47(1-2): p. 55.

79.   R. A.K.N, *Preferred orientations in nickel electro-deposits: I. The mechanism of development of textures in nickel electro-deposits.* Journal of Electroanalytical Chemistry (1959), 1963, 6(2): p. 141.

80.   S. Psarrou, P. Gyftou and N. Spyrellis, *Electron Microscopy Study of Nickel and Nickel Composite Electrocoatings.* Microchimica Acta, 2001, 136(3): p. 159.

81.   T. Borkar and S. P. Harimkar, *Effect of Electrodeposition Conditions and Reinforcement Content on Microstructure and Tribological Properties of Nickel Composite Coatings.* Surf. Coat. Tech., 2011, 205(17–18): p. 4124.

82.   F. Wang, S. Arai and M. Endo, *Electrochemical Preparation and Characterization of Nickel Ultra-Dispersed PTFE Composite Films from Aqueous Solution.* Materials Transactions, 2004, 45: p. 1311.

83.   S.-C. Wang and W.-C. J. Wei, *Kinetics of Electroplating Process of Nano-sized Ceramic Particle / Ni Composite.* Materials Chemistry and Physics, 2003, 78(3): p. 574.

84.   Y. L. Wang, Y. Z. Wan, S. M. Zhao, H. M. Tao and X. H. Dong, *Electrodeposition and Characterization of Al_2O_3-Cu(Sn), CaF_2-Cu(Sn) and talc-Cu(Sn) Electrocomposite Coatings.* Surf. Coat. Tech., 1998, 106(2-3): p. 162.

85.   J.-H. Ouyang, X.-S. Liang, J. Wen, Z.-G. Liu and Z.-L. Yang, *Electrodeposition and Tribological Properties of Self-lubricating Ni–$BaCr_2O_4$ Composite Coatings.* Wear, 2011, 271(9–10): p. 2037.

86.   P. Narasimman, M. Pushpavanama and V. M. Periasamy, *Effect of Surfactants on the Electrodeposition of Ni-SiC Composites.* Portugaliae Electrochimica Acta, 2012, 30(1): p. 1.

87.   V. P. Greco, *Review and Update on Electrocomposites* US Army Armament Research, Development and Engineering Center, 1992.

88.   G. Sharma, R. K. Yadava and V. K. Sharma, *Characteristics of Electrocodeposited Ni–Co–SiC Composite Coating.* Bulletin of Materials Science, 2006, 29: p. 491.

89.   C. F. Malfatti, H. M. Veit, T. L. Menezes, J. Zoppas Ferreira, J. S. Rodriguês and J. P. Bonino, *The Surfactant Addition Effect in the Elaboration of Electrodepositated NiP-SiC Composite Coatings.* Surf. Coat. Tech., 2007, 201(14): p. 6318.

90.   N. K. Shrestha, M. Kawai and T. Saji, *Co-deposition of B_4C Particles and Nickel Under the Influence of a Redox-Active Surfactant and Anti-Wear Property of the Coatings.* Surf. Coat. Tech., 2005, 200(7): p. 2414.

91.   K. H. Hou, M. D. Ger, L. M. Wang and S. T. Ke, *The Wear Behaviour of Electrocodeposited Ni-SiC Composites.* Wear, 2002, 253(9-10): p. 994.

92.   C. Guo, Y. Zuo, X. Zhao, J. Zhao and J. Xiong, *Effects of Surfactants on Electrodeposition of Nickel - Carbon Nanotubes Composite Coatings.* Surf. Coat. Tech., 2008, 202(14): p. 3385.

93. N. K. Shrestha, M. Masuko and T. Saji, *Composite Plating of Ni/SiC Using Azo-Cationic Surfactants and Wear Resistance of Coatings.* Wear, 2003, 254(5–6): p. 555.

94. D. P. Weston, Y. Q. Zhu, D. Zhang, C. Miller, D. G. Kingerley, C. Carpenter, S. J. Harris and N. J. Weston, *Co-electrodeposition of Inorganic Fullerene (IF-WS₂) Nano-particles with Cobalt From a Gluconate Bath with Anionic and Cationic Surfactants.* Electrochim. Acta, 2011, 56(19): p. 6837.

95. A. Velichenko, V. Knysh, T. Luk'yanenko, D. Devilliers and F. Danilov, *Electrodeposition of Composite Materials PbO2-Ti and Their Physicochemical Properties.* Russian Journal of Electrochemistry, 2008, 44(11): p. 1251.

96. Z.-X. Niu, F.-H. Cao, W. Wang, Z. Zhang, J.-Q. Zhang and C.-N. Cao, *Electrodeposition of Ni-SiC Nanocomposite Film.* Transactions of Nonferrous Metals Society of China, 2007, 17(1): p. 9.

97. Y. Xia, S. Sasaki, T. Murakami, M. Nakano, L. Shi and H. Wang, *Ionic Liquid Lubrication of Electrodeposited Nickel - Si₃N₄ Composite Coatings.* Wear, 2007, 262(7-8): p. 765.

98. L. M. Wang, *Effect of Surfactant-Assistant Electrodeposition in Ni Matrix.* Journal of The Electrochemical Society, 2009, 156(6): p. D204.

99. T. S. N. Sankara Narayanan and S. K. Seshadri, *Electro- and Electroless Plated Coatings for Corrosion Protection*, in *Corrosion Science and Technology: Mechanism, Mitigation and Monitoring* Narosa Publishing House: New Delhi, 2008.

100. M. Paunovic and M. Schlesinger, *Fundamentals of Electrochemical Deposition* New Jersey: Johm Wiley ans Sons 2006.

101. P. T. Tang, *Utilising Electrochemical Deposition for Micro Manufacturing*, in *Multi-Material Micro Manufacture*, S. Dimov and W. Menz, Editors., Whittles Publishing Ltd: Cardiff, UK, 2008.

102. P. J. Withers and H. K. D. H. Bhadeshia, *Residual stress Part 2 – Nature and origins.* Materials Science and Technology, 2001, 17: p. 366.

103. M. Y. Popereka and V. V. Koshmanov, *Effect of Organic Additives in Electrolytes on Internal Stresses in Electrodeposited Iron.* Soviet materials science, 1966, 2(6): p. 453.

104. G. Richardson and B. Stein, *Comparative Study of Three Internal Stress Measurement Methods.* Reflexite Precision Technology Center, 1997: p. 1.

105. A. Brenner and S. Senderoff, *A Spiral Contractometer for Measuring Stress in Electrodeposits.* Journal of Research of the National Bureau of Standards, 1949, 42(2): p. 89.

106. S. Survilienë, L. Orlovskaja, G. Bikulcius and S. Biallozor, *Effect of MoO₂ and TiO₂ on Electrodeposition and Properties of Chromium Coating.* Surf. Coat. Tech., 2001, 137(2–3): p. 230.

107. V. Medelien, *The Influence of B₄C and SiC Additions on the Morphological, Physical, Chemical and Corrosion Properties of Ni Coatings.* Surf. Coat. Tech., 2002, 154(1): p. 104.

108. A. Ramalho, M. C. Oliveira and L. F. Menezes, *Sliding Friction: Global Versus Local Analysis*, in *Friction, Wear and Wear protection*, A. Fischer and K. Bobzin, Editors., Wiley-VCH: Weinheim, 2009.

109. J. W. Dini, *Wear* in *Electrodeposition The Materials Science of Coatings and Substrates* Noyes Publications: California, 1993.

110. E. Gnecco and E. Meyer, *Fundamentals of Friction and Wear on the Nanoscale* Berlin: Springer, 526, 2007.

111. W. J. Bartz, *Tribological Relationship as Basis for the Solution of Friction and Wear Problems.* Handbook of Tribology and Lubricaiton   1994, 8.

112. A. S. M. A. Haseeb, U. Albers and K. Bade, *Friction and Wear Characteristics of Electrodeposited Nanocrystalline Nickel - Tungsten Alloy Films.* Wear, 2008, 264(1–2): p. 106.

113. K. Holmberg and A. Matthews, in *Coatings Tribology Properties, Techniques and Applications in Surface Engineering*, D. Dowson, Editor   Elsevier: Amsterdam, 1994.

114. M. Surender, B. Basu and R. Balasubramaniam, *Wear Characterization of Electrodeposited Ni - WC Composite Coatings.* Tribol. Int., 2004, 37(9): p. 743.

115. W.-H. Lee, S.-C. Tang and K.-C. Chung, *Effects of Direct Current and Pulse Plating on the Co-deposition of Nickel and Nanometer Diamond Powder.* Surf. Coat. Tech., 1999, 120–121(0): p. 607.

116. L. Du, B. Xu, S. Dong, H. Yang and W. Tu, *Study of Tribological Characteristics and Wear Mechanism of Nano-particle Strengthened Nickel-based Nomposite Coatings Under Abrasive Contaminant Lubrication.* Wear, 2004, 257(9-10): p. 1058.

117. G. Heidari, H. Tavakoli and S. Mousavi Khoie, *Nano SiC-Nickel Composite Coatings from a Sulfamat Bath Using Direct Current and Pulsed Direct Current.* J. Mater. Eng. Perform.

118. Y.-J. Xue, X.-Z. Jia, Y.-W. Zhou, W. Ma and J.-S. Li, *Tribological Performance of Ni-CeO$_2$ Composite Coatings by Electrodeposition.* Surf. Coat. Tech., 2006, 200(20-21): p. 5677.

119. L. Chen, L. Wang, Z. Zeng and J. Zhang, *Effect of surfactant on the electrodeposition and wear resistance of Ni–Al2O3 composite coatings.* Materials Science and Engineering: A, 2006, 434(1–2): p. 319.

120. B. Wielage, T. Lampke, M. Zacher and D. Dietrich, *Electroplated Nickel Composites with Micron- to Nano-sized Particles.* Key Engineering Materials, 2008, 384: p. 283.

121. M. R. Vaezi, S. K. Sadrnezhaad and L. Nikzad, *Electrodeposition of Ni-SiC Nano-composite Coatings and Evaluation of Wear and Corrosion Resistance and Electroplating Characteristics.* Colloids and Surfaces A: Physicochemical and Engineering Aspects, 2008, 315(1-3): p. 176.

122. L. Shi, C. Sun, P. Gao, F. Zhou and W. Liu, *Mechanical Properties and Wear and Corrosion Resistance of Electrodeposited Ni-Co / SiC Nanocomposite Coating.* Applied Surface Science, 2006, 252(10): p. 3591.

123. L. Benea, P. L. Bonora, A. Borello and S. Martelli, *Wear Corrosion Properties of Nano-structured SiC-nickel Composite Coatings Obtained by Electroplating.* Wear, 2002, 249(10-11): p. 995.

124. I. Garcia, J. Fransaer and J. P. Celis, *Electrodeposition and Sliding Wear Resistance of Nickel Composite Coatings Containing Micron and Submicron SiC Particles.* Surf. Coat. Tech., 2001, 148(2-3): p. 171.

125. D. D. Roshon, *Electroplated Diamond-Composite Coatings for Abrasive Wear Resistance* IBM Journal of Research and Development, 1978, 22(6): p. 681.

126. T. M. Gubarevich and L. E. Chernukho, *Ultradisperse Diamond Modifications in the Composite Gilding Process Synthesis, Properties and Applications of*

Ultrananocrystalline Diamond, D. Gruen, O. Shenderova, and A. Vul', Editors., Springer Netherlands, p. 345, 2005.

127.   P. Y. Detkov, V. A. Popov, V. G. Kulichikhin and S. I. Chukhaeva, *Development of Composite Materials Based on Improved Nanodiamonds Molecular Building Blocks for Nanotechnology*, G. Mansoori, et al., Editors.,   Springer Berlin / Heidelberg, p. 29, 2007.

128.   X. Sun and J. Li, *Friction and Wear Properties of Electrodeposited Nickel–Titania Nanocomposite Coatings.* Tribology Letters, 2007, 28(3): p. 223.

129.   Astm-G99-95a, *Standard Test Method for Wear Testing with a Pin-on-Disk Apparatus*, 2000, ASTM International.

130.   *http://www.surtec.com/en/products/product-overview/nickel-plating-68/surtec-855-322/, 2013.*

131.   D. P. Murphy, *Metal Cleaning*, in *ASM Handbook - Alkaline Cleaning*, 1982.

132.   R. N. Gay and W. K. Raymond, *Process for Electroplating Nickel Over Stainless Steel*, 4764260, 3, 1988.

133.   Astm-B281-88, *Standard Practice for Preparation of Copper and Copper-Base Alloys for Electroplating and Conversion Coatings1*, 2001, ASTM International.

134.   Malvern, *Zetasizer Nano S.* 2013.

135.   E. Saraloglu Guler , İ. Karakaya and E. Konca, *Effect of Electroplating Parameters on Internal Stress in Ni-MoS$_2$ Composite Plating.* TMS (The Minerals, Metals & Materials Society) Annual Meeting Supplemental Proceedings, 2013: p. 191.

136.   P. M. S. Monk, *Linear Sweep and Cyclic Voltammetry at Solid Electrodes*, in *Fundamentals of Electroanalytical Chemistry* John Wiley and Sons Ltd.   : England, 2001.

137.   C. H. Hamann, A. Hamnett and W. Vielstich, *Electrochemistry* Weinheim: Wiley-VCH, 1998.

138.   M. Ibrahim, *Black Nickel Electrodeposition From a Modified Watts Bath.* J. Appl. Electrochem., 2006, 36(3): p. 295.

139.   E. Saraloglu Guler, İ. Karakaya and E. Konca, *Effect of Electrodeposition Parameters on the Current Density of Hydrogen Evolution Reaction in Ni and Ni-MoS$_2$ Composite Coatings.* Int. J. Electrochem. Sci., 2013, 8: p. 5496

140.   N. Yamada, H. Shoji, Y. Kubo and S. Katayama, *Preparation of Inorganic-Organic Hybrid Films Containing Particles Using Electrophoretic Deposition Method.* Journal of Materials Science, 2002, 37(10): p. 2071.

141.   J. G. Manjunath, B. E. Kumara Swamy, O. Gilbert, G. P. Mamatha and B. S. Sherigara, *Sensitive Voltammetric Determination of Dopamine at Salicylic Acid and TX-100, SDS, CTAB Modified Carbon Paste Electrode.* Int. J. Electrochem. Sci., 2010, 5: p. 682

142.   J. G. Manjunatha, B. E. Kumara Swamy, G. P. Mamatha, U. Chandra, E. Niranjana and B. S. Sherigara, *Cyclic Voltammetric Studies of Dopamine at Lamotrigine and TX-100 Modified Carbon Paste Electrode.* Int. J. Electrochem. Sci., 2009, 4: p. 187

143.   B. N. Chandrashekar, B. E. Kumara Swamy, K. R. Vishnu Mahesh, U. Chandra and B. S. Sherigara, *Electrochemical Studies of Bromothymol Blue at surfactant Modified Carbon Paste Electrode By using Cyclic Voltammetry.* Int. J. Electrochem. Sci., 2009, 4: p. 471

144.   B. N. Popov, K.-M. Yin and R. E. White, *Galvanostatic Pulse and Pulse Reverse Plating of Nickel-Iron Alloys from Electrolytes Containing Organic Compounds on a Rotating Disk Electrode.* J. Electrochem. Soc., 1993, 140(5).

145. I. Garcia, A. Conde, G. Langelaan, J. Fransaer and J. P. Celis, *Improved Corrosion Resistance Through Microstructural Modifications Induced by Codepositing SiC Particles with Electrolytic Nickel.* Corrosion Science, 2003, 45(6): p. 1173.

146. M.-C. Chou, M.-D. Ger, S.-T. Ke, Y.-R. Huang and S.-T. Wu, *The Ni - P - SiC Composite Produced by Electro-codeposition.* Materials Chemistry and Physics, 2005, 92(1): p. 146.

147. P. A. Young, *Lattice Parameter Measurements on Molybdenum Disulphide.* Brit. J. Appl. Phys., 1968, 1(2): p. 936.

148. R. Weil, *The Structures of Electrodeposits and the Properies That Depend on Them.* Annu. Rev. Mater. Sci., 1989, 19: p. 165.

149. J. Amblard and M. Froment, *New Interpretation of Texture Formation in Nickel Electrodeposits.* Faraday Symposia of the Chemical Society, 1977, 12(0): p. 136.

150. D. Y. Li and J. A. Szpunar, *A Monte Carlo simulation approach to the texture formation during electrodeposition—II. Simulation and experiment.* Electrochim. Acta, 1997, 42(1): p. 47.

151. M. Saitou, S. Oshiro and Y. Sagawa, *Scaling Behavior of Internal Stress in Electrodeposited in Nickel Thin Films.* Journal of Applied Physics, 2008, 104(093518): p. 1

152. E. Beltowska-Lehman, A. Goral and P. Indyka, *Electrodeposition and Characterization of Ni / Al$_2$O$_3$ Nanocomposite Coatings.* Archieves of Metallurgy and Materials, 2011, 56(4): p. 919.

153. F. Czerwinski, *The Microstructure and Internal Stress of Fe - Ni Nanocrystalline Alloys Electrodeposited without a Stress-reliever.* Electrochim. Acta, 1998, 44(4): p. 667.

154. M. A. Chowdhury, D. M. Nuruzzaman and M. L. Rahaman, *Variation of Friction Coefficient of Copper with Sliding Velocity and Relative Humidity.* Journal of Advanced Research in Mechanical Engineering, 2010, 1(3): p. 142.

155. S. Tongay, S. S. Varnoosfaderani, B. R. Appleton, J. Wu and A. F. Hebard, *Magnetic Properties of MoS$_2$: Existence of Ferromagnetism.* Applied Physics Letters 2012, 101: p. 123105.

156. Y. Yamaguchi, *Tribology of Plastic Materials.* Friction Amsterdam, 1990.

157. R. G. Bayer, *Design for Wear Resistance.* ASM Handbook, 1997, 20: p. 603.

158. G. H. Xu, M. Zhu, J. Liu, Z. Zhou and H. Liang, *The Effect of Pre-treatment of Substrate on Fretting Tribological Behaviour of MoS$_2$ Coatings.* Wear, 2003, 255: p. 246.

APPENDIX A

THE VOLTAMMOGRAMS FOR 16 EXPERIMENTS AT 100 mV/s SCAN RATE VALUES
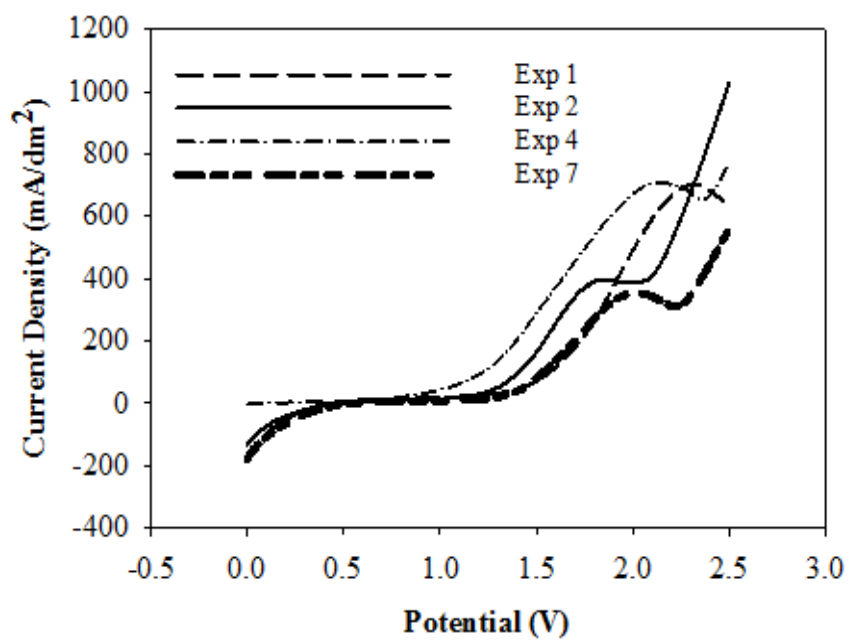

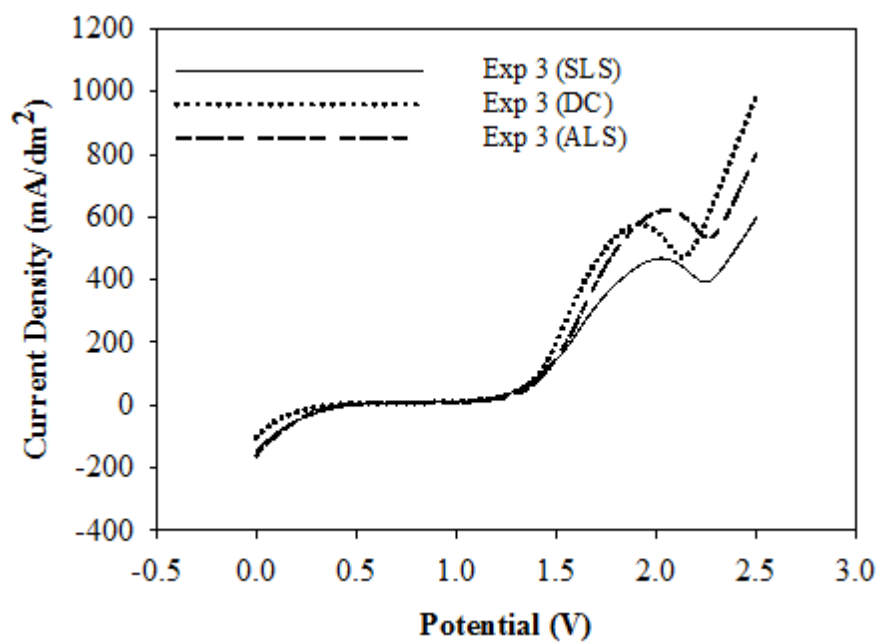**Figure A.1 The voltammograms for experiments 1, 2, 4 and 7**

Figure A.2 The voltammograms for experiment 3 using surfactants SLS, DC and ALS
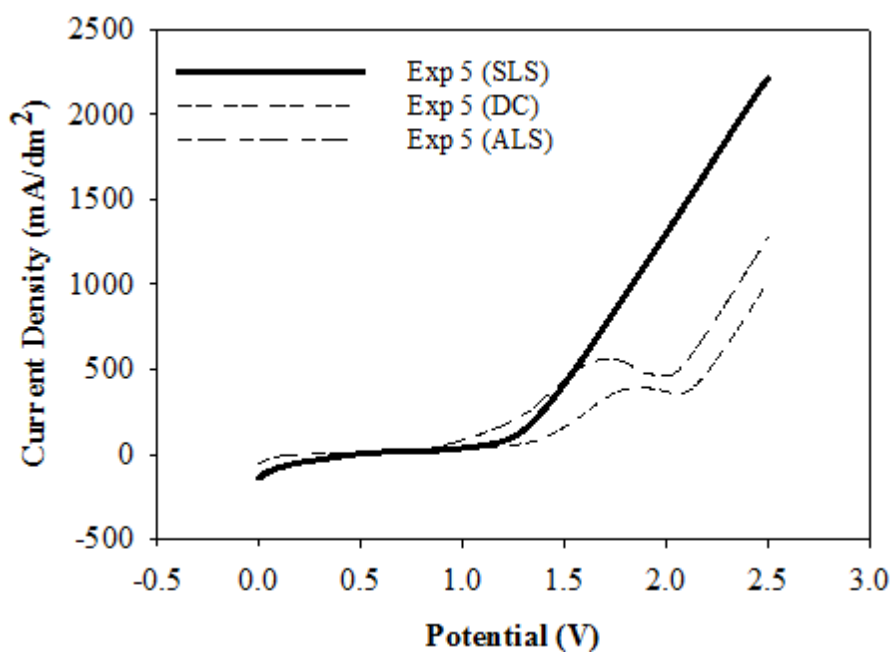

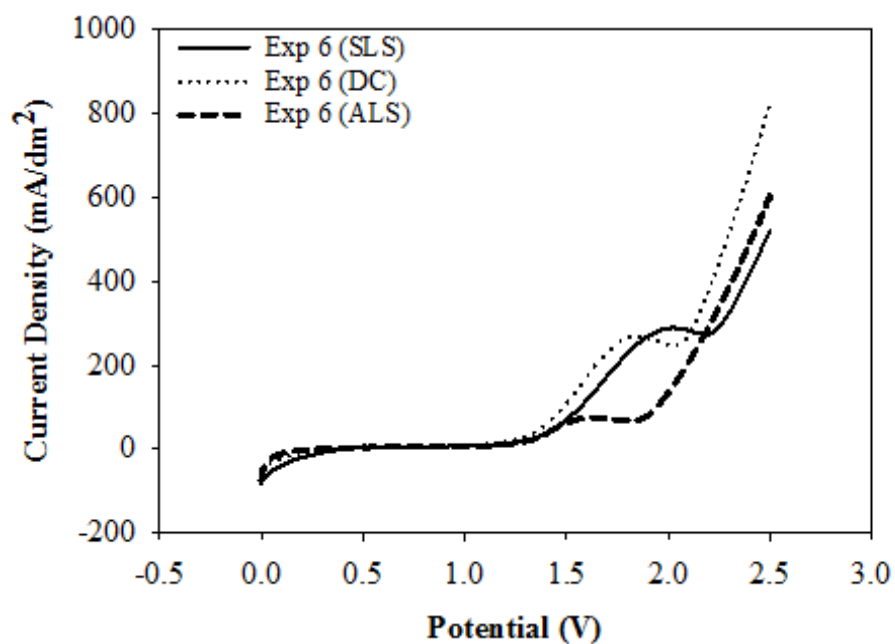**Figure A.3 The voltammograms for experiment 5 using surfactants SLS, DC and ALS**

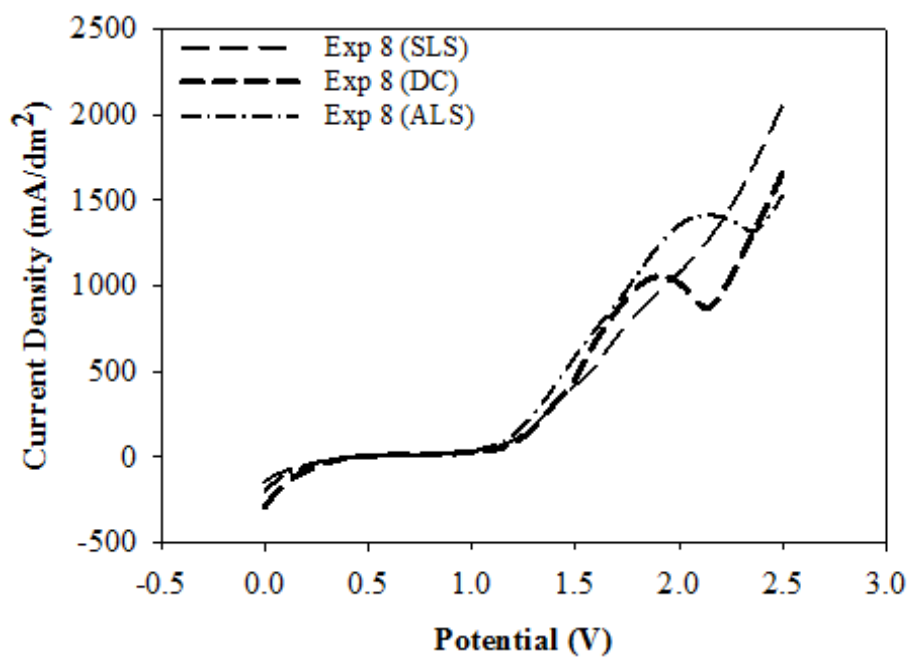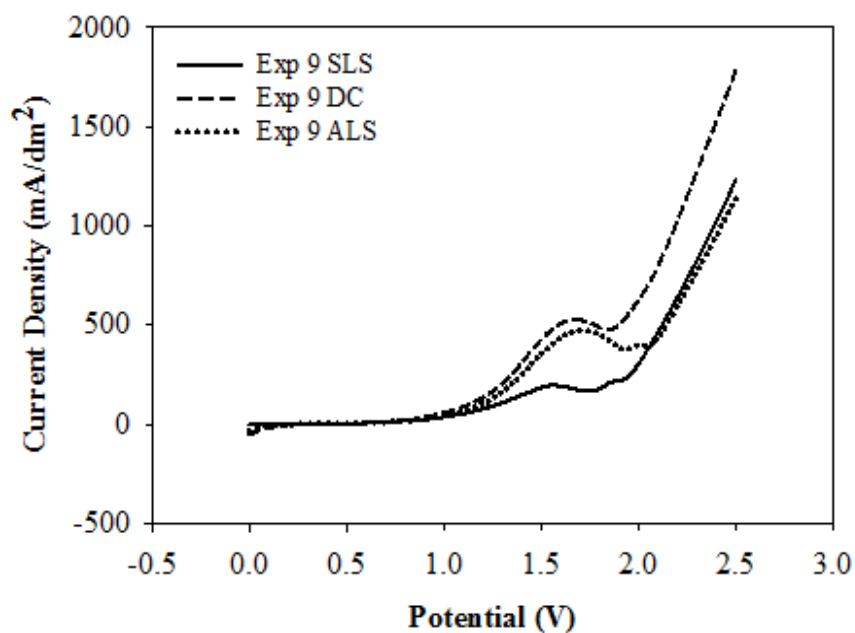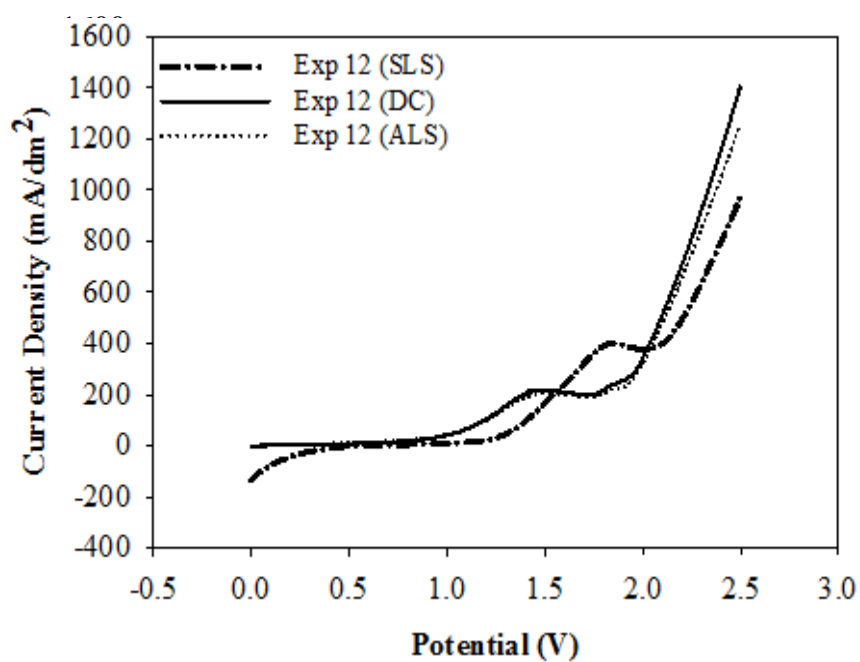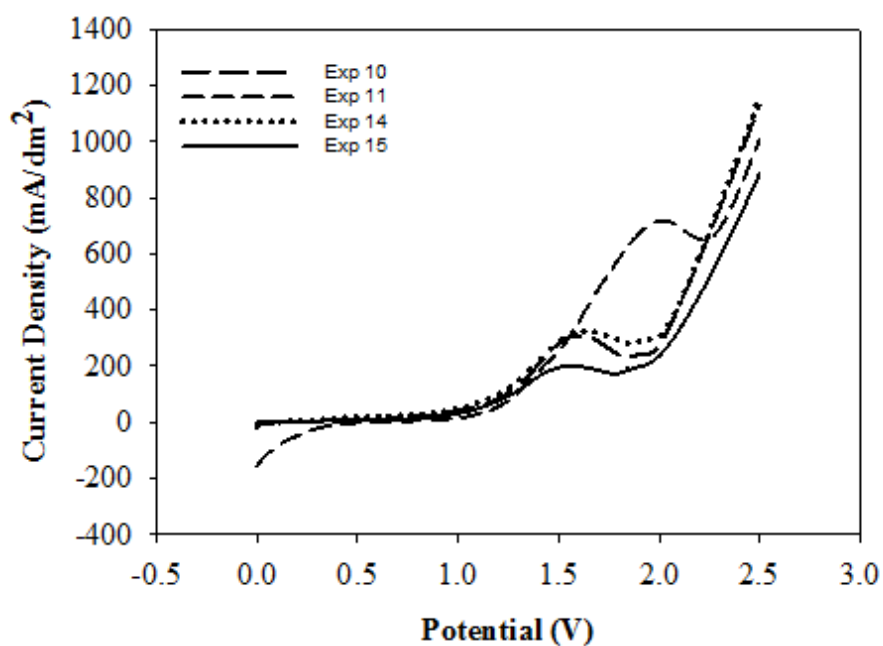**Figure A.4 The voltammograms for experiment 6 using surfactants SLS, DC and ALS**

Figure A.5 The voltammograms for experiment 8 using surfactants SLS, DC and ALS

Figure A.6 The voltammograms for experiment 9 using surfactants SLS, DC and ALS

Figure A.7 The voltammograms for experiment 12 using surfactants SLS, DC and ALS

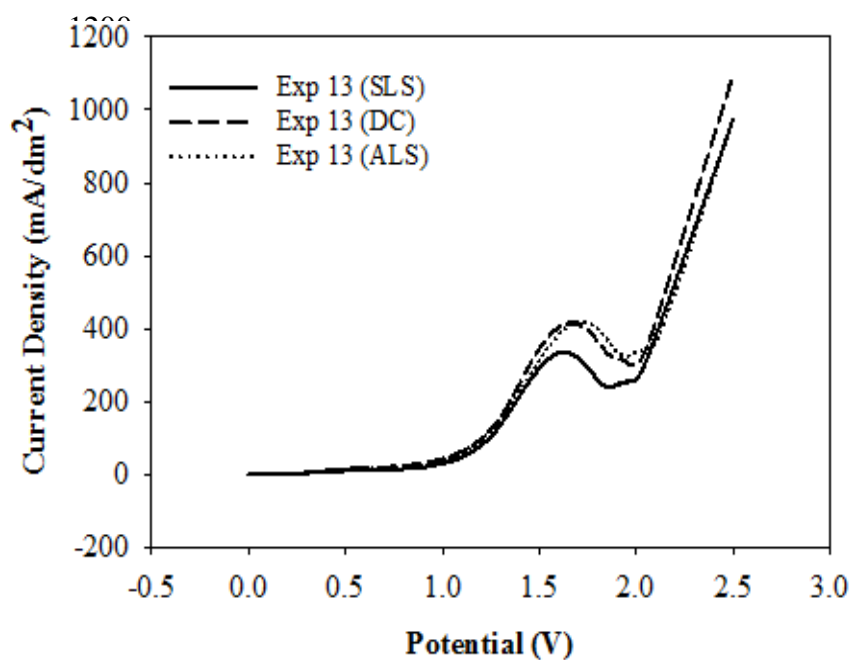**Figure A.8 The voltammograms for experiments 10, 11, 14 and 15**

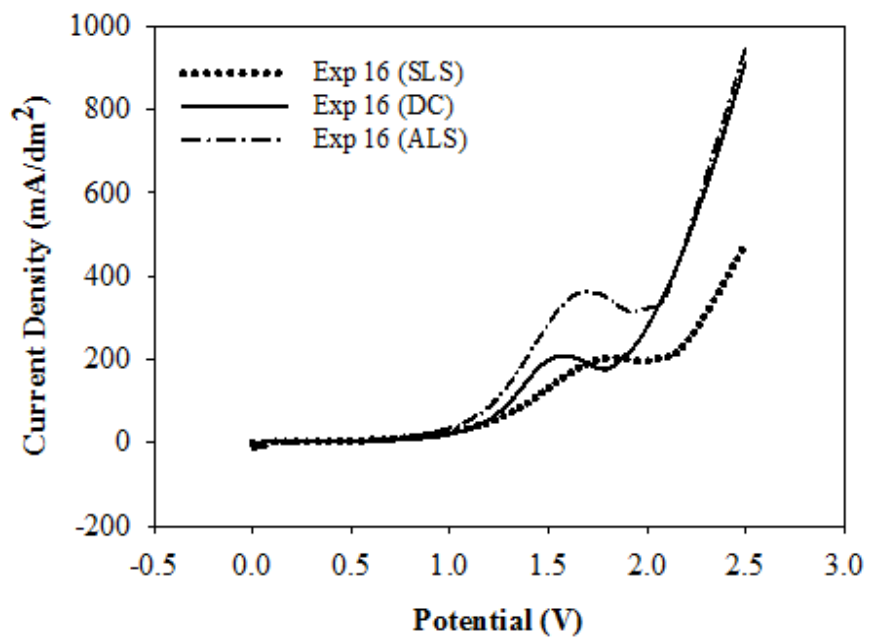**Figure A.9 The voltammograms for experiment 13 using surfactants SLS, DC and ALS**

Figure A.10 The voltammograms for experiment 16 using surfactants SLS, DC and ALS
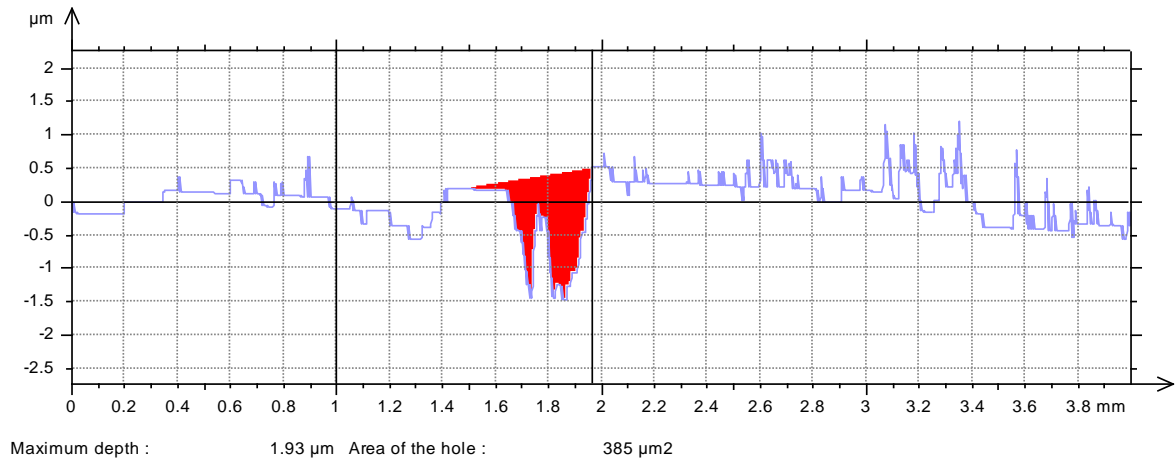
APPENDIX B

CROSS-SECTIONAL WEAR TRACK PROFILES

Maximum depth :   1.93 µm   Area of the hole :   385 µm2

Figure B.1 Wear track profile for experiment 1(measurement 1)

Maximum depth :   3.23 µm   Area of the hole :   692 µm2
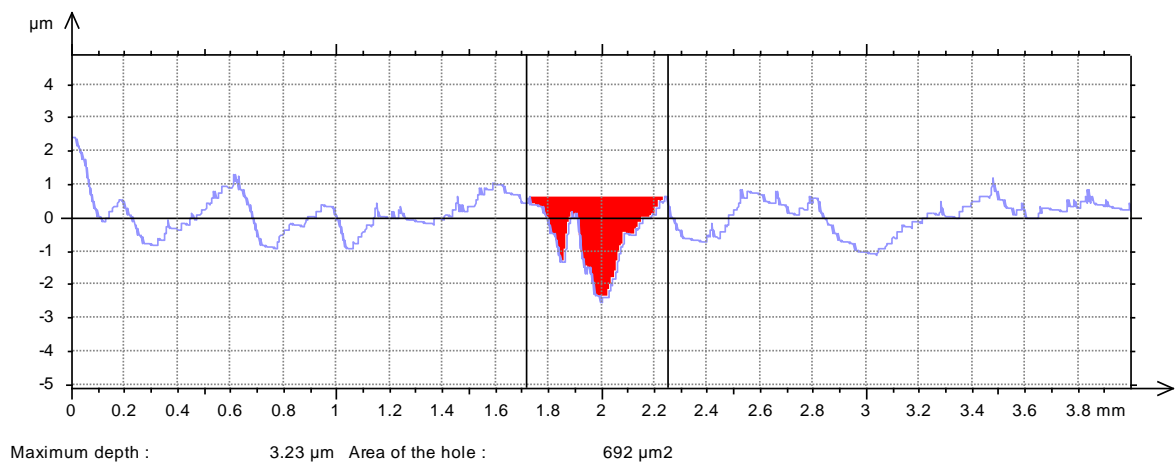
Figure B.2 Wear track profile for experiment 1(measurement 2)

88

Maximum depth :   2.73 µm   Area of the hole :   640 µm2
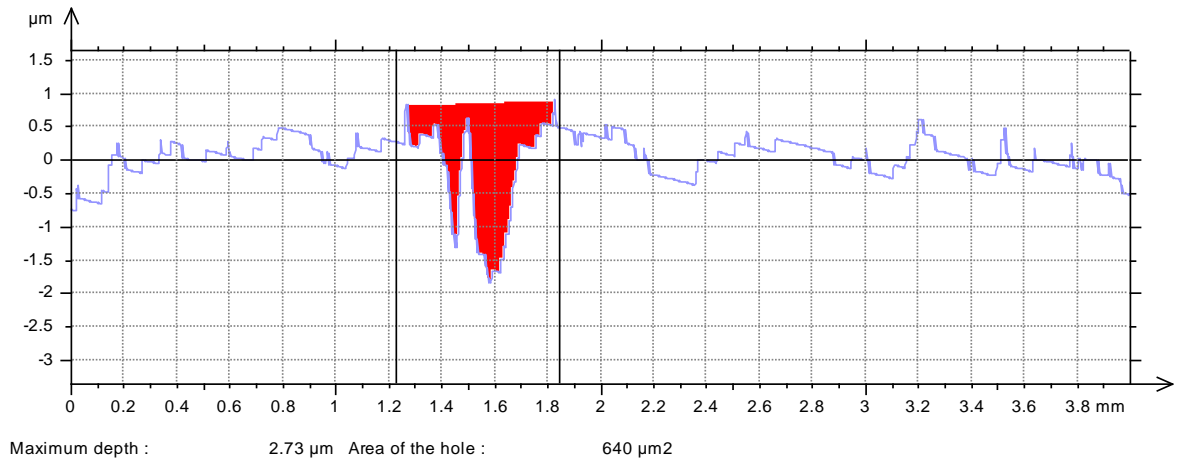
Figure B.3 Wear track profile for experiment 1(measurement 3)

Maximum depth :   2.9 µm   Area of the hole :   707 µm2
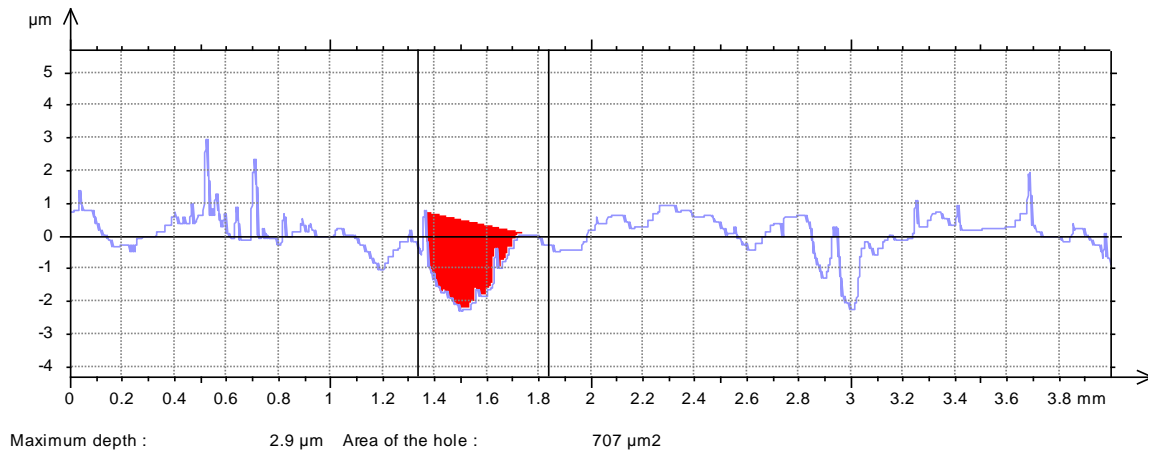
Figure B.4 Wear track profile for experiment 3(measurement 1)

Maximum depth :   5.87 µm   Area of the hole :   2402 µm2
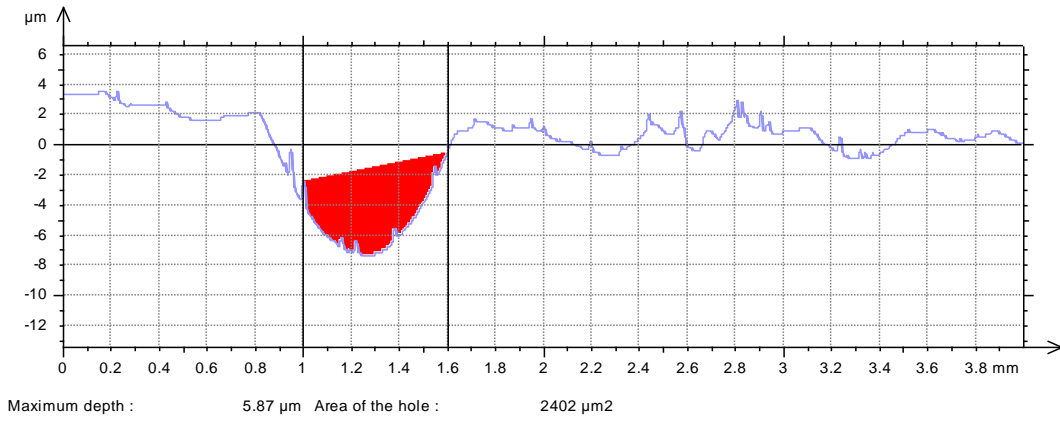
Figure B.5 Wear track profile for experiment 3 (measurement 2)
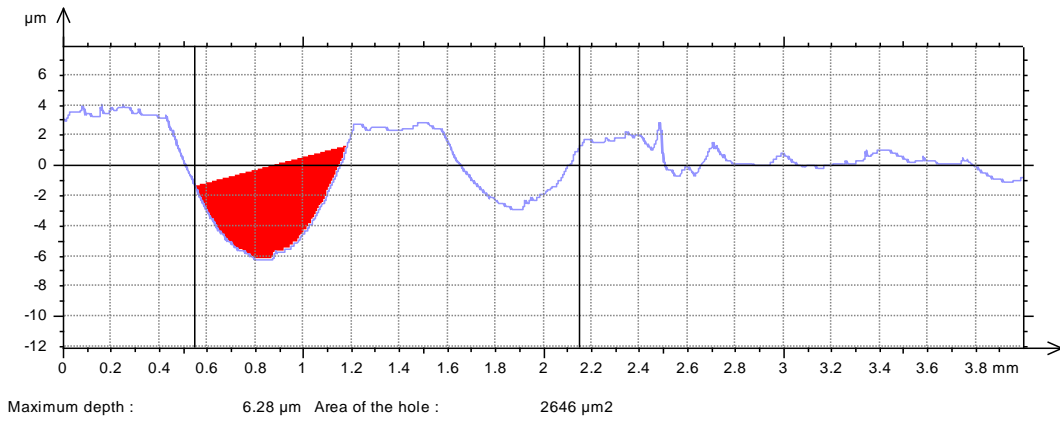
Maximum depth :   6.28 µm   Area of the hole :   2646 µm2

Figure B.6 Wear track profile for experiment 3(measurement 3)

Maximum depth :   4.52 µm   Area of the hole :   1696 µm2

Figure B.6 Wear track profile for experiment 4 (measurement 1)

Maximum depth :   11.3 µm   Area of the hole :   6366 µm2
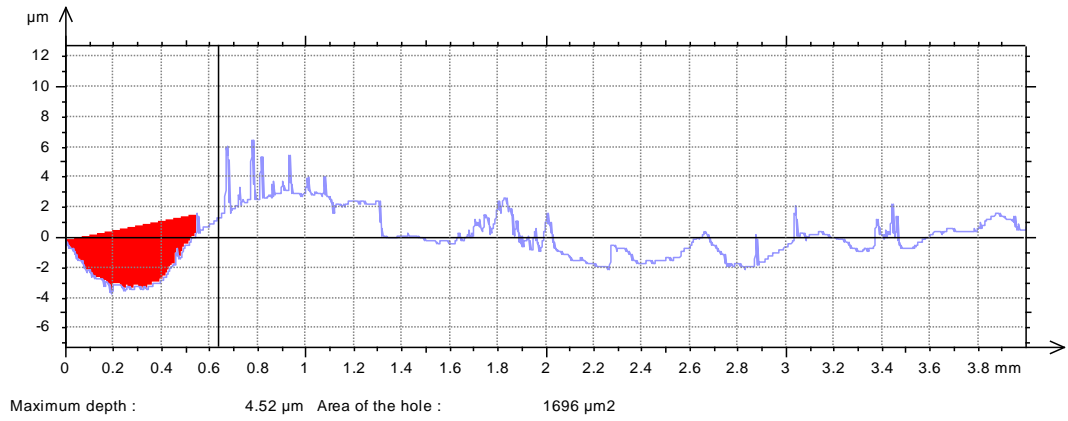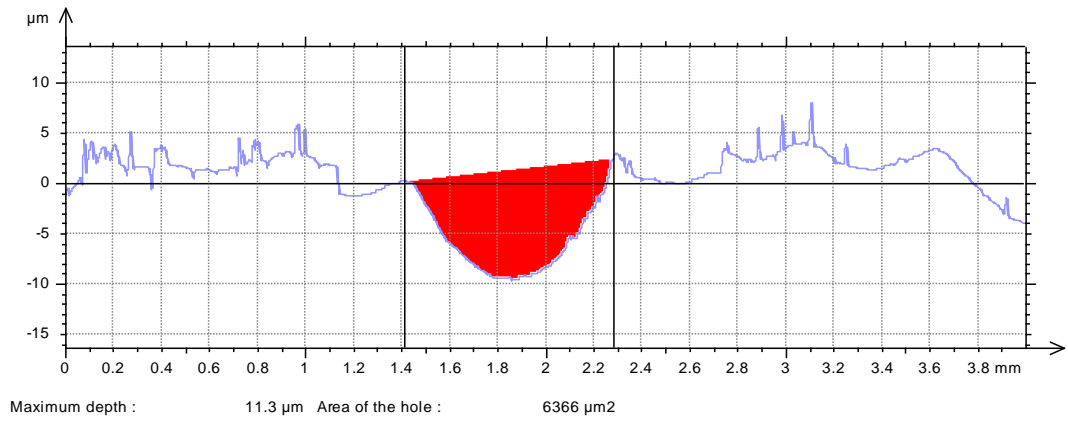
Figure B.7 Wear track profile for experiment 4 (measurement 2)

Maximum depth :   18.2 µm   Area of the hole :   8653 µm2

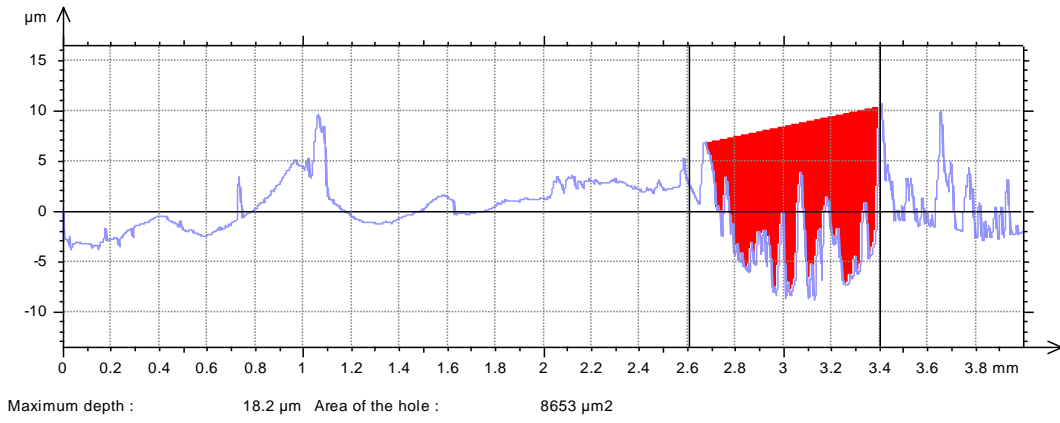**Figure B.8 Wear track profile for experiment 4 (measurement 3)**

PERSONAL INFORMATION
Surname, Name: Saraloğlu Güler, Ebru
Nationality: Turkish (TC)
Date and Place of Birth: 26 February 1984, Kdz. Ereğli
Marital Status: Married
Phone: +90 312 210 59 15
Fax: +90 312 210 25 18
email: saebru@metu.edu.tr

EDUCATION

Degree	Institution	Year of Graduation
PhD	METU Metallurgical and Materials Engineering	2013
MS	METU Metallurgical and Materials Engineering	2008
BS	METU Metallurgical and Materials Engineering	2006
High School	Burak Bora Anadolu High School, İstanbul	2002

WORK EXPERIENCE

Year	Place	Enrollment
2006-Present	METU Metallurgical and Materials Engineering Dept.	Research Assistant

FOREIGN LANGUAGES
Advanced English, German

ACTIVITIES & PAPERS:

Tubitak Project 105M174 (2006-2008): Production of Aluminum Alloys by Severe Plastic Deformation (Investigator)

Paper: Saraloglu E, Tan E, Gur CH; Effect of ECAP and Post-aging Processes on 2024 Aluminum Alloy; Steel Research International 79 (**2008**) Metal Forming special issue Vol.2 467-471

International Conference paper: Saraloglu E, Tan E, Gur CH; Eş Kanallı Açısal Presleme ve Yaşlandırma İşlemlerinin 2024 Al Alaşımının Mekanik Özelliklerine Etkisi, CD Proc 14th International Metallurgy & Materials Congress, 16-18 ekim **2008**, İstanbul, 15-20. (speaker)

International Conference paper: Saraloglu E, Tan E, Gur CH; Effect of ECAP and Post-aging Processes on 2024 Aluminum Alloy, Metal Forming 12th Int. Conf. **2008**, Krakow

Thesis: Effect of ECAP and Subsequent Het Treatments on Microstructure and Mechanical Properties of 2024 Aluminum Alloy (August, **2008**)

Entrepreneurship certificate 2011 (fromTubitak)

International Conference paper: Guler Saraloglu E, Karakaya, I. and Konca, E (**2012**) Effect of Electroplating Parameters on "HER" Current Density in Ni-MoS$_2$ Composite Plating, in Supplemental Proceedings: Materials Processing and Interfaces, Volume 1 (ed TMS), John Wiley & Sons, Inc., Hoboken, NJ, USA. (speaker)

International Conference paper: Guler Saraloglu E., Konca, E. and Karakaya, İ. (**2013**) Effect of Electroplating Parameters on Internal Stress in Ni-MoS$_2$ Composite Plating, in TMS2013 Supplemental Proceedings (ed TMS), John Wiley & Sons, Inc., Hoboken, NJ, USA.

International Conference: Guler Saraloglu E, Karakaya, I., Konca, E, Ozturk, A. and Erdoğan, M. (**2013**) Investigation of the Tribological Behavior of Electrocodeposited Ni-MoS$_2$ Composite Coatings, in International Conference on Metallurgical Coatings and Thin Films, San Diego, CA, USA

International Conference: Guler Saraloglu E, Karakaya I., Konca, E. and Erdoğan, M. (**2013**) Investigation of Internal Stress Levels and Characteristics during Electrocodeposition of Ni-MoS$_2$ Composite Coatings, in International Conference on Metallurgical Coatings and Thin Films, San Diego, CA, USA (poster presentation)

Paper: Guler Saraloglu E., Konca, E. and Karakaya, İ.; Effect of Electrodeposition Parameters on the Current Density of Hydrogen Evolution Reaction in Ni and Ni-MoS$_2$ Composite Coatings; International Journal of Electrochemical Science (**2013**) Vol.8 5496 – 5505

Paper: Guler Saraloglu E., Karakaya, İ. and Konca, E.; Effects of current density, coating thickness, temperature, pH and particle concentration on internal stress during Ni-MoS$_2$ electrocodeposition; Surface Engineering (**2013**) (revised)

Microsoft Software certificate 2013 Microsoft Certified Solution Developer, Education place: Bilge Adam, Education dates: 19.01.2013 - 08.09.2013, Education content: Programming in C#, Database Design and Programming, Developing Azure and Web Services, Programming in HTML 5 with Javascript and CSS3, Developing ASP. NET 4.5 MVC Web Applications, Project Management

HOBBIES
Computer software, Playing chess, Latin Dance Sports, Swimming